2007-05-07

Origin and Tectonic Evolution of Gondwana Sequence Units Accreted to the Banda Arc: A Structural Transect through Central East Timor

Elizabeth Anick Zobell
Brigham Young University - Provo

ORIGIN AND TECTONIC EVOLUTION OF GONDWANA SEQUENCE UNITS ACCRETED TO THE BANDA ARC: A STRUCTURAL TRANSECT THROUGH CENTRAL EAST TIMOR

by

Elizabeth A. Zobell

A thesis submitted to the faculty of

Brigham Young University

in partial fulfillment of the requirement for the degree of

Master of Science

Department of Geological Sciences

Brigham Young University

August 2007

BRIGHAM YOUNG UNIVERSITY

GRADUATE COMMITTEE APPROVAL

of a thesis submitted by

Elizabeth A. Zobell

This thesis has been read by each member of the following graduate committee and by majority vote has been found to be satisfactory.

Date	Ronald A. Harris, Chair
Date	John H. McBride
Date	Michael J. Dorais

BRIGHAM YOUNG UNIVERSITY

As chair of the candidate's graduate committee, I have read the thesis of Elizabeth A. Zobell in its final form and have found that (1) its format, citations, and bibliographical style are consistent and acceptable and fulfill university and department style requirements; (2) its illustrative materials including figures, tables, and charts are in place; and (3) the final manuscript is satisfactory to the graduate committee and is ready for submission to the university library.

____

Date

____

Ronald A. Harris
Chair, Graduate Committee

Accepted for the Department

____

Michael J. Dorais
Graduate Coordinator

Accepted for the College

____

Thomas W. Sederberg
Associate Dean, College of Physical and Mathematical Sciences

ABSTRACT

ORIGIN AND TECTONIC EVOLUTION OF GONDWANA SEQUENCE UNITS ACCRETED TO THE BANDA ARC: A STRUCTURAL TRANSECT THROUGH CENTRAL EAST TIMOR

Elizabeth A. Zobell

Department of Geological Sciences

Master of Science

Petrographic and age analysis of sandstones, detailed structural analysis and gravity modeling were conducted to investigate the origin of the Gondwana Sequence in the Timor Region, and to better constrain the tectonic evolution of the active Banda Arc. Our field studies and U/Pb zircon age analysis helped assign most units to either Asian or Australian affinity. Detrital zircon from uplifted Banda forearc units (Asian affinity) have U/Pb ages as young as 80 Ma (Standley and Harris, in press). In contrast, analysis of detrital zircon from Gondwana Sequence sandstones accreted to the Banda Arc from Savu to East Timor are no younger than 234.6 ± 4.0 Ma, and have peak ages at 301 Ma and 1873 Ma with some Archean ages. These age constraints provide a reliable new application for distinguishing rocks units as Asian or Australian affinity.

Petrographic and provenance analysis of Triassic Australian affinity greywacke units yield QFL abundances consistent with a proximal, syn-rift, intracratonic or recycled orogen source, from the northeast. The Mount Isa region to the east has the most similar peak U/Pb zircon ages to the Gondwana Sequence. However an extension of this terrane to the west, which would have rifted away during Jurassic breakup, is required to account for the immaturity of the sandstones.

Structural measurements of Gondwana Sequence units accreted to the Banda Arc show a northwest - southeast paleo and current maximum stress direction, and vergence mostly to the southeast. Individual thrust sheets are 3 km thick and account for 50% total shortening. The deformational grain of Timor is a hybrid of the east-west strike of Banda Arc and northeast-southwest strike of incoming Australian continental margin structures.

The Banda forearc, which is 200 km wide north of Savu, progressively narrows towards East Timor. In order to constrain the location of the forearc, three area-balanced structural models were tested against the gravity field of the Banda Arc. The best fit model requires internal shortening and under-stacking of the forearc beneath the arc, which may account for the cessation of volcanism and uplifted coral terraces north of East Timor.

ACKNOWLEDGEMENTS

Funding for the project was provided by the National Science Foundation (EAR 0337221). Assistance in East Timor was provided by the Oil, Gas and Energy Directorate (OGED) of East Timor (Mr. Amandio Gusmao Soares, Francisco Ferreira and Mr. Vicente de Pinto Costa and their staff), and the Natural Resources Division of East Timor (Lourenço Pedro and Francesco Monteira). Inacio Freitas Mereira, the Dean of the Faculty of Engineering at the National University of East Timor, arranged for Timorese student counterparts. Wine Langeraar, National Mapping Adviser to East Timor, made available maps and aerial photographs. I would like to thank Ron Harris for his encouragement and insight throughout this project. I would also like to thank Noemia Viegas from the National University of East Timor who helped as a dedicated field assistant, Eujay McCartain from Western Australia University for field support, Mike Vorkink for providing samples from Savu, and Miranda Livingston for assistance in data entry. George Gehrels and Victor Valencia from the University of Arizona assisted in the detrital zircon analysis. Funding for the Arizona LaserChron Center is provided by the National Science Foundation (EAR 0443387). Gravity models were generated using GM-SYS with help from John McBride. Cross-sections were balanced using Lithotect.

TABLE OF CONTENTS

INTRODUCTION

The Banda Orogen is an active arc-continent collision at the convergent boundary between the Asian and Australian plates (Figure 1) and is commonly used as a modern analog for the tectonic evolution of other collisions (Finney et al., 1996, Huang, 2000; Leech, 2005; Huang, 2006; Reusch, 2006). However, many fundamental questions about the structure of the collision zone remain unanswered and various parts of the orogen are poorly understood, such as 1) what happens to the pre-collisional forearc, 2) limits for total shortening, 3) whether basement is involved in building of the orogenic wedge and 4) what is the mechanism for crustal shortening? We chose to investigate these questions by conducting a detailed structural analysis through the central part of East Timor, which exposes the deepest structural levels of the orogen. A gravity profile (Kaye and Milsom, 1988; Chamalaun et al., 1975) through this region also allows us to test various models proposed for subsurface structural and tectonic features, such as deformation of the upper plate and basement involved in thrust near the surface. We have also investigated the origin of rock units near the suture zone in order to distinguish tectonic affinities.

Three major lithologic units make up the Banda Orogen, the Banda Terrane is found at the highest structural level, and the Gondwana and Kolbano Sequences which form the bulk of the orogenic wedge. The Banda Terrane is well documented as a fragment of Asian affinity forearc material of the Banda Arc upper plate (Standley and Harris, in press; Harris, 2006). The Gondwana Sequences was deposited in intracratonic basins during the initial rifting of Gondwana. The source for these units is unknown. The Kolbano Sequence represents post-rift units that were deposited on the slope of the northwest Australian passive continental margin.

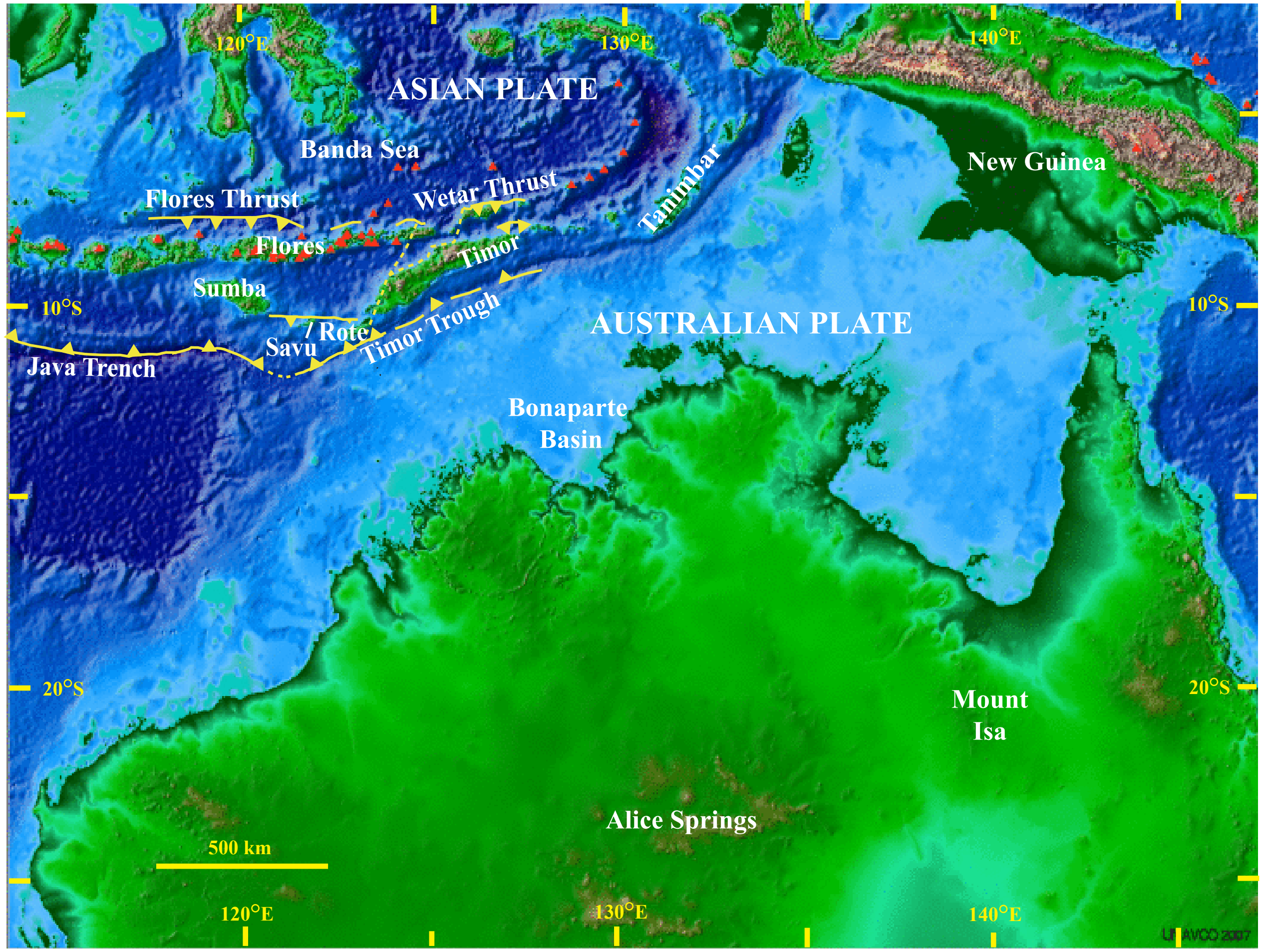

Figure 1: Location map of the Banda Arc region showing active faults (yellow), and active volcanoes (red triangles) (modified from Harris, 2006). Deformation localized at the Java Trench is progressivelydistributed away from the deformation front (Timor Trough) into the forearc and backarc.

We investigated the origin of Gondwana Sequence units by conducting a petrographic provenance study and U/Pb age analysis of detrital zircon. The stratigraphy of Gondwana Sequence units in the Banda Arc has been described by Audley-Charles (1968), Gianni (1971), Bird and Cook (1991) and Hunter (1993). These studies provided a general litho-stratigraphic description of the Gondwana Sequence, but constraints for the origin of these units and their structure are still lacking. Vorkink (2004) conducted a detailed structural analysis of Savu and found that discrete thrust sheets accommodated for shortening of Triassic-Jurassic Gondwana Sequence units. From reconnaissance structural studies throughout Timor, Harris (1991) shows that Gondwana Sequence units form a duplex beneath the Banda Terrane and the northern part of an imbricate fan of Kolbano sequence units. We conducted a detailed structural analysis of Gondwana Sequence units in a north-south corridor through East Timor from Manatutu to Fatu Berliu (Figure 2). We have also constructed crustal and lithospheric scale cross-sections across Timor through this corridor that are constrained by gravity models in order to test what happens to the Banda forearc during collision.

GEOLOGIC SETTING

The Banda Arc consists of two island chains separated by a forearc basin. Timor forms part of the uplifted accretionary wedge that has evolved into the Banda Orogen fold and thrust belt. The Banda Orogen consists mostly of Australian continental margin units accreted in front of, and beneath forearc basement of the Banda Sea plate. The formation of the Banda Arc is related to opening of the Banda Sea by slab rollback during

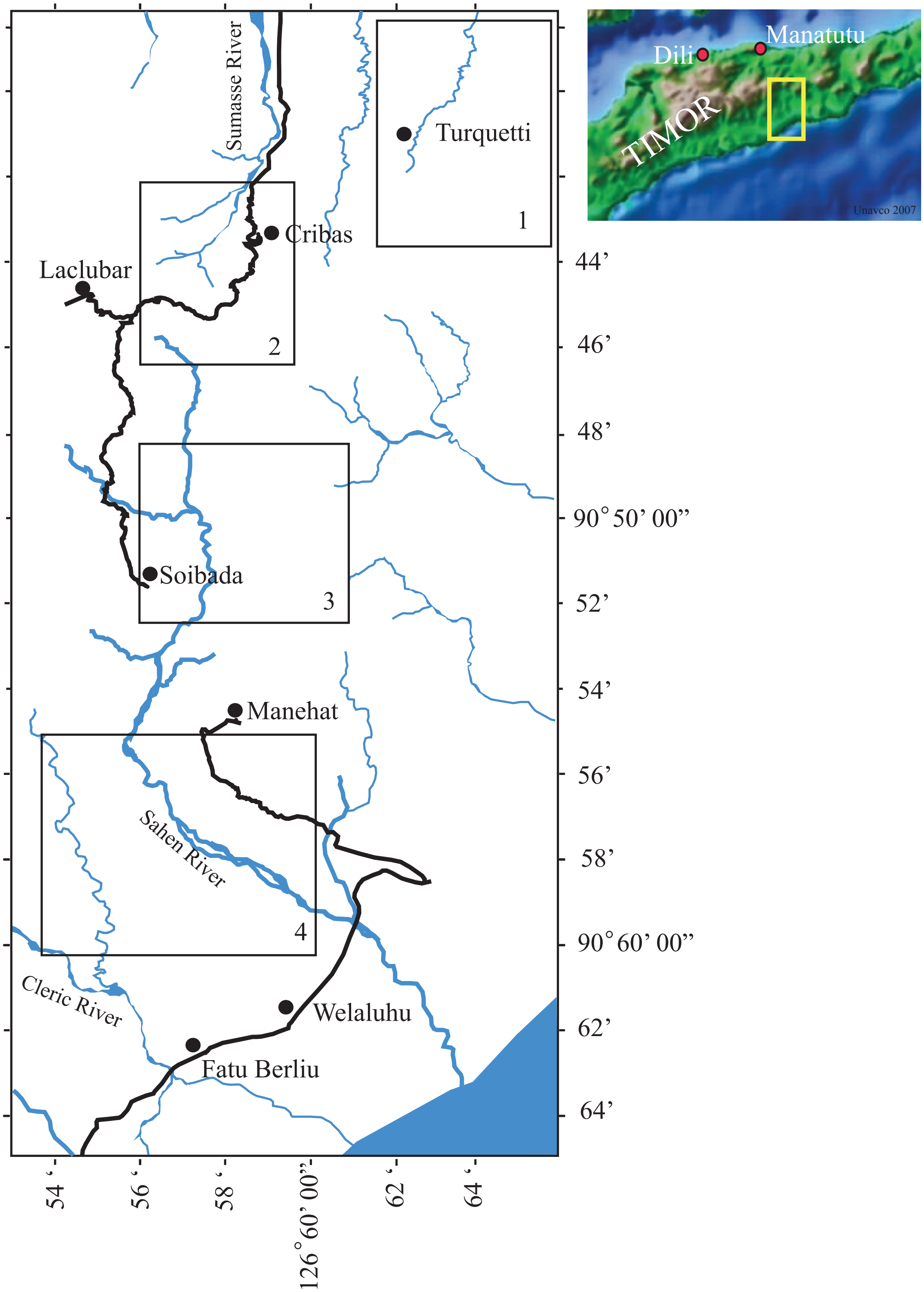

Figure 2: Location map for the structural transects. 1: Turquetti transect, 2: Cribas transect, 3: Northern Soibada transect, 4: Southern Soibada and Fatu Berliu transects. Rivers are in grey and roads are in black.

the Late Miocene (Harris, 2006). The outer fringes of the Australian continental margin reached the Banda Arc subduction zone at 5-8 Ma (Johnston and Bowin, 1981). This initial collision occurred near the center of the island of Timor and propagated obliquely to the west towards Savu and to the east towards Taninbar (Harris, 1991).

Sedimentary cover sequences of the Australian continent involved in this collision consists of Permian through Jurassic siliciclasic and carbonate deposits (Audley-Charles, 1968) (Figure 3). The Wailuli Formation, which is composed of shale and mudstone, caps the Gondwana Sequence. This formation is overlain by an unconformity marking the breakup of Gondwanaland. Post-rift passive margin deposits that accumulated on the Australian slope and rise consists mostly of Cretaceous to Pliocene chert, limestone, and shale with minor sandstone that were deposited on the subsiding Australian margin (Carter et al., 1976).

During the collision of the Australia continental margin with the Banda Arc a decollement formed within the relatively weak Wailuli Formation near the breakup unconformity separating pre- and post-rift units. This allowed Kolbano units to detach and create an imbricate stack against the front of the Banda Terrane (Carter et al., 1976). Beneath the Kolbano imbricate stack lays relatively undeformed Gondwana Sequence, which was thrust below the Banda Terrane. Evidence for the decollement in the Wailuli Formation includes the locations of the post- versus pre-rift rock units in Timor (Figure 4 and 5). Post-rift units are dominantly located on the southern portion of the island near and extent to the Timor Trough and shortened pre-break-up Gondwana Sequence units make up the bulk of the island. The location of Wailuli Formation decollement is further

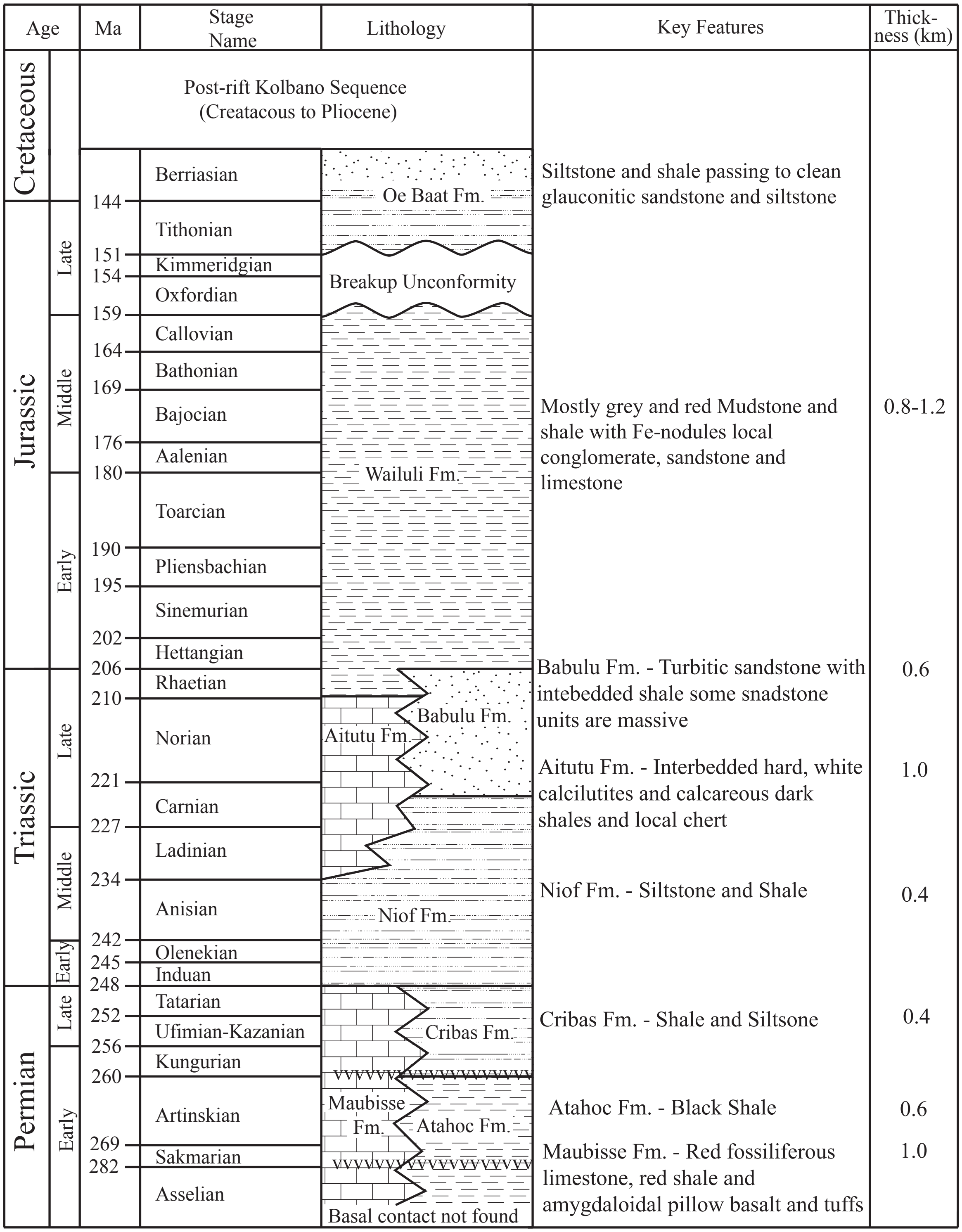

Figure 3: Gondwana Sequence stratigraphic column. The Aileu Complex is associated with the Maubisse Formation.

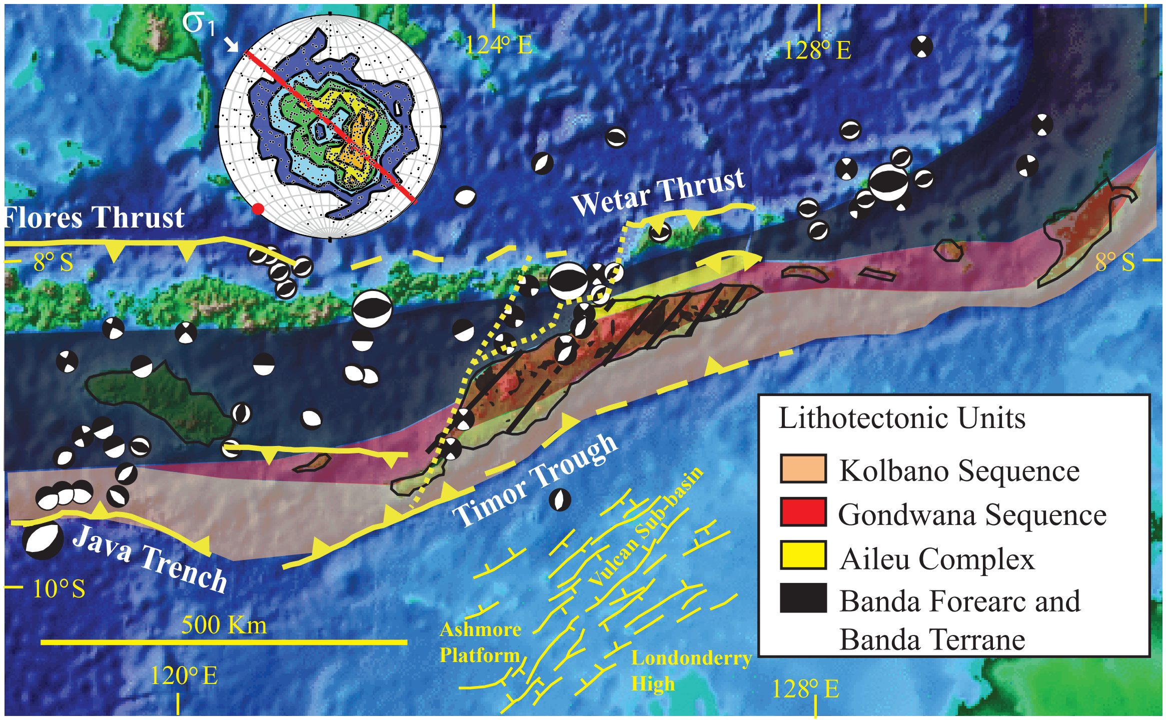

Figure 4: Map showing extent of major lithotectonic units in the Banda Orogen, fault plane solutions, and active faults. The Banda Terrane is forearc crust that forms klippen overlying the Gondwana Sequence in Timor. Black lines are hinge lines of antiforms in Timor, which parallel the structure of the northwest Australian continental margin (shown in yellow) (Petkovik et al., 2000). Stereograph shows poles to bedding plane measurements from Timor (N= 914) predict a σ_1 direction (red line) and fold axis (red circle) parallel to observed structures (See structural analysis).

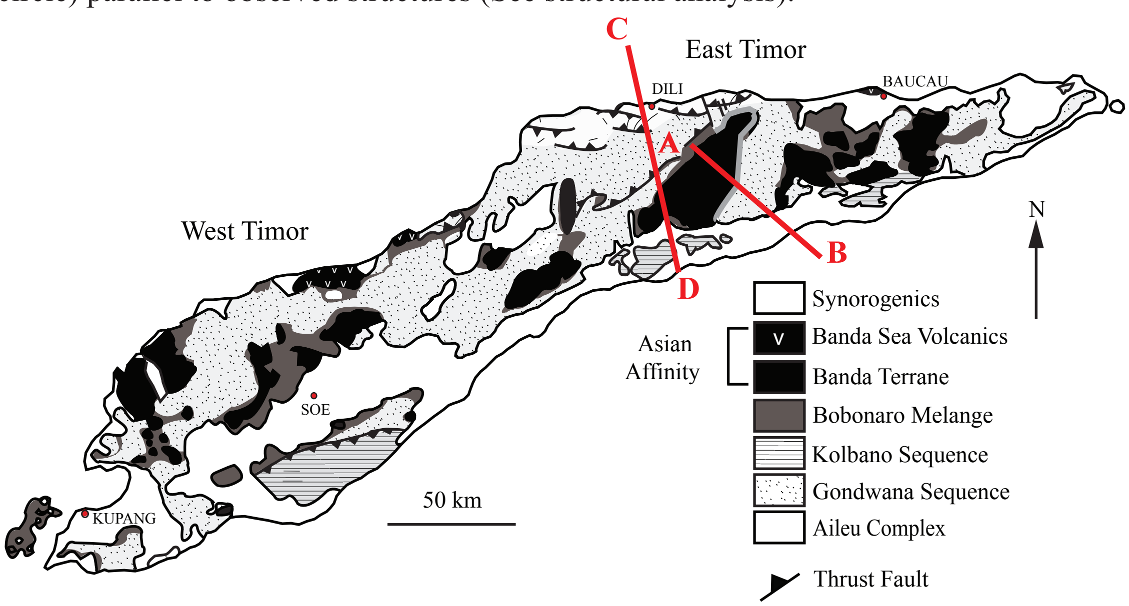

Figure 5: Map of the major lithotectonic units of Timor. Kolbano Sequence in mainly found in southern Timor and Gondwana in Northern Timor. The Banda Terrane structurally overlies the Gondwana Sequence.

constrained by drilling (Sani et al., 1995) and seismic profiles (Reed et al., 1986; Karig et al., 1987).

TECTONIC AFFINITY

Many of the lithologic units of the Banda Orogen are similar to each other though they may have different tectonic affinities. Lithostratigraphic analysis alone has led to rival hypothesis about whether units have an Australian or Asian affinity. The age and origin of the Gondwana Sequence and the Banda Terrane units within the Banda Orogen has remained a debate after years of research (Grady, 1975; Carter et al., 1976; Chamalaun and Grady, 1978; Bird and Cook, 1991; Charlton, 2002). Recent age and geochemical analysis (Standley and Harris, in press; Harris, 2006) have clearly demonstrated which units belong to the Banda Terrane, and that these units are Asian affinity. Late Cretaceous detrital zircons found in 35-45 Ma amphibolite facies metamorphic rocks, arc affinity volcanic units and fossils assemblages with equatorial Asian association define the Banda Terrane of the Asian plate. The Permian-Jurassic Gondwana Sequence, on the other hand, was in mid-latitudes and nowhere near a plate boundary during the events that formed the Banda Terrane. Detrital zircons found in these Gondwana Sequence units should have only pre-Triassic and older detrital zircons ages including some derived from the Proterozoic-Archean Australian craton.

The first suggestions for an Australian origin of Gondwana Sequence units were published by Wanner (1913) and Brouwer (1942). A detailed study of sandstones in West Timor by Bird and Cook (1991) indicate a proximal source from the north and northeast. Their study compared the petrology of West Timor sandstones to those found on the Australian continental shelf and found a difference in sources between West Timor and the nearby Bonaparte Basin. In this study we investigated the provenance of Gondwana Sequence sandstones in Savu, West Timor and East Timor and analyzed ages of detrital zircon from some of these samples. Determining affinities of the major rock units of the Banda Orogen is a necessary step in investigating the nature of an active collisional suture.

Gondwana Sequence Unit Descriptions

The Gondwana Sequence can be divided into two series, the Permian-Triassic Aileu-Maubisse Series, and the Permian-Jurassic Kekneno Series (Lemoine, 1959). The stratigraphic relationship between the two series is ambiguous, but is inferred as transitional (Sawyer et al., 1993). The Kekneno Series consists of the Atahoc, Cribas, Niof, Aitutu, Babulu and the Wailuli Formations.

Aileu Complex

The Aileu Complex stretches from the north coast of western East Timor inland to the northern part of the Ramelau Range and is also found on the island of Kisar (Harris, 2006) and perhaps on other islands to the east (Figure 4). The Aileu complex consists of Permian-Triassic (?) psammite that grades southward into limestone and basalt associated with the Maubisse Formation (Berry and McDougall, 1986; Prasetyadi and Harris, 1996). On the north coast of central East Timor these units are metamorphosed into pelitic schist, marble, phyllite and amphibolite. Some metamorphism may have occurred during the rifting event that formed the edge of the Australian continental margin, but the main phase of metamorphism is associated with late Miocene onset of collision in central Timor (Berry and McDougall, 1986; Harris, 1991; Harris et al., 1998).

Maubisse Formation

The Maubisse Formation is a red, crinoidal limestone that was deposited during the Permian through Triassic, and represents the oldest rocks exposed in the Banda Orogen (de Roever, 1940; Audley-Charles, 1968). Pillow lavas found within the Maubisse Formation have geochemical signatures of within-plate and ocean-ridge basalt, which is interpreted as representing the onset of rifting (Berry and Jenner, 1982). Clastic sedimentary units found in the Maubisse Formation show a fining toward the south (Carter et al., 1976). Rocks similar to the Maubisse Formation have been documented on the Sahul Shoals of the undeformed Australian continental margin (Grady and Berry, 1977).

Atahoc Formation

The Atahoc Formation is most likely transitional with the Maubisse Formation and is Permian in age. This formation is mainly shales with some fine grained sandstones and volcanics. The basal contact has not been found and the upper contact is amygdaloidal basalt (Sawyer et al., 1993).

Cribas Formation

The Permian Cribas Formation overlies the Atahoc formation and is most likely interfingered with the Maubisse Formation. This formation contains shales and silty shales with clay and ironstone nodules. The presence of these nodules indicates an anoxic condition during its deposition (Charlton et al., 2002). Sandstone is found in the upper portion of the Cribas Formation. This sandstone is interpreted as being part of a submarine fan complex (Hunter, 1993) deposited on a shallow shelf (Bird, 1987).

Niof Formation

The Triassic Niof Formation is recognized in West Timor and may comprise the upper part of the Cribas Formation in East Timor. It consists of thin interbedded claystone, brown, gray and black shale, and sandstone. Bird and Cook (1991) interpreted the deposition of the Niof as turbidites in shallow to deep water. The upper portion of the Niof is interbedded with the Aitutu formation.

Aitutu Formation

The Triassic Aitutu Formation is the most distinctive unit of the Gondwana Sequence. It is a rhythmically bedded white to pink limestone with thin interbeds of dark grey shale. The Aitutu Formation was deposited on an open marine outer shelf (Sawyer et al., 1993). It is the most lithologically distinct unit of the Kekneno Series and is used as a marker unit for structural reconstructions.

Babulu Formation

The Triassic Babulu Formation is only recognized in central Timor (Gianni, 1971; Bird and Cook, 1991) and Savu (Vorkink, 2004), and may comprise the base of the Wailuli Formation in East Timor. The Babulu Formation consists of sandstone, shale and silts with some massive sandstones beds. Deposition of this unit most likely occurred in a proximal near shore to shelf break (Sawyer et al., 1993) through turbidity currents from a prograding delta (Bird and Cook, 1991).

Wailuli Formation

The Late Triassic to Jurassic Wailuli Formation is a thick succession of mostly smectite-rich mudstone (Harris et al., 1998) with some well bedded marl, calcilutite, micaceous shale and quartz arenite. Towards the top of the formation are conglomerate and red shale units (Audley-Charles, 1968). It commonly serves as a decollement for imbrication of the overlying Kolbano Sequence; and as a roof thrust for the Gondwana Sequence duplex zone.

Provenance of the Gondwana Sequence

We investigated possible source regions for Gondwana Sequence sandstones by petrographic studies and U/Pb age analysis of detrital zircon. Samples of Triassic Gondwana Sequence sandstone were collected from Savu, West Timor and East Timor. Modal abundances for classification and sedimentary provenance were determined using a three hundred point count of thin sections, percent errors of the point count are reported according the Tornado Chart for point counting reliability (van der Plas and Tobi, 1965) (Table 1). Sandstone maturity was investigated as a means of estimating transported distances based on rounding, presence of heavy minerals, presence of lithic clasts, and size and freshness of feldspars.

Table 1: Modal composition of sandstones with percent errors. ET = East Timor, WT = West Timor, SV = Savu

Sample	Location	Mono	Undulose	Poly	Micro	K-Spar	Plag	Lithics	Mica	Opaques	Matrix	Cement
EZ-69	ET	12.3 ± 3.9	5.0 ± 2.1	8.0 ± 3.1	3.3 ± 1.0	0 ± 0	0.6 ± 0.2	9.6 ± 3.5	1.0 ± 0.5	4.0 ± 2.2	0 ± 0	56.0 ± 5.7
EZ-70	ET	20.0 ± 4.5	20.0 ± 4.5	3.3 ± 1.0	2.0 ± 1.0	0 ± 0	0.6 ± 0.2	3.3 ± 1.0	3.0 ± 1.0	11.9 ± 3.7	35.3 ± 5.6	1.0 ± 0.5
EZ-88	ET	15.3 ± 4.0	22.0 ± 4.7	10.6 ± 3.6	0 ± 0	0 ± 0	2.6 ± 1.0	15.0 ± 4.0	5.0 ± 2.4	4.6 ± 2.3	24.6 ± 4.8	0 ± 0
EZ-151	ET	16.0 ± 4.1	13.0 ± 3.9	13.6 ± 3.9	0 ± 0	0 ± 0	3.6 ± 1.0	10.3 ± 3.5	1.3 ± 0.5	2.0 ± 1.0	29.3 ± 5.3	3.0 ± 1.0
89 HS-11A	WT	21.3 ± 4.6	18.0 ± 4.3	2.3 ±1.0	3.6 ± 1.0	0 ± 0	1.6 ± 0.5	5.6 ± 2.6	1.0 ± 0.5	0 ± 0	46.3 ± 5.8	0 ± 0
89 HS 14	WT	31.3 ± 5.3	6.6 ± 2.5	12.6 ± 3.8	0 ± 0	1.0 ± 0.5	2.0 ± 1.0	11.9 ± 3.8	4.0 ± 2.2	0.3 ± 0.2	30.0 ± 5.3	0.3 ± 0.2
89 HS-16A	WT	24.4 ± 4.7	18.6 ± 4.4	7.4 ± 2.8	0 ± 0	0 ± 0	2.6 ± 1.0	1.0 ± 0.5	0.8 ± 0.5	0 ± 0	33.8 ± 5.5	0 ± 0
90 HS 45	WT	18.8 ± 4.4	10.0 ± 3.5	10.2 ± 3.5	3.4 ± 1.0	0 ± 0	3.2 ± 1.0	24.0 ± 4.8	3.0 ± 1.0	1.0 ± 0.5	26.4 ± 5.0	0 ± 0
90 HS-73C	WT	26.3 ± 5.0	10.0 ± 3.5	16.6 ± 4.1	0.5 ± 0.2	2.3 ± 1.1	0.6 ± 0.2	6.6 ± 2.5	2.0 ± 1.0	1.3 ± 0.5	0 ± 0	34.5 ± 5.6
RA-24A	WT	6.0 ± 2.2	42.3 ± 5.6	1.0 ± 0.5	0 ± 0	0 ± 0	3.0 ± 1.0	2.0 ± 1.0	23.0 ± 4.8	2.3 ± 1.0	0 ± 0	20.6 ± 4.6
SV-9	SV	32.0 ± 5.3	37.0 ± 5.6	1.6 ± 1.0	0 ± 0	0.6 ± 0.2	0.3 ± 0.2	0.3 ± 0.2	1.0 ± 0.5	0 ± 0	27 ± 5.1	0 ± 0
SV-28C	SV	29.0 ± 5.2	9.6 ± 3.3	2.6 ± 1.0	0 ± 0	0 ± 0	0.3 ± 0.2	0.3 ± 0.2	0 ± 0	0 ± 0	0 ± 0	57.9 ± 5.7
SV-155A	SV	25.0 ± 4.9	8.6 ± 3.2	6.3 ± 2.2	2.6 ± 1.0	0 ± 0	2.6 ± 1.0	2.2 ± 1.0	2.3 ± 1.0	0 ± 0	51 ± 5.8	0 ± 0
SV-159	SV	12.3 ± 3.9	11.0 ± 3.7	10.3 ± 3.5	3.6 ± 1.0	0.3 ± 0.2	0.6 ± 0.2	1.2 ± 0.5	0 ± 0	0 ± 0	60.6 ± 5.6	0 ± 0
SV-164	SV	36.0 ± 5.5	34.6 ± 5.6	1.0 ± 0.5	0.3 ± 0.2	0 ± 0	0 ± 0	2.0 ± 1.0	1.0 ± 0.5	1.3 ± 0.5	23.66 ± 4.8	0 ± 0
SV-Bab	SV	26.0 ± 5.0	8.0 ± 3.0	4.9 ± 2.2	1.24 ± 0.5	0 ± 0	1.2 ± 0.5	12.4 ± 4.0	3.7 ± 1.0	0 ± 0	0 ± 0	42.2 ± 5.6

U/Pb zircon age analyses were conducted on six detrital zircon bearing Triassic Gondwana Sequence sandstones in East Timor and Savu were analyzed. These samples were crushed and the <940μm size fraction was magnetically separated using the Carpco and Frantz magnetic separators. Heavy minerals were separated using tetraboroethelene. Zircons were then hand picked for analysis. Small sample size (we analyzed a total of 304 zircon grains) prevented a random selection from a large pool of zircons. U-Pb geochronology of zircons was conducted by laser ablation multicollector inductively coupled plasma mass spectrometry (LA-MC-ICPMS) at the Arizona LaserChron Center. Probability ages are based on $^{206}Pb/^{238}U$ for <1000 Ma grains and on $^{206}Pb/^{207}Pb$ for >1000 Ma grains. This division at 1000 Ma results from the increasing uncertainty of $^{206}Pb/^{238}U$ ages and the decreasing uncertainty of $^{206}Pb/^{207}Pb$ ages as a function of age. A full description of methods for detrital zircon analysis can be found in Gehrels et al. (2006).

Petrography

Gondwana Sequence sandstones we analyzed are mostly texturally immature, with large framework grains that are sub-angular to sub-rounded (Figure 6). Modal abundances show high percentages of quartz, but all samples have significant amounts of fresh, twinned feldspar (Figure 7), fresh mica (Figure 8) and lithic fragments (Figure 9). Modal abundances, in combination with high percentages of matrix, or matrix replacing cement show a compositional immaturity.

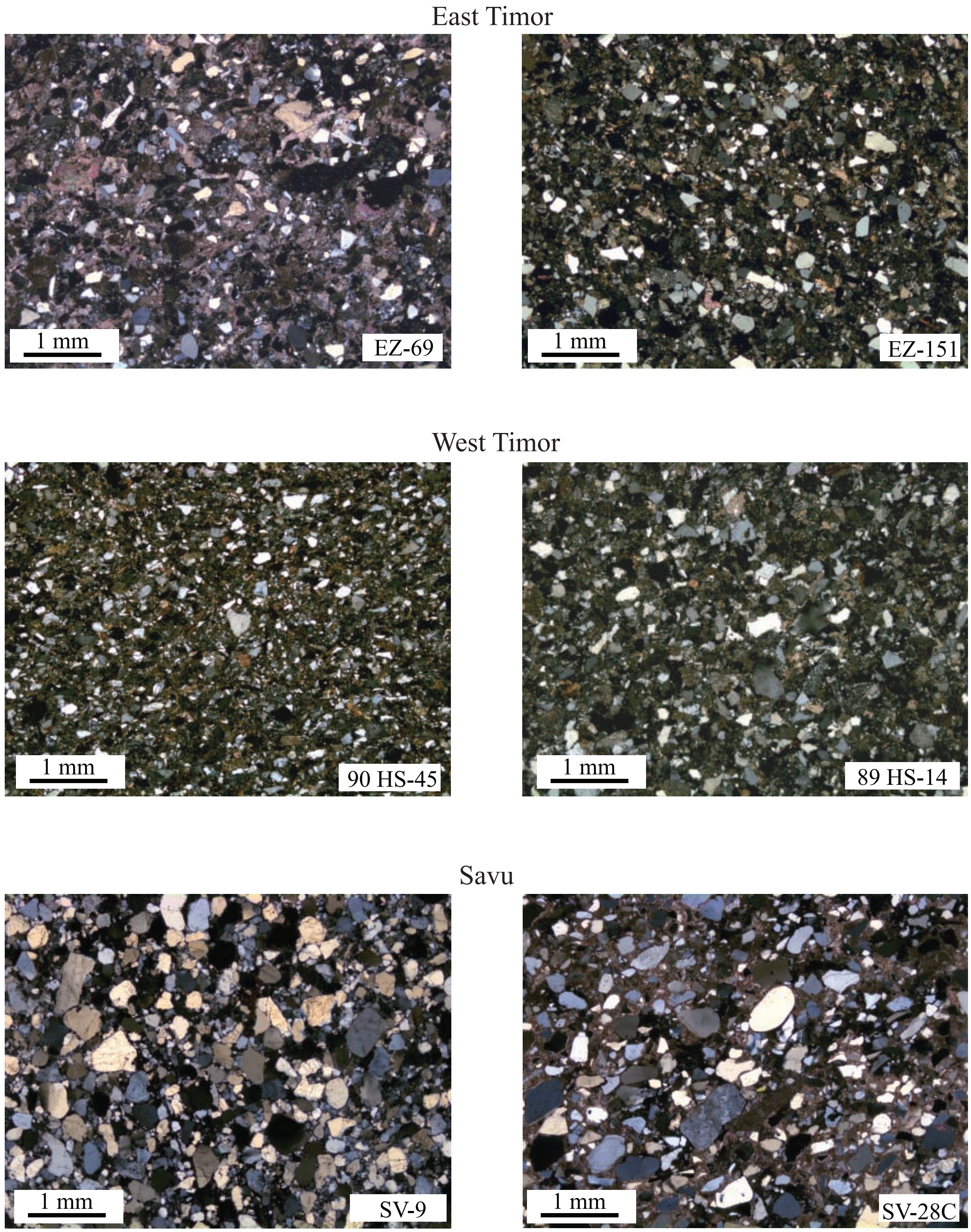

Figure 6: Photomicrographs in cross polarized light showing sub-angular to sub-rounded sandstone textures of representative Triassic Gondwana Sequence sandstone from Timor and Savu.

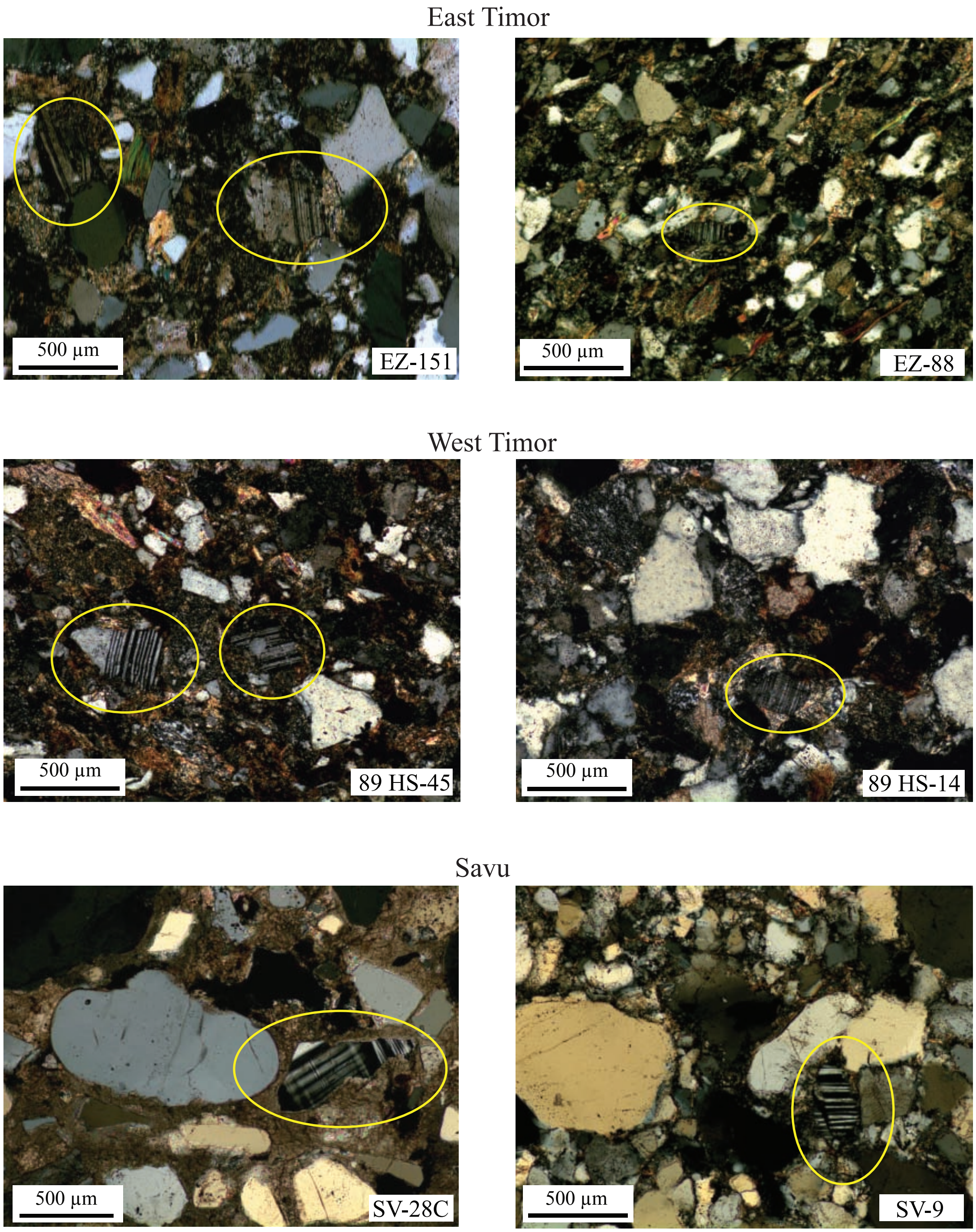

Figure 7: Photomicrographs in crossed polarized light of representative Triassic Gondwana Sequence sandstone from Timor and Savu showing the presence of fresh twinned feldspar grains (circled).

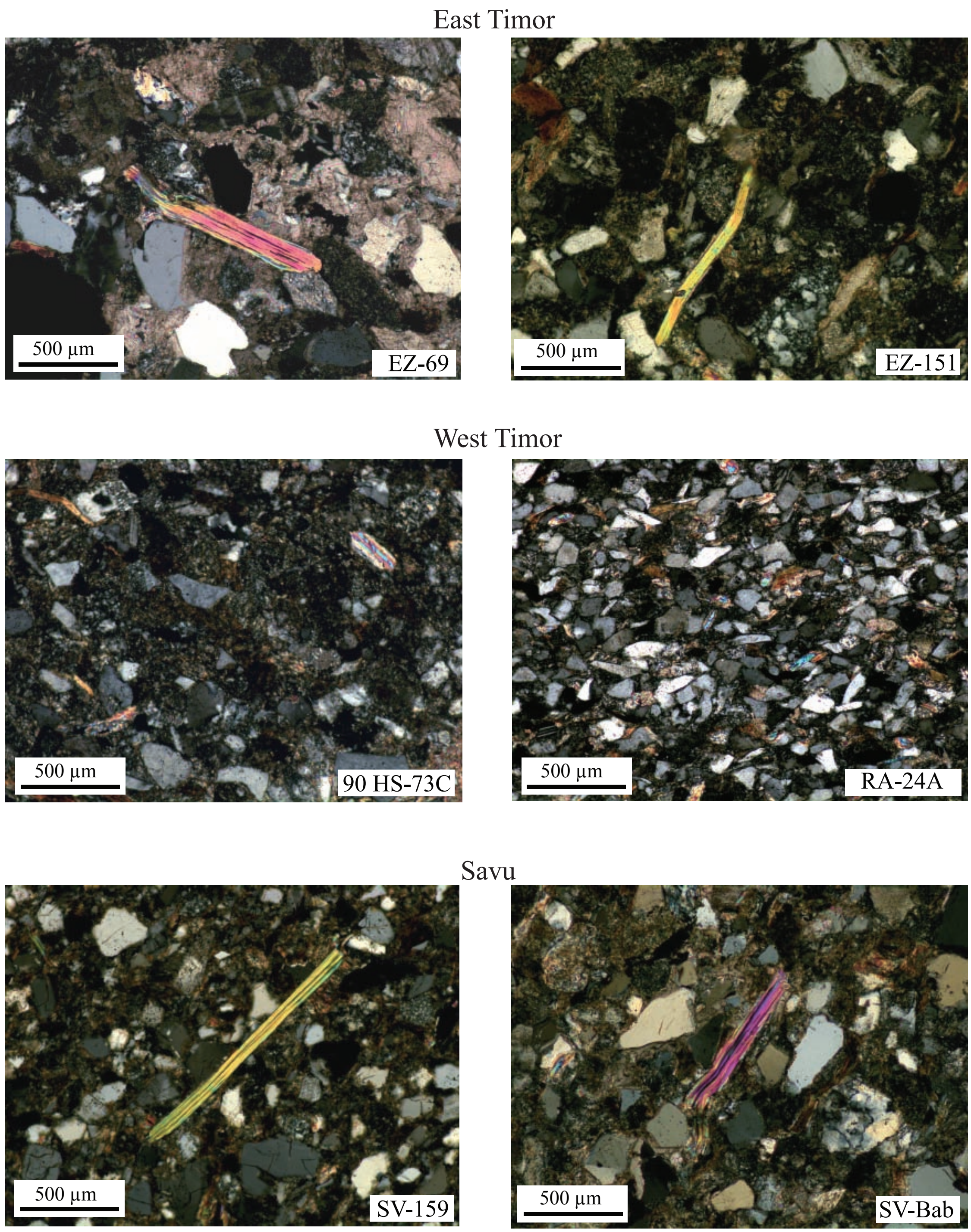

Figure 8: Photomicrographs in cross polarized light of representative Triassic Gondwana Sequence sandstone from Timor and Savu showing the presence of fresh micas.

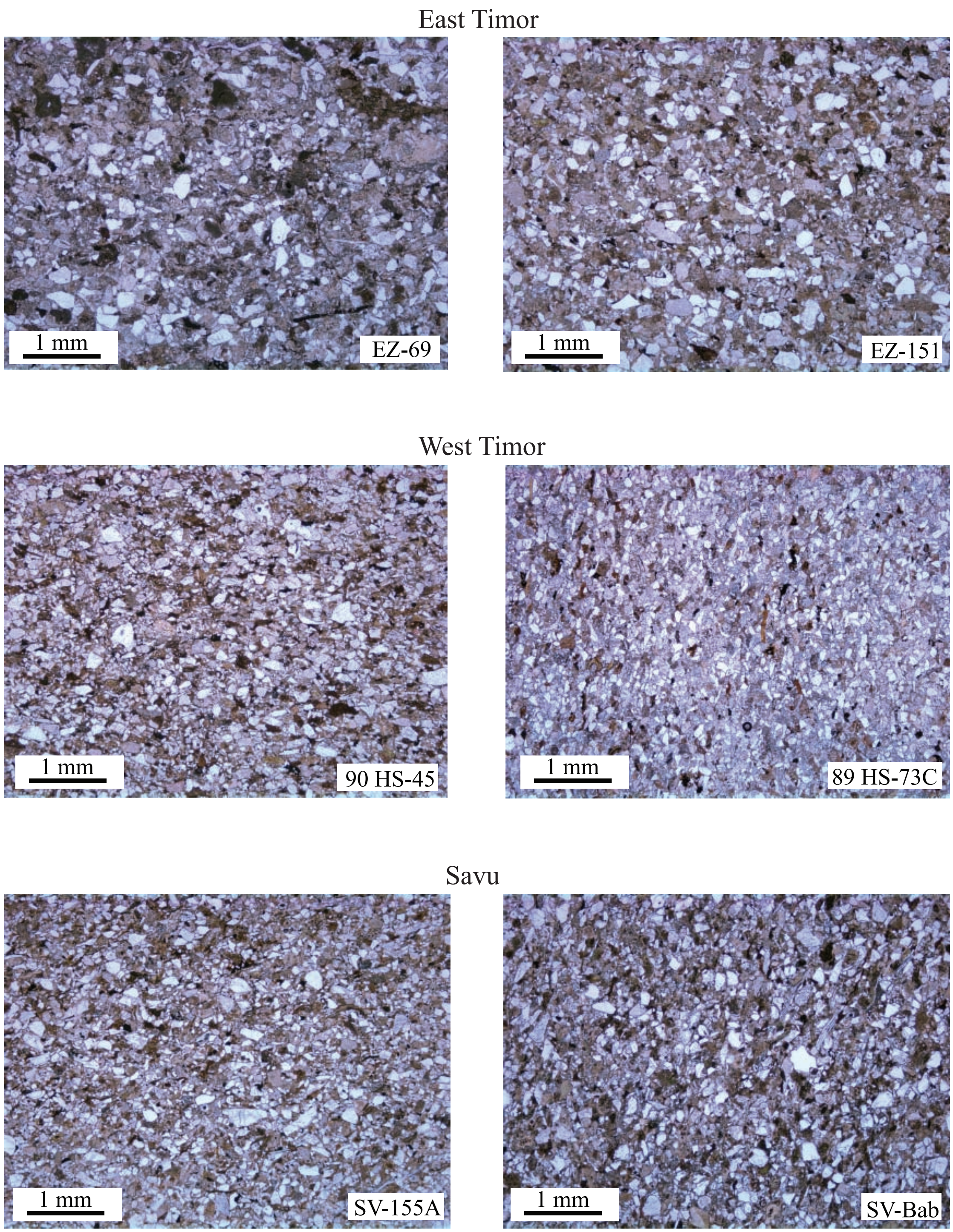

Figure 9: Photomicrographs in plain polarized light of representative Triassic Gondwana Sequence sandstone from Timor and Savu showing the abundance of lithic grains (dark brown) and martix (light brown).

Classifications

Most sandstone samples plot as quartz wackes to lithic wackes (Figure 10) on the classification diagram of Williams (1982). Dickinson (1983) classification diagrams for sedimentary provenance indicate a recycled orogen provenance for most Gondwana Sequence sandstones throughout the Banda Orogen (Figure 11).

Detrital Zircon Analysis

In order to determine the age of the source area for Triassic units of the Gondwana Sequence detrital zircons were extracted from six sandstone samples. Five of these samples are from the island of Savu in Indonesia and one sample is from East Timor.

Zircons found in sandstones of the Gondwana Sequence are amber to clear, and pink to mauve in color with variable amounts of abrasion. Proterozoic zircons vary in color, but Paleozoic zircons are only amber to clear. Both abraided and pristine zircons are present although there is no apparent relationship between abrasion and age. Many zircons are concordant for all the samples, and some weak discordance is also found (Figure 12).

Peak ages show the largest peak at 254-385 and a smaller one at 1788 – 1874 (Figure 13 and 14). The mean ages for these two peaks are 301 Ma and 1882 Ma. Other minor peaks are found at 423-555 Ma, 847-912 Ma, 1157-1364 Ma and 2456-2738 Ma. Similar age ranges have been reported for the Permian Aileu Complex in Kisar (Harris, 2006) and northern East Timor (Ron Berry, personal communication). Detrital apatite fission track model ages for Gondwana Sequence Permian through Triassic sandstone

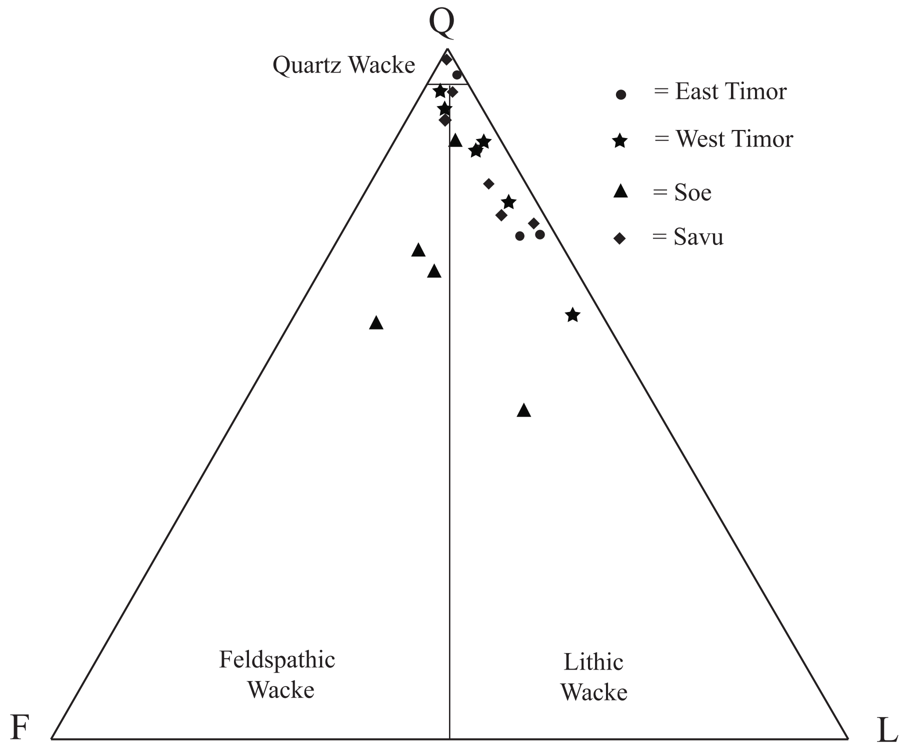

Figure 10: QFL diagram after Williams et al., (1982) for classification of sandstone from the Triassic Gondwana Sequence.

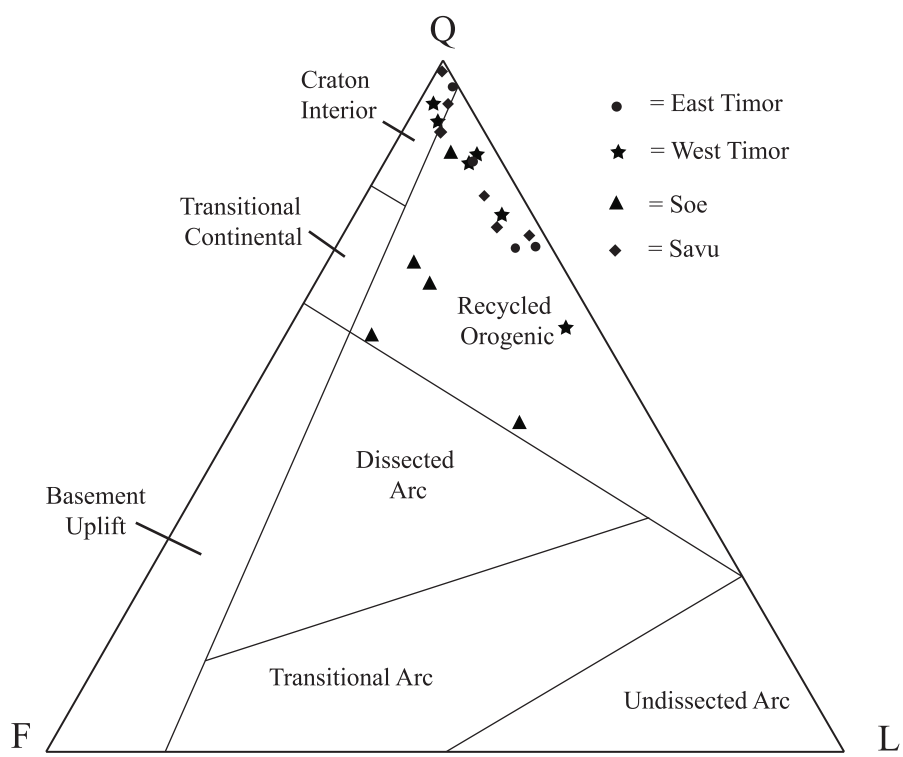

Figure 11: QFL sedimentary provenance based on Dickenson (1983) for Triassic Gondwana Sequence sandstone.

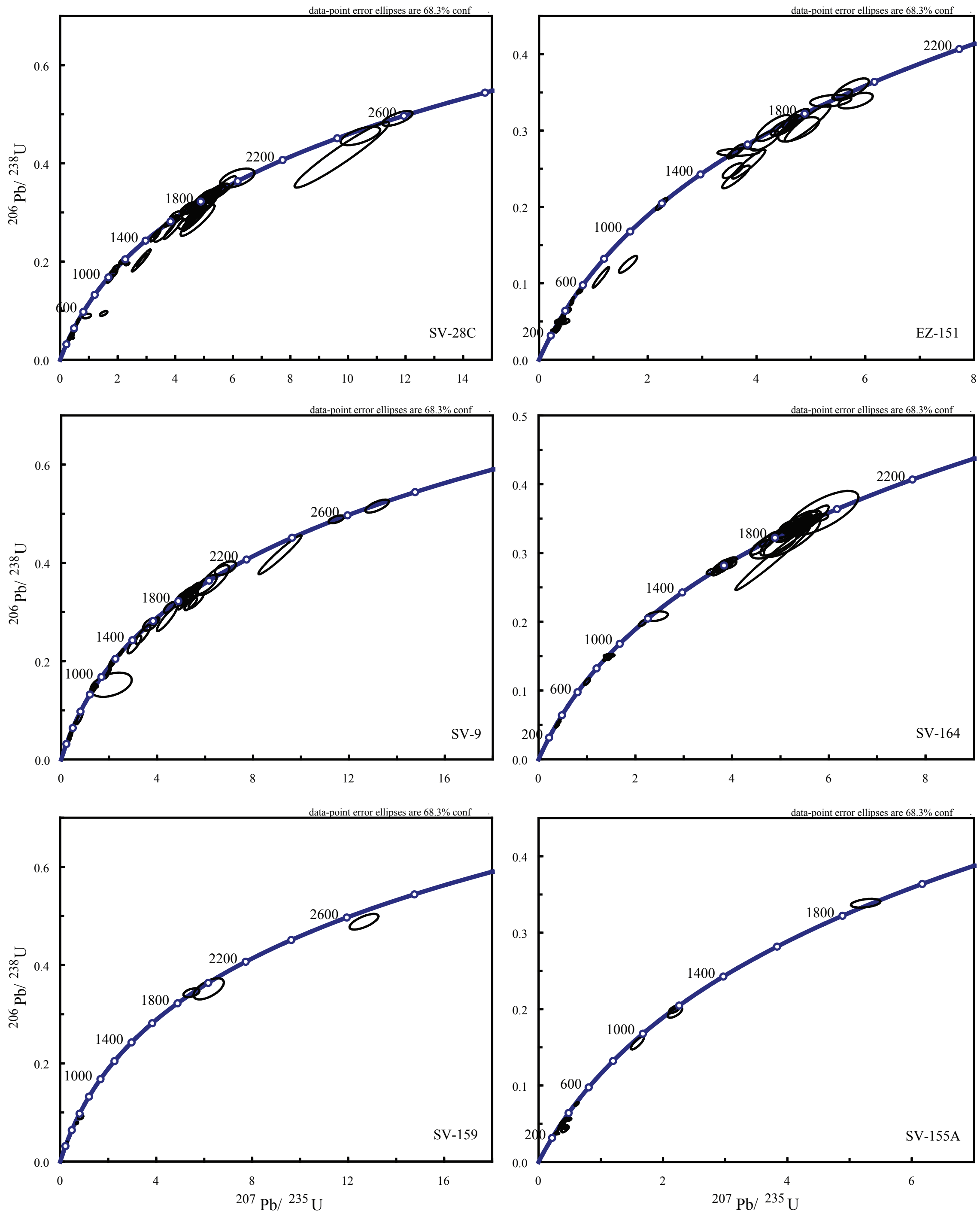

Figure 12: Concordia diagrams from detrital zircon analysis of Gondwana Sequence sandstones (see text). SV sampes are from Savu. Sample EZ-151 is from East Timor.

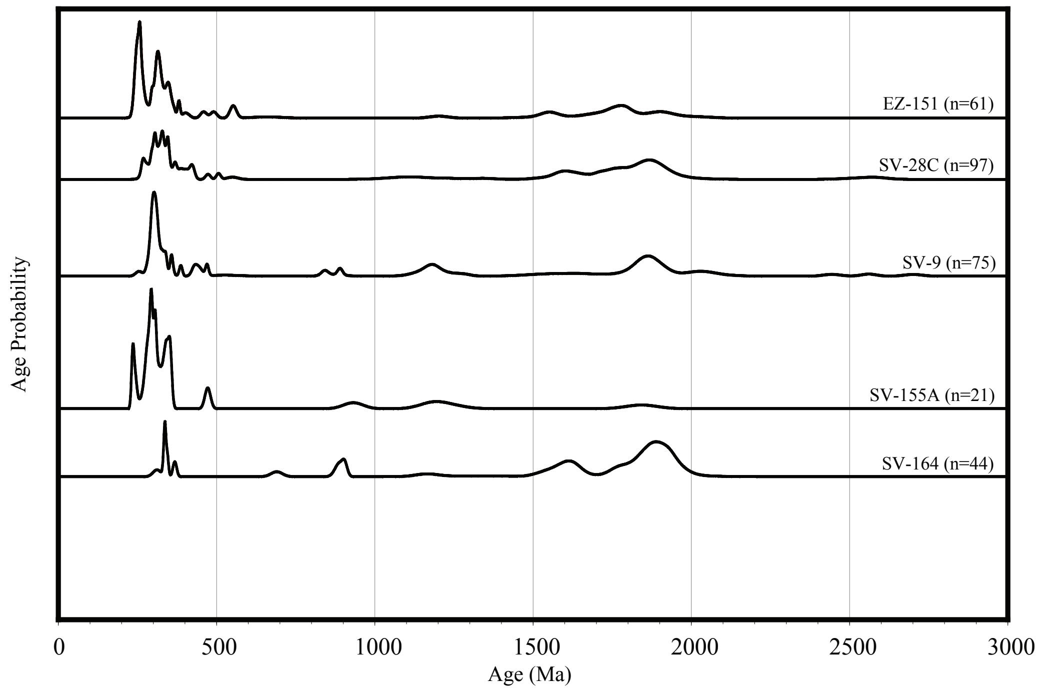

Figure 13: Probability age plots of detrital zircon analyses. These plots have been normalized so the area under the curve is the same for each sample regardless of number of analyses. Sample SV-159 has been excluded from this graph because of small number of grains analyzed.

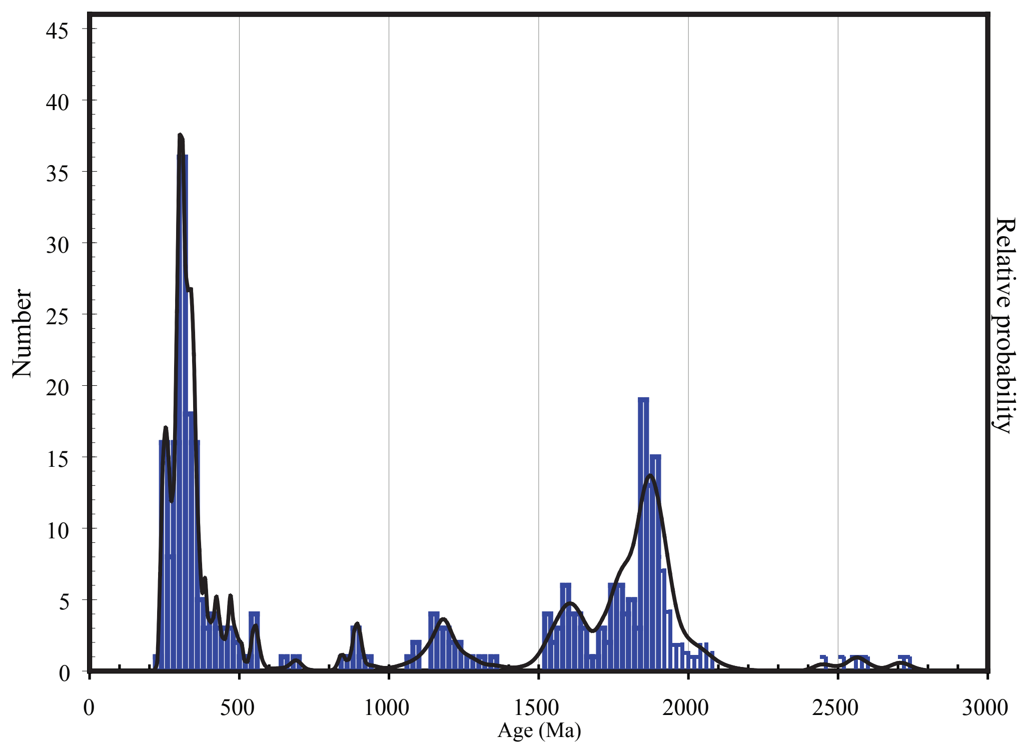

Figure 14: Probability age plot of all detrital zircon analyses from this study. Major peaks are at 301 Ma and 1882 Ma. The youngest gain analyzed is 234.6 ± 4 Ma and the oldest grains are Archean, with a maximum age of 2725.3 ± 37.6.

throughout Timor yield a similar source age of between 300 and 400 Ma (Harris et al., 2000). These results indicate that the source for Gondwana Sequence sandstones throughout the Banda Orogen is most likely the same from Savu to Kisar.

Origin of the Gondwana Sequence

Previous studies of the Triassic Babulu Formation of West Timor indicate a proximal source based on heavy mineral concentrations and wood fragments in sandstone (Cook, 1986; Bird and Cook, 1991). Petrographic analyses reported here of samples from East Timor and Savu also indicate a proximal source. These features include twinned feldspars, fresh biotite, and abundant lithic grains. These components of the sandstone would preferentially breakdown during long transport and extensive processing. The abundance of sub-angular grains also supports a short transport history.

Paleocurrent measurements of the Babulu Formation from silty turbidite ripples show a northeastern source, and paleocurrent measurements from sandy turbiditic flutes and ripples show an easterly source. Sediments were most likely shed from delta fronts and followed a subsiding basin (Bird and Cook, 1991). The petrographic analysis from this study reveals and increase in rounding from East Timor in the northeast to Savu in the southwest (Figure 6), which is consistent with the southwest paleocurrents as reported by Bird and Cook (1991).

A region to the east of the northwest Australian margin with similar zircon age ranges as that of the Gondwana Sequence is Northern Queensland in Australia. The Coen region of Northern Queensland underwent two major periods of crustal growth one during the Proterozoic (1800-1550 Ma) and another during the Palaeozoic (430-280 Ma)

(Blewett and Black, 1998). The Barramundi Orogeny at 1870 Ma (Page and Williams, 1988) corresponds to the Proterozoic peak age of 1872 Ma. Other Proterozoic events in the region include granitic plutons that intruded the Mount Isa region at 1800 Ma, 1740 Ma, 1690 Ma and 1670 Ma (Blake and Stewart, 1992).

Paleozoic events that correspond to Gondwana Sequence detrital zircons are also found in Northern Queensland. Apatite fission track ages from the Mount Isa Inlier crystalline rocks vary from 231 to 390 Ma (Spikings et al., 1997), which overlap those of the Timor Region. The youngest zircon analyzed from the Gondwana Sequence was 234.6 ± 4 Ma. The Kennedy Province, which extends from Cairns to Mornington Island in Australia, was emplaced at 300 Ma (Blewett and Black, 1998) which corresponds to the mean peak age from the Gondwana Sequence.

The chemistry of the Kennedy Province volcanics indicates that they erupted in an intraplate setting not associated with subduction (Blewett and Black, 1998). Provenance classifications of the Gondwana Sequence (Figure 11) do not have a significant arc signature that would be associated with subduction, as indicated by low percentages of lithics and feldspars.

A provenance study of New Guinea metasedimentary rocks that were deposited during the Mid to Late Permian report Northern Queensland as a sedimentary source (van Wyck and Williams, 2002). Similarities in peak ages between New Guinea and the Gondwana Sequence imply that they may have a similar sedimentary provenance. The depositional ages of these units are relatively close, which could indicate that the source region of Northern Queensland was shedding detrital material from the Permian through the Triassic westward along rift zones to northwest Australian margin.

Bird and Cook (1991) compared the sandstones of West Timor to age equivalent sandstones of the Bonaparte Basin and determined that they had different source locations based on modal abundances and heavy mineral content. Bonaparte Basin sandstones are also more mature than Timor Gondwana Sequence sandstones. Deposition in the Bonaparte Basin from Northern Queensland was prevented by the shape of the Australian Craton. This could explain differences seen in the sedimentology of the Gondwana Sequence and the Bonaparte Basin despite their close proximity to each other.

Although there is a strong correlation between Queensland granite ages and Timor region Gondwana Sequence detrital zircons, the distances the detritus would have to travel are inconsistent with the immature Gondwana Sequence sandstones. Paleogeographic reconstructions of the northwest Australian margin during the Permian through Jurassic (Stampfli and Borel, 2002) shows terranes to the north and northeast of the current Banda Orogen. These terranes rifted from the continent during the Jurassic to form Agroland, which is now located in southern Tibet (Charlton, 2000; Stampfli and Borel, 2002). We propose that the granites found in Queensland continued to the north into Argoland, providing a proximal source for the Gondwana Sequence.

There are other parts of northwest Australia with similar U/Pb zircon ages to those from Gondwana Sequence sandstones, such as the central and northwestern Australian Craton. Orogenic events during the Proterozoic that have similar age ranges as the detrital zircons of the Gondwana Sequence are the Halls Creek Orogeny, 1837 – 1826 Ma, (Bodorkos et al., 2000) and the Mount Stafford tectonic event.1818 – 1775 Ma (Collins and Williams, 1995). Reported age ranges for the Alice Springs Orogeny in central Australia between 270 – 350 Ma (Dunlap, 1996) overlap for Paleozoic age ranges from the Gondwana Sequence. These sources, however, would require between 600 and 1000 km of transport. With a distal aerial source, the biotite, feldspar and lithic grains would not be as abundant and pristine as they are in the samples. This source region would also result in a southern source for the Gondwana Sequence. Since age equivalent sandstones from the Bonaparte Basin are more mature that those of the Banda Orogen (Bird and Cook, 1991) it is unlikely that these areas contributed as a source region. These possible source areas are also inconsistent with paleocurrent directions.

The Sibumasu Terrane, which was rifted from the northwest edge of Australia during the Permian (Burrett and Stait, 1986) and now forms portions of western Yunnan, Burma, northwest Thailand, western Malaysia, and northwest Sumatra (Metcalfe, 1996) has been suggested as a source for the Maubisse Formation due to fining southwards (Carter et al., 1976). The Malay Peninsula has Proterozoic Basement (Liew and Page, 1985), which indicates that it rifted from Australia as part of the Sibumasu Terrane. The major Paleozoic event for this region is the emplacement of the Malay-Thai Tin Granites. These granites yield ages around 220 Ma (Cobbing et al., 1992), which is younger than any detrital zircons from Timor region Gondwana Sequence units.

Paleogeographic reconstruction of Southeast Asia during the Permian and Triassic show rapid northward movement of the Sibumasu Terrane after it rifted from the Australian continent (Metcalfe, 2000; Stampfli and Borel, 2002). The ages of the Malay-Thai Tin Granites and the paleogeography of the Sibumasu Terrane indicate that this is not a possible source region for the Gondwana Sequence.

We conclude that the best possible source region for the Gondwana Sequence sandstones is Argoland, which rifted from the Australian continent during the Jurassic. This region satisfies sandstone maturity and paleocurrent data, but we must infer that Argoland is part of the Mount Isa granite belt.

Rock Unit Affinities

Banda Terrane volcanic units have igneous zircons of 32 Ma (Harris, 2006) and detrital zircons in metamorphic units are as young as 80 Ma (Standley and Harris, in press). The youngest analyzed zircon from the Gondwana Sequence is 234.6 ± 4.0 Ma. This contrast in ages provides a new application for determining tectonic affinities of various terranes that make up the Banda Orogen.

EAST TIMOR STRUCTURAL ANALYSIS

Structural measurements of bedding, fold axial surface, fault and fractures planes were acquired in four traverses of East Timor (Figure 2) in order to determine the geometry of accreted Gondwana Sequence units and to construct a kinematic evolution.

Bedding plane measurements from West and East Timor mostly strike northeast-southwest and indicate a northwest-southeast shortening direction during the collision of the Australian continent with the Banda Arc (Figure 15). The maximum principle compressional stress direction (σ_1) is inferred from the direction of shortening, which is perpendicular to pi-pole of poles to bedding. The fold hinge line is parallel to the pi-pole and is sub-parallel to the axis of the island of Timor. Most axial surfaces dip to the northwest, showing a dominantly southeast vergence direction for shortening of

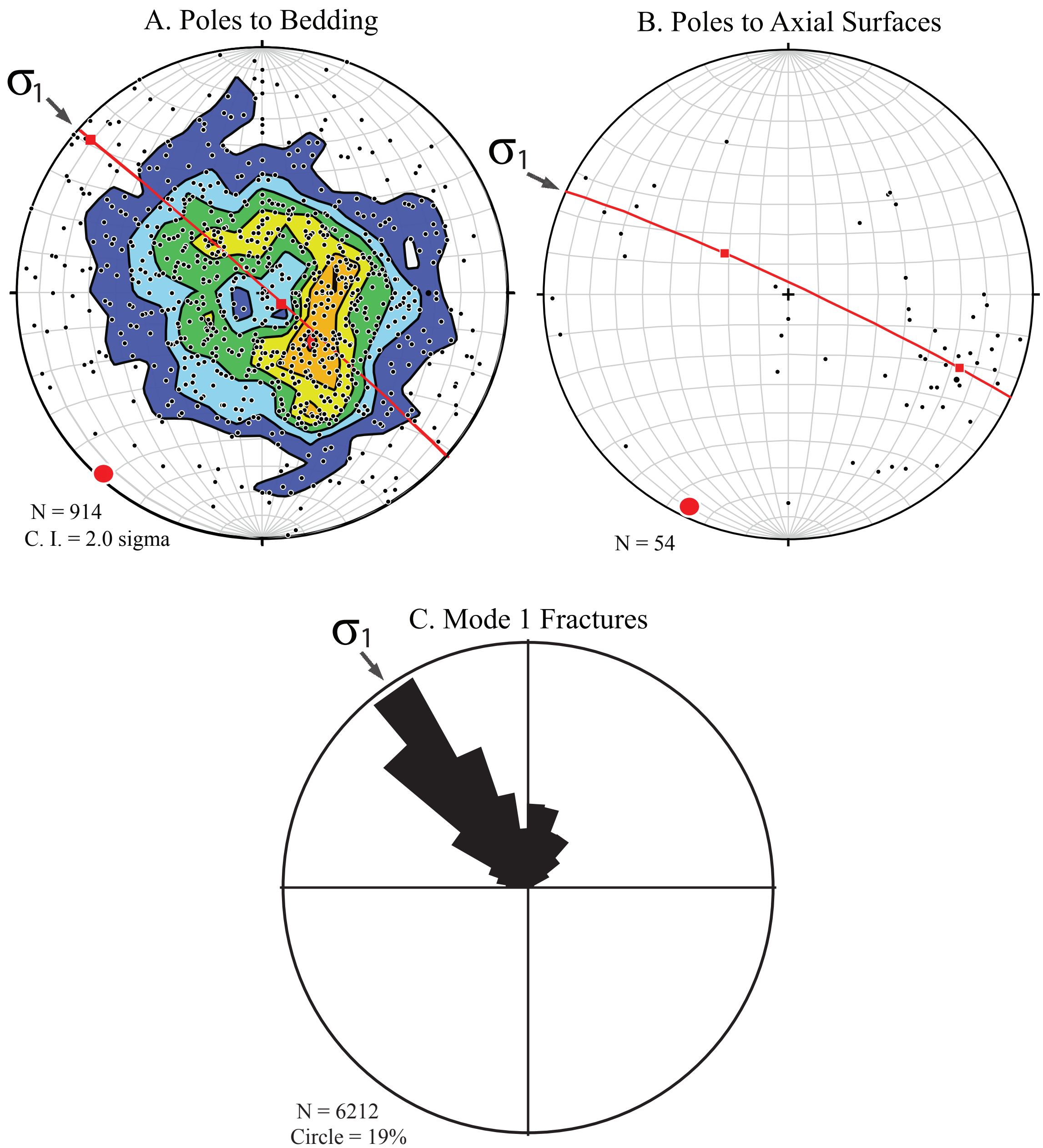

Figure 15: Structural measurements throughout Timor (lower hemisphere equal area projection). A) Stereograph of poles to bedding planes from East and West Timor, including measurements taken from the Cribas to Fatu Berliu and Maubisse regions. Cylindrical best fit line (red) approximates σ_1, pole to cylindrical best fit line is approximation of fold hinge lines. B) Poles to fold axial surfaces from the Cribas to Fatu Berliu corridor. Pole to cylindrical bast fir predicts orientation of fold hinge lines. C) Mode one fracture measurements from syn-orogenic deposits throughout Timor and Alor (Mikolas and Harris, 1996). The large pedal shows the prevailing regional stresses near parrallel to cylindrical best fit of poles to bedding planes. Secondary direction is parallel to plate motion vector (Genrich et al., 1996).

Gondwana Sequence (Figure 15). Mode 1 fracture measurements from the Gondwana Sequence show random distribution due mostly to their pre-orogenic structural inheritance development. However, fracture measurements from syn-orogenic units on the island of Timor and Alor (Mikolas and Harris, 1996) indicate a maximum stress direction that is northwest-southeast (Figure 15). The same orientation of fractures is seen in sonar images of the pre-collisional accretionary wedge south of Sumba (Breen et al., 1986). The secondary stress direction in the northeast-southwest direction is similar to the short axis of borehole breakouts drilled on the Australian continental shelf (Hillis, 1991).

Macroscopic folds in East Timor are mostly asymmetric with a steeply inclined to overturned forelimb. Line length shortening of folds varies from 7 and 82 percent, with an average of 35 percent (N=14). Broad amplitude, recumbent and chevron folding are all present (Figure 16). Most folds are concentric with flexural slip of competent units, flexural flow of shale and mudstone, and some neutral surface deformation.

The four transects from the Cribas region of East Timor were divided into structural domains based on bedding plane measurements. The Turquetti transect (Figure 17) crosses the previous mapped Cribas anticline of Audley-Charles (1968), which he interpreted as a series of east-west trending anticlines and synclines. One structural domain in this region has opposing dips, suggesting an anticline. However bedding plane attitudes and axial surfaces in this area show a southwest-northeast trend as opposed to the previously mapped east-west trend. The Aitutu anticline to the west also has a well-documented southwest-northeast strike (Harris et al., 2000).

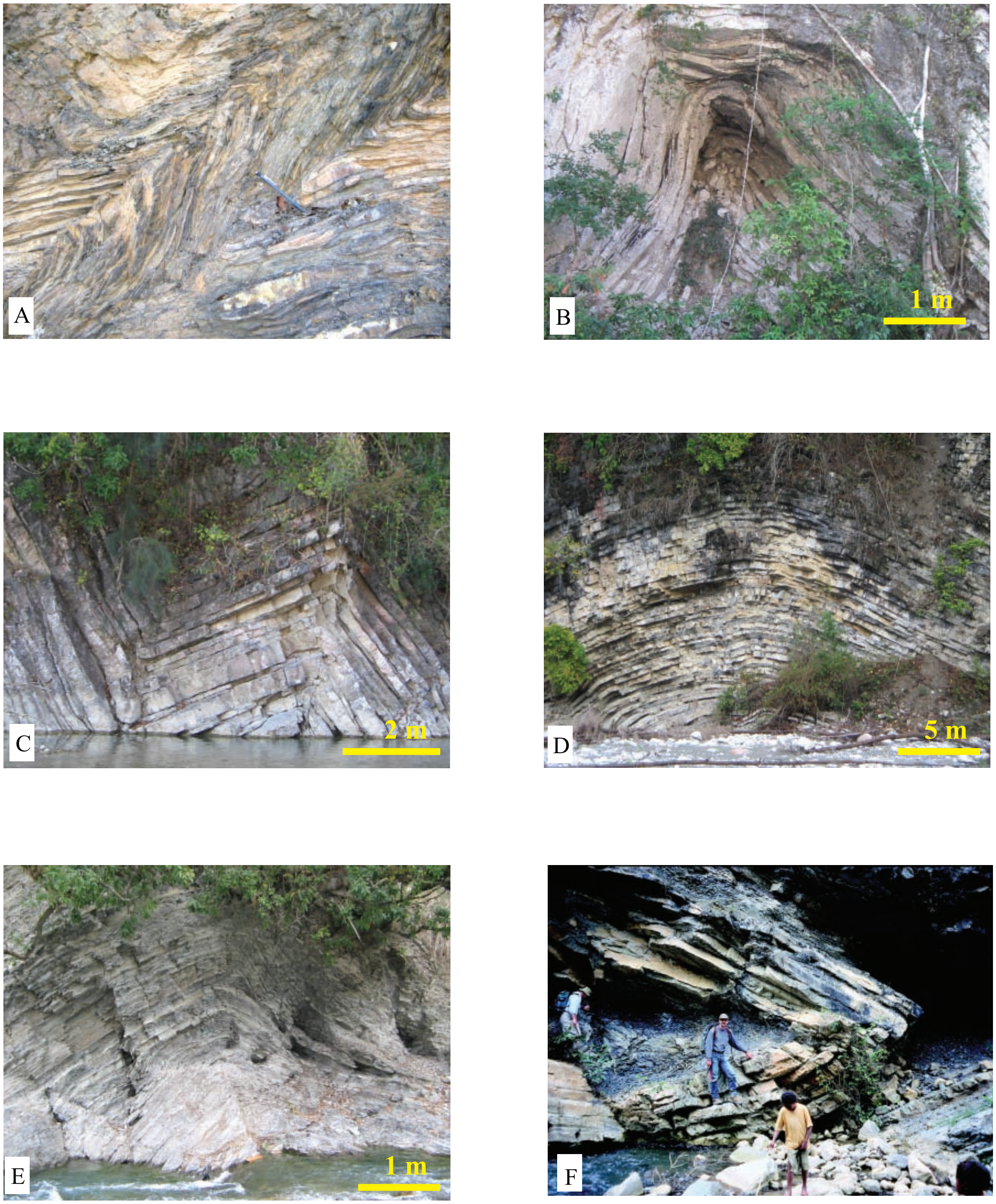

Figure 16: Mesoscale structures from central East Timor. A) Overturned fold from Turquetti traverse, looking west. B) Upright anticline from Soibada traverse, looking east. C) Asymmetric upright fold from Soibada traverse, looking northeast. D) Soibada traverse, looking west. E) Asymmetric upright fold from the Soibada traverse, looking northwest. F) Recumbant fold verging south from the Aitutu region, looking northeast.

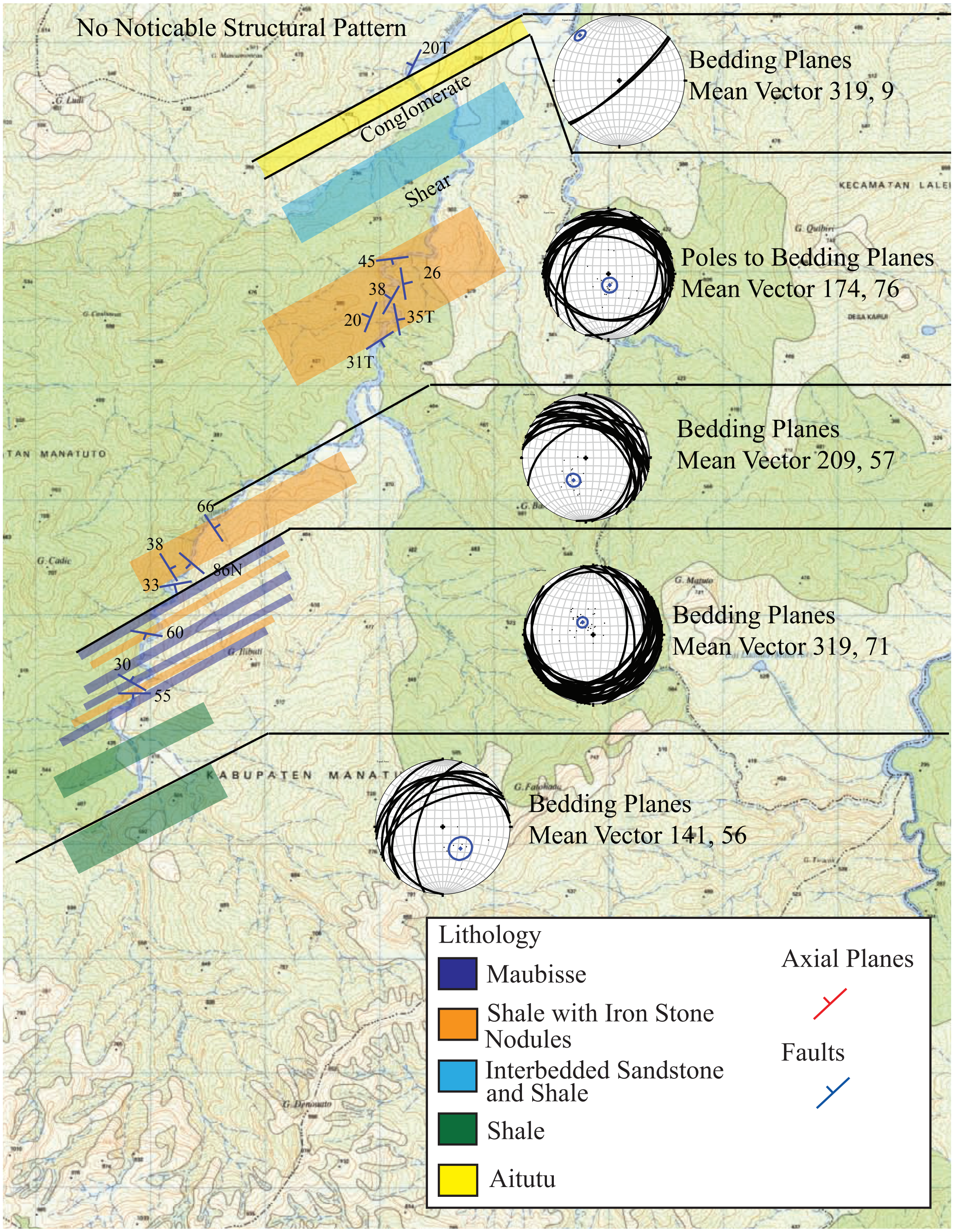

Figure 17: Turquetti structural map with rock types and units. Black lines indicate structural domain boundaries. Blue dot on stereographs represent the mean vector, and blue circle represents the 95% confidence cone. (See figure 2 for location).

Distinct structural domains from the Cribas transect (Figure 18) are not found. Bedding measurements from this area dominantly dip to the northwest, which is similar to fold backlimb measurements from other traverses. The lack of forelimb structural domains could be a result of the more durable orientation of backlimb dip slopes.

In the northern portion of the Soibada transect (Figure 19) there are numerous meso-scale folds. Strike domains trend in a southwest-northeast direction. The southern portion of the Soibada transect is geometrically similar features to the north (Figure 20). Abundant axial surfaces measurements from the Soibada transect clearly indicate a northwest-southeast maximum stress direction and mostly southeast vergence.

The Fatu Berliu transect (Figure 20) has a number of small dip domains with alternating dip directions. An abundance of short wavelength folds results in the small dip domain boundaries.

Structural measurements and structural domain boundaries all support a northwest-southeast maximum stress direction for the deformation of the Banda Orogen. This observation explains general patterns of the distribution of geologic units throughout Timor. Klippen of Banda Terrane are preserved mostly in northeast-southwest trending synclinoriums (Figure 4) parallel to the Aitutu and Cribas anticlines, and meso-scale folds in the Gondwana Sequence. Previous explanations for the orientation of these massifs included large strike-slip faults cutting through the island (Charlton, 2002), yet no evidence for the inferred faults is found. We propose that the synclines where the Banda Terrane outcrops are a result in part of structural inheritance-that the Gondwana Sequence is influenced by older rift structures, some of which may be reactivated pre-collision structural geometry of the passive continental margin Australian shelf.

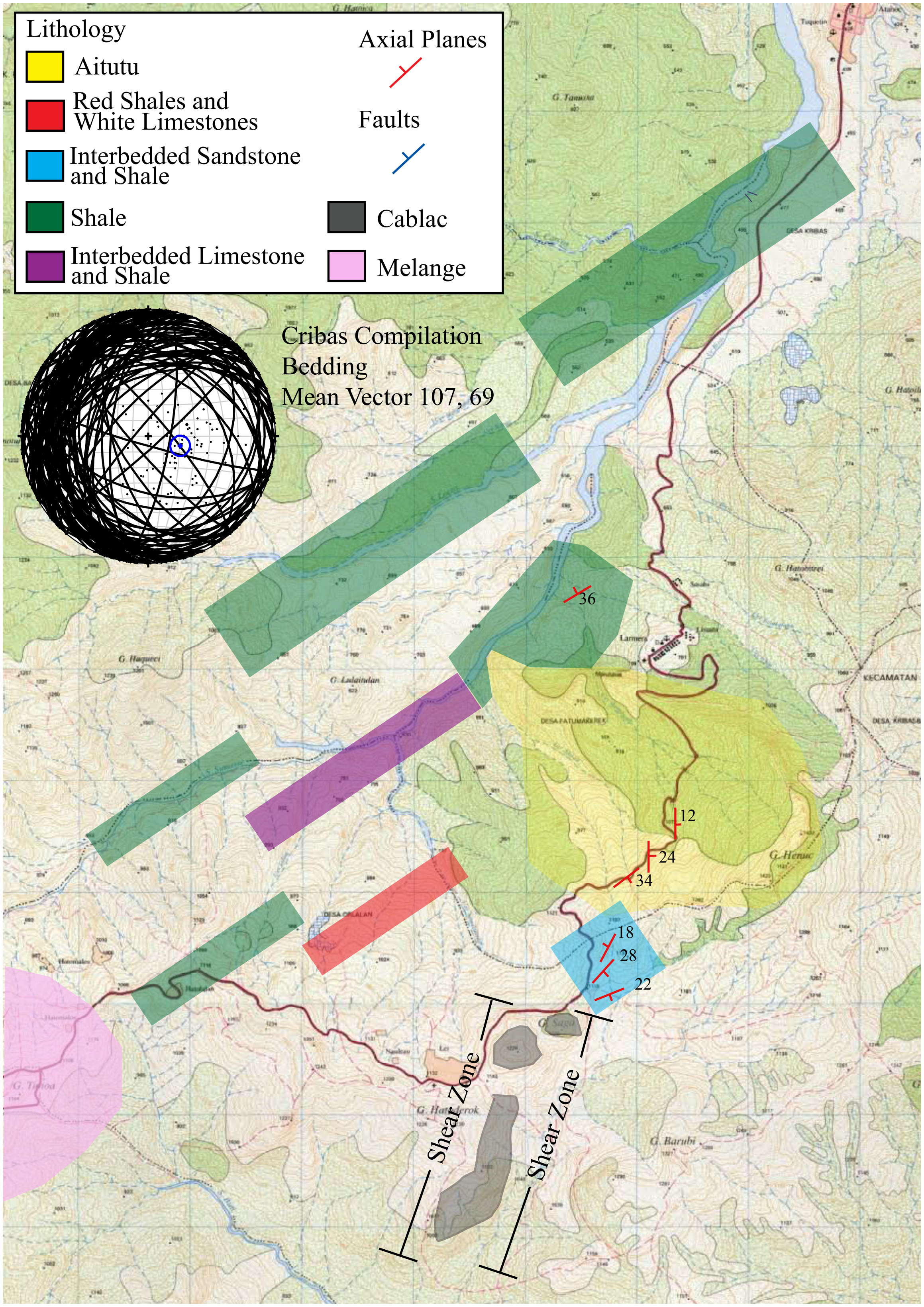

Figure 18: Cribas structural map with lithologic units. Structural domains are not spatially distinct. (See figure 2 for location).

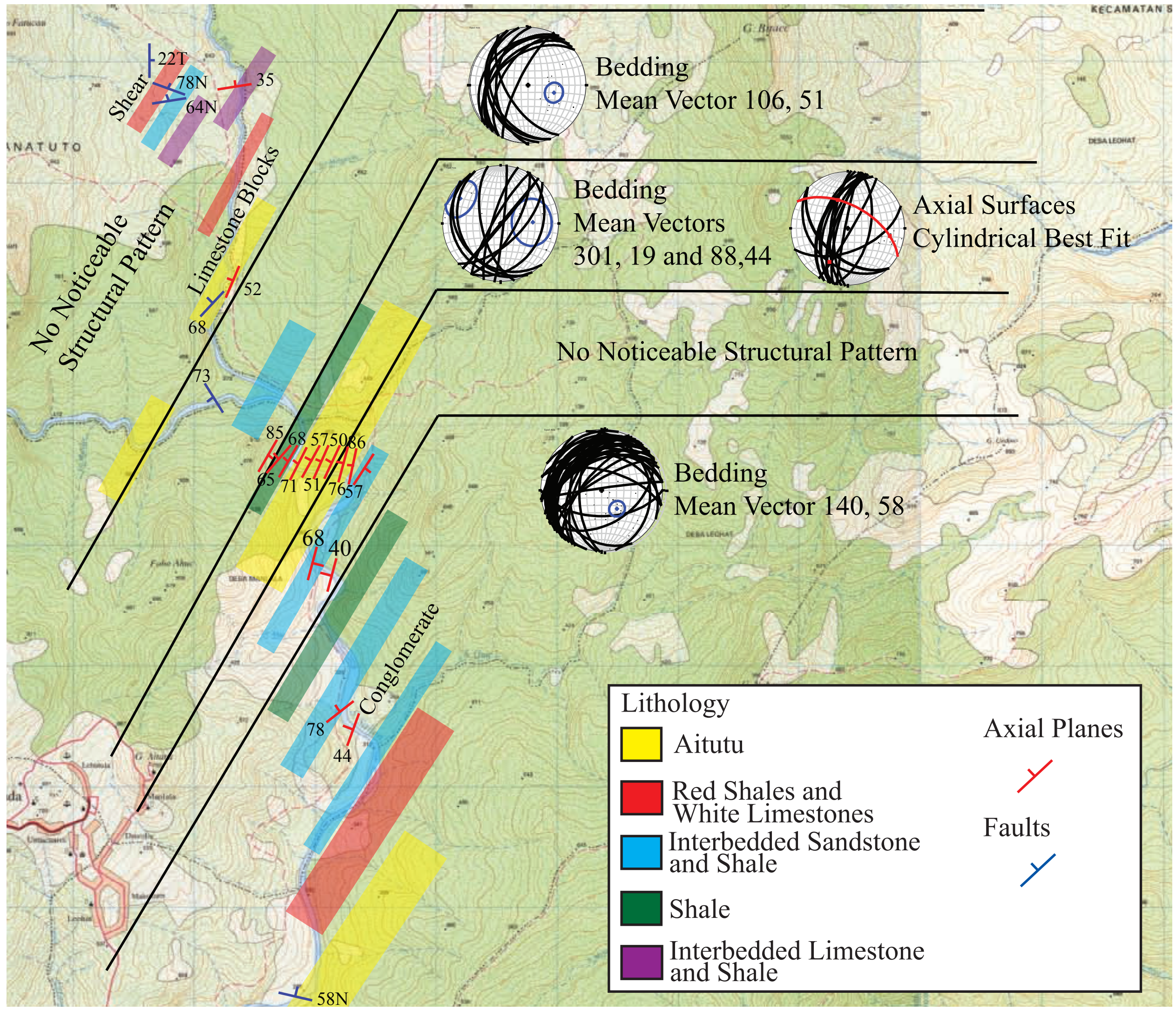

Figure 19: Northern Soibada structural domain map with rock types and units. Black lines indicate boundaries between structural domains. (See figure 2 for location).

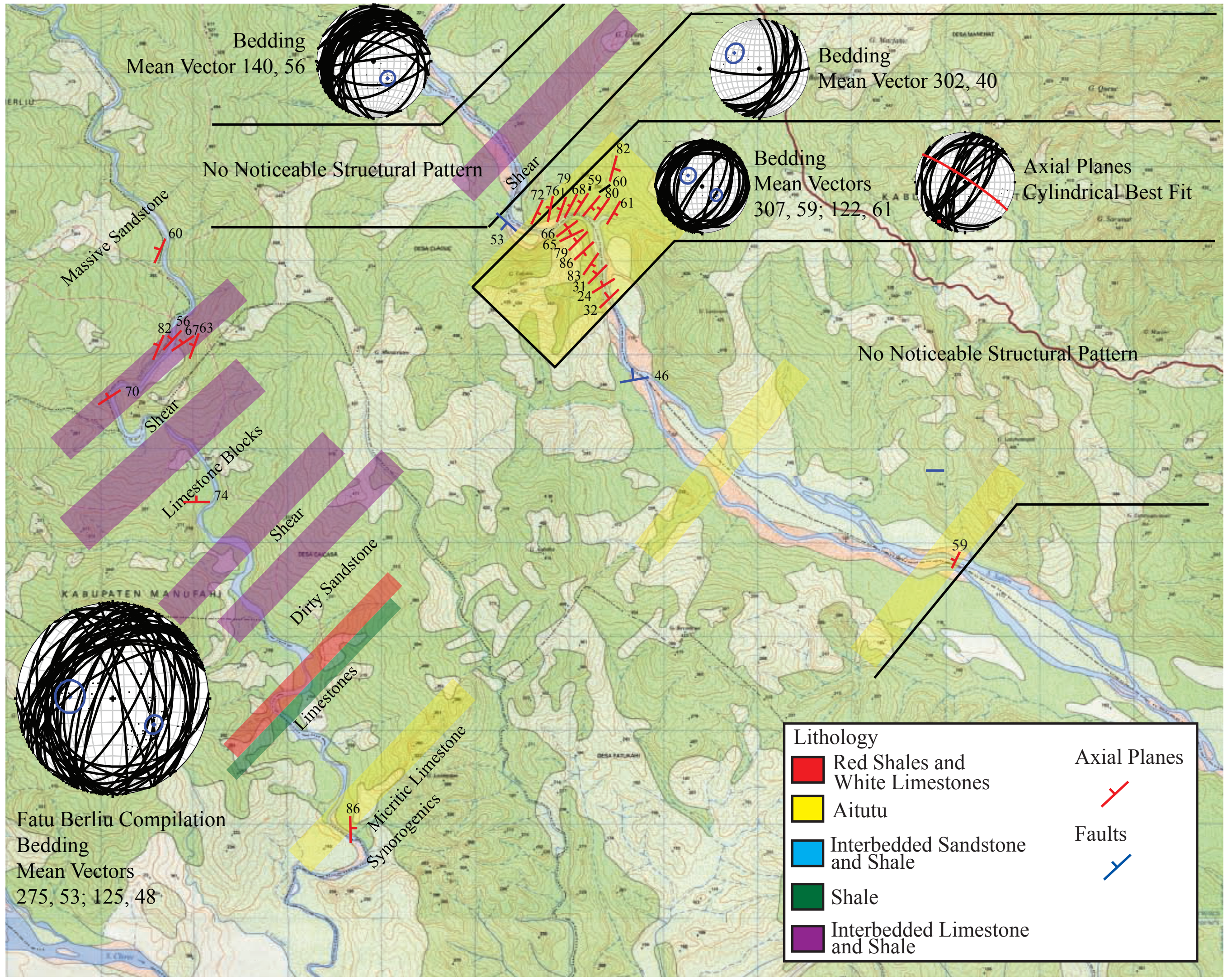

Figure 20: Southern Soibada (right) and Fatu Berliu (left) structural domain maps with rock types and units. Black lines indicate boundaries between structural domains. (See figure 2 for location).

Cross Section

Although most Gondwana Sequence units are gently dipping to the northwest, dip domains of steeply inclined beds are also found in numerous locations along the cross-island structural transect. These observations, along with those of meso-scale folds, indicate fault propagation or detachment folding mechanisms. Structural domains of intense folding found in the Soibada traverse we infer formed as a result of flexural slip deformation within larger fold structures. Just how large the folds are, and how they maybe related to thrusting, were determined through lithostratigraphic analysis.

Lithostratigraphic similarities between clastic-rich units of the Gondwana Sequence can make it difficult to establish stratigraphic position. The Aitutu Formation is the most reliable marker unit for structural reconstructions, but other lithologic features were also used, such as red shale interbedded with white limestones and conglomerates found mostly in the Wailuli Formation of the Soibada traverse (Figures 19 and 20). Massive sandstones were also found with Halobia-bearing shales, which we interpret as the Babulu Formation (Figure 19) at the top of the Aitutu. The Babulu Formation is interbedded with the top of the Aitutu and the base of the Wailuli Formation (Figure 3) but exposure in East Timor is not common. The Niof Formation, like the Babulu Formation is interbedded with the Aitutu Formation (Figure 3), this formation is also not commonly exposed in East Timor. Repetition of these units associated with stratigraphic truncation thrust shortening with minor folding.

These observations provide general geometric constraints for reconstructing the size of thrust sheets and depths of detachment. The lack of pre-Permian or post-Jurassic units in the repeated sections of Gondwana Sequence indicates multiple detachments and duplex structures. Cretaceous to Pliocene units of the Kolbano Sequence are detaching above the Wailuli Formation and the Gondwana Sequence is detaching from pre-Permian units. The roof thrust of the duplex along most, if not all of the structural transect is the Lolotoi Complex and in places its sedimentary cover, which are both part of the Asian affinity Banda Terrane. The basal detachment of the duplex has not been observed.

The exposed Banda Terrane is part of a synclinorium, we propose as a structural low in the duplex zone. Gravity models predict that the Banda Terrane is no more than 3 km thick (Chamalaun et al., 1975). We projected structure into the region from the west to construct a forward model with variation in the length and displacement of thrust sheets to produce a synform for the Banda Terrane (Figure 21). The northern thrust stack in the model represents the Aitutu anticline region, which plunges beneath the Banda Terrane (Standley and Harris, in press). The southern thrust stack is constrained by exposures in the Soibada region.

After generating a forward model that fit the general geometry needed to create a synform beneath the Banda Terrane, the model was modified to fit the observed data (Figure 22). The angle of the thrust faults was increased in order to shorten the spacing between the tops of the trust sheets, indicating that the amount of displacement of younger thrust sheets is greater than predicted by the model. Thrust sheets were added or removed using similar geometries as needed to satisfy the observed data. The final model was restored and line balanced. Restoration of the cross-section predicts an initial line length for the sedimentary package of 101 km and a deformed length of 48 km. This shows that the deformed section has been shortened by approximately 48%. With a

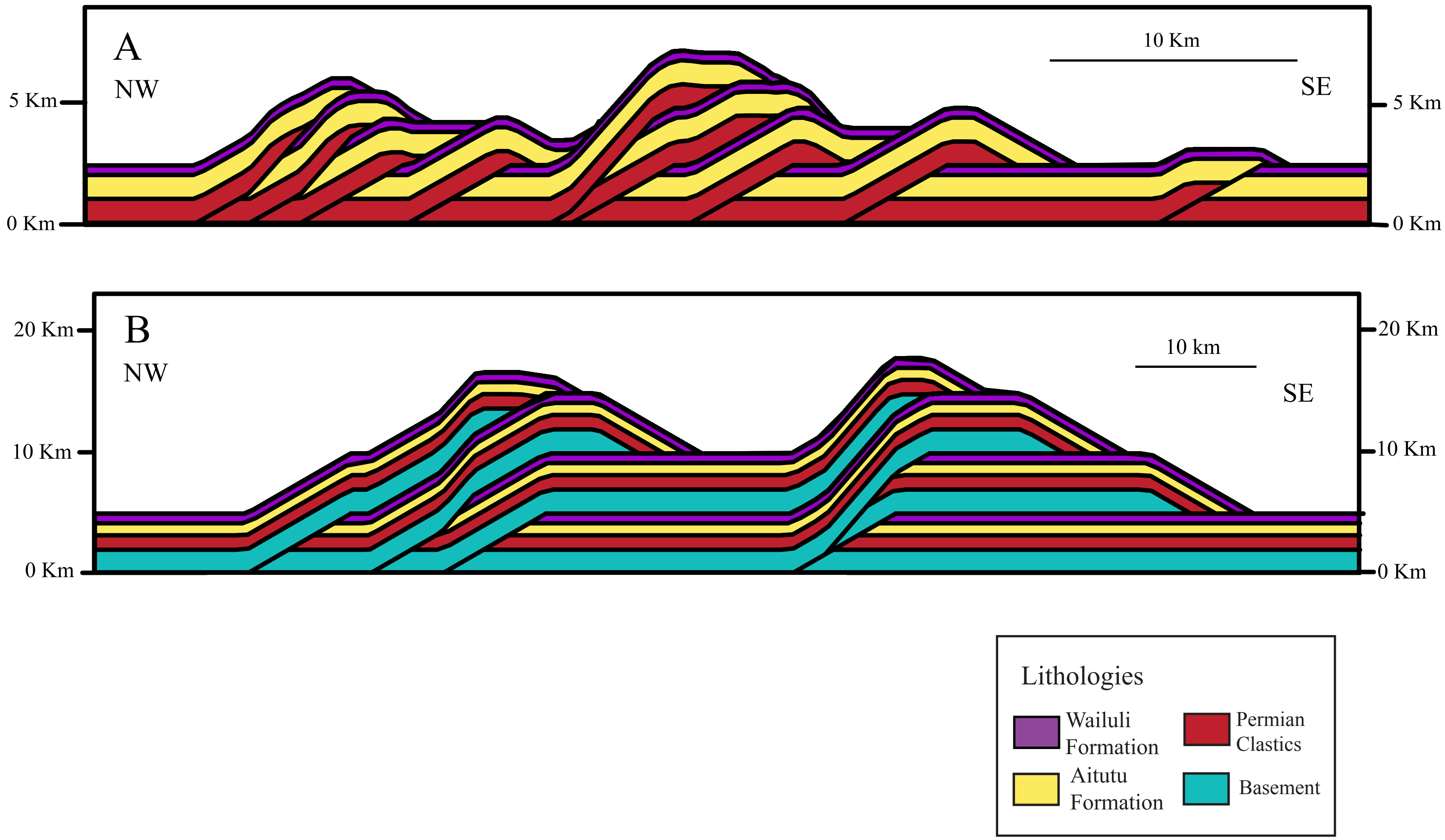

Figure 21: Forward models of thrusting on Timor. A) thrusting of the Kekneno Series with a top of basement decollment. B) 2 km of basement involved in thrusting. Basement involved thrusting creates structural relief that is greater than observed, and would expose basement at the surface.

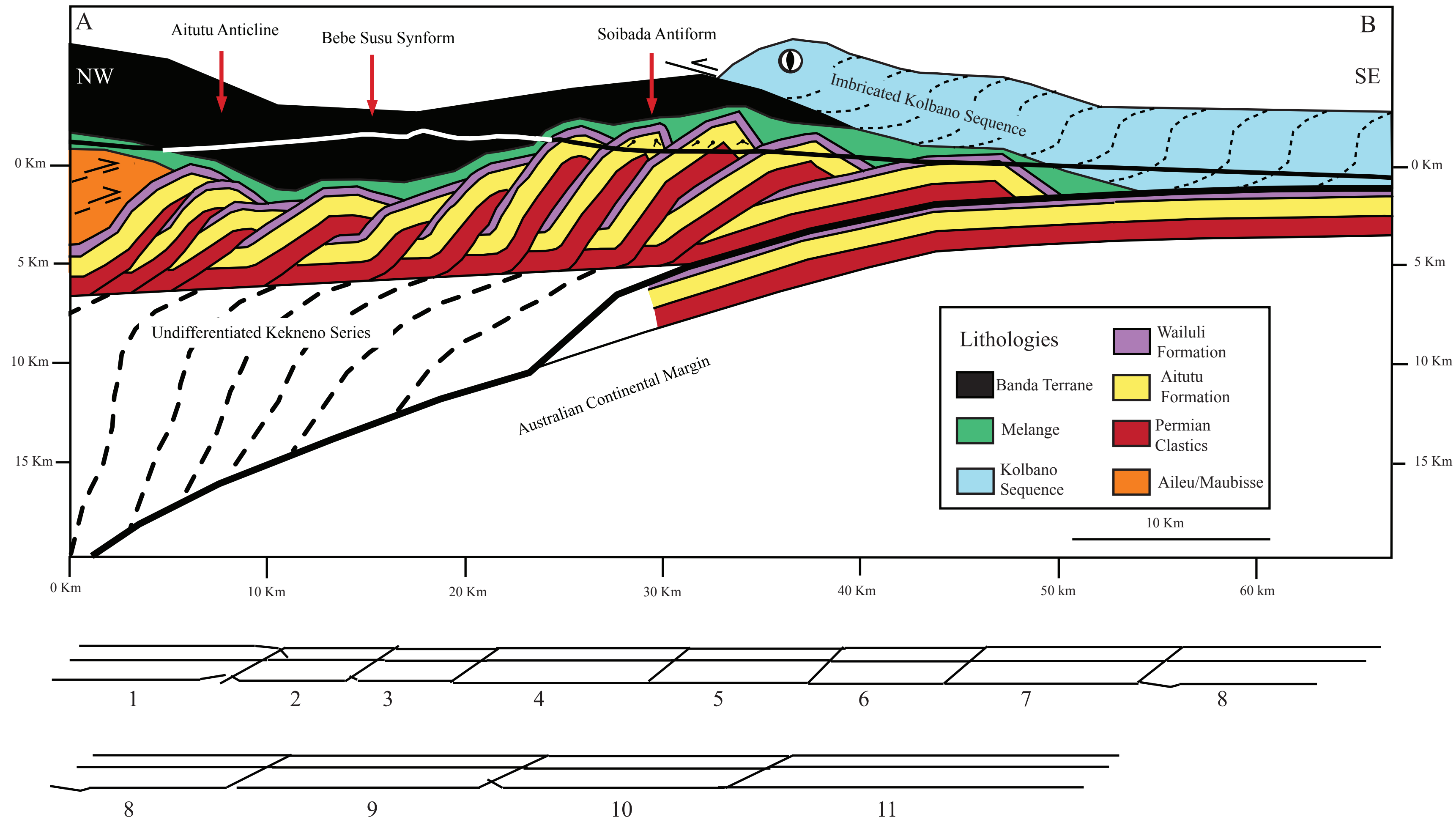

Figure 22: Cross-section showing duplexed Kekneno Series beneath the Banda Terrane. Line of section shown on Figure 5. Balance section includes the top of Wailuli, Aitutu and Permian clastics. Thrust sheets on restored section are numbered in order of deformation (1 is accreted first). Thrust sheet number eight has is included on lower section for reference.

convergence rate of 68 km/Ma this deformation would take less than 1 Ma if all the convergence was taken-up at this location when it was connected to the deformation front.

The geometry of the ramp anticlines of each thrust sheet in relation to the Banda Terrane roof thrust leave large gaps. These gaps between the thrust sheets and the Banda Terrane are filled with mélange as is commonly observed throughout Timor, where the eroded tops of thrust sheets protrude through blankets of mélange (Harris et al., 1998).

The question of what is below the Gondwana Sequence duplex depends on the geometry of the orogenic wedge, the dip of its basal thrust and how much space there is to fill. The northern-most Aileu complex experienced peak metamorphism at 20 km depth at the onset of collision around 5-8 Ma (Berry and McDougal, 1986); therefore the orogenic wedge must extend at least to this depth. Measurements of the total area of the orogenic wedge (1243 km^2) divided by the pre-shortened thickness of the Gondwana Sequence of 3 km indicates an initial line length for the undeformed section of 414 km. The deformed length of the accretionary wedge from the Wetar Suture (north coast of Timor) to the Timor is trough is 155 km. This indicates a maximum of 63% shortening of the Gondwana Sequence in a northwest-southeast direction sub-parallel to the trends of lithotectonic units and uplifted parts of the orogen. Total shortening is most likely less than this due to the involvement of some pre-Permian units in the deformation. GPS velocity measurements indicate that the Australian plate is moving to the north-northeast relative to the Asian plate at a rate of 68 mm/yr (Genrich et al., 1996; Nugroho et al., 2004). Northwest-southeast transport of the Gondwana Sequence is oblique to this motion and is inferred to be controlled by the orientation of the plate boundary and inheriting structure of the Australian margin (Figure 4). The plate boundary was near east-west before collision and has taken on the west-southwest to east-northeast orientation of the northwest Australian continental margin (Harris, 1991).

The depth of the orogenic wedge presents a space problem within the orogenic wedge between the basal detachment of the Gondwana Sequence duplex and the basal thrust of the orogen. Extending the Gondwana Sequence duplex to the base of the orogen requires long, narrow thrust sheets, not viable with structural models or consistent with the strength of the rocks involved. One possible solution to this problem is to increase the thickness of the thrust sheets by including pre-Permian basement. However, by so doing there is a non-viable increase in structural relief, and there would also be exposures on the surface of pre-Permian units, which are not documented anywhere in the Banda Arc (Figure 21). In order to fill the necessary area we propose that there are multiple duplex zones beneath the upper-most stack of Gondwana Sequence. With the above section accounting for only 1 Ma of the total 5-8 Ma of deformation a larger section of Gondwana Sequence is required to account for the total shortening estimate. Therefore we conclude that there are multiple duplex zones of Gondwana Sequence in the Banda Orogen accretionary wedge.

GRAVITY MODELING AND TECTONIC EVOLUTION OF THE BANDA FOREARC

The question of how the Banda forearc upper plate responds to the collision of the Australian continental is one that is pertinent to the tectonic evolution of arc-continent collision in general The sutures of most ancient collision zones obscure the tectonic evolution of the pre-collisional forearc region. Whether this large slab of lithosphere in the Banda Arc is underthrust (Price and Audley Charles, 1983), overthrust (Hamilton, 1979), or laterally-displaced by strike-slip faulting (Rutherford et al., 2001) is unconstrained. Deep seismic profiles through the Banda Arc were unable to resolve the position or geometry of the forearc (Snyder et al., 1996).

Here we use the known gravity field to test various models proposed for the tectonic evolution of the forearc. The Banda forearc is 200 km wide north of Savu, and at least 30 km thick near Sumba. However, in the collision zone it progressively narrows towards East Timor where it is not found. Although thin fragments of forearc are found structurally overlying Australian affinity units on Timor Island, these klippen only account for a small amount of pre-collisional forearc volume. Gondwana Sequence units found directly beneath these thin klippen of Banda Terrane show no evidence of having been thrust beneath a thick forearc slab, with the exception of the northern-most Aileu Complex (Harris et al., 2000). We use the gravity field to determine the location of the large forearc slab. The density contrast between the forearc and the Australian continental margin units have a large effect on the gravity field.

Gravity measurements from onshore central East Timor were acquired along the north-south road from Dili to the south coast through villages of Aileu, Maubisse and Same (Chamalaun et al., 1976). We projected these measurements onto a straight line oriented in a north-south direction. The line continues offshore where gravity measurements were estimated from the bouguer anomaly map of Kaye and Milsom (1988). No terrane correction has been applied; however the expected size of the correction is less then the wavelengths of features in the model, which is a two dimensional approximation.

The obliquity of the collision is such that Savu is at the initial stages of arc-continent collision, while East Timor is the most deformed area of the Banda Orogen (Harris, 1991). We use the forearc geometry in Savu as a template for the undeformed forearc of the Banda Orogen (Vorkink, 2004). Structural models for East Timor must account for the area of forearc observed in Savu. Previous models for the deformation of the Banda forearc include the insertion model in which the forearc is thrust below the accretionary wedge of Timor and delaminates the upper cover sequences from the lower Australian continental crust (Harris, 1991; Audley-Charles, 2004). A similar model to this was also presented by Price and Audley-Charles (1983), but in this model the forearc delaminates the Australian crust from its underlying mantle. Another model for the deformation of the forearc is the displacement model of Harris (2003). In this model the forearc is displaced to the north with the zone of active volcanism. A model proposed by Rutherford et al., (2001) displaces the forearc north of Timor laterally to the west through strike slip faulting. We also propose a new model here in which the forearc and the backarc have been thickened through a series of thrusts. We test each model here against the observed gravity fixing all other variables except the position of forearc lithosphere.

The densities of each body in the models were maintained throughout each test. Densities for surface units in the Banda Orogen were measured directly by Chamalaun et al., (1975). Density values in those areas not accessible for direct measurements were inferred using the Nafe-Drake curve and seismic velocities measured by Bowin et al., (1980). We chose an upper mantle density of 3.6 g/cm^3 based on seismic velocities rather than measurements of mantle rocks on the surface, due to problems with using surface measurements as a proxy for conditions in the mantle.

In order to address the problem of non-uniqueness for gravity models the following geological and geophysical constraints were used for each test:

1. A wedge of accreted Australian Continental margin units that account for at least 250 km of shortening and are 20-25 km thick near the point of highest topography.
2. Klippen of Banda Terrane between 3 and 5 km thick.
3. 25 km thick volcanic arc with a density of 2.8 g/cm^3.
4. South dipping Flores/Wetar thrust system north of the Banda Arc (Silver et al., 1983; 1986; Breen and Silver, 1989; and Snyder et al., 1996).
5. Continental margin crust that is 40 km thick and is transitional with oceanic crust that is 8 km thick over a distance of 300 km (Symonds et al., 1998).
6. A continental lithospheric thickness of 230 km (Bowman and Kennet, 1990) and an oceanic lithosphere thickness of 80 km (Caldwell and Turcotte, 1979).
7. Continental lower crust with a density of 2.7 g/cm^3, continental upper mantle density of 3.6 g/cm^3 (Bowin et al., 1980) with a thickness of 230 km (Bowman and Kennet, 1990) and an asthenospheric density of 3.7 g/cm^3.
8. Oceanic crustal thickness of 10 km and a density of 2.8 g/cm^3 (Bowin et al., 1980). An oceanic upper mantle density of 3.6 g/cm^3 (Bowin et al., 1980) and an upper mantle thickness of 80 km (Caldwell and Turcotte, 1979)
9. Forearc cross-sectional area of 5886 km^2.

10. Forearc orogenic wedge densities of 2.2 g/cm^3 for the Wailuli Formation and synorogenics, 2.4 g/cm^3 for the Kolbano Sequence, 2.67 g/cm^3 for the Gondwana Sequence, 2.9 g/cm^3 for the Aileu and the Banda Terrane (Chamalaun et al., 1975).

The forearc insertion model assumes no internal deformation of the forearc, which maintains its integrity by inserting into the incoming Australian continental margin and delaminating cover from basement units. This model was presented most recently by Audley-Charles (2004), but the boundary conditions do not fit the observed gravity field (Figure 23). It is also important to note that the entire area of the forearc present in the undeformed Savu section (Vorking, 2004) is not accounted for in the model presented by Audley-Charles (2004). Modifying the underthrust model to accommodate the full area of the forearc does not fit the observed gravity, and still requires further modifications before it can be considered a viable solution for the collision zone (Figure 24).

Another proposed model for the forearc is to displace the entire subducting slab, and location of the active arc to the north, as presented by Harris (2003). This model would explain the presence of volcanoes in the Banda Sea north of the Banda Arc (Figure 1). The location of the forearc in this model is ambiguous, but using the geometries presented better satisfies the onshore gravity, but does not account for the steep gravity gradient north of Timor (Figure 25). The same reason for a misfit in this model also applies to the lateral displacement model of Rutherford et al. (2001).

The best-fit model that accounts for the full area of forearc lithosphere requires internal thickening of the forearc and stacking it beneath the region that includes the north coast of Timor and the now inactive volcanic arc (Figure 26).

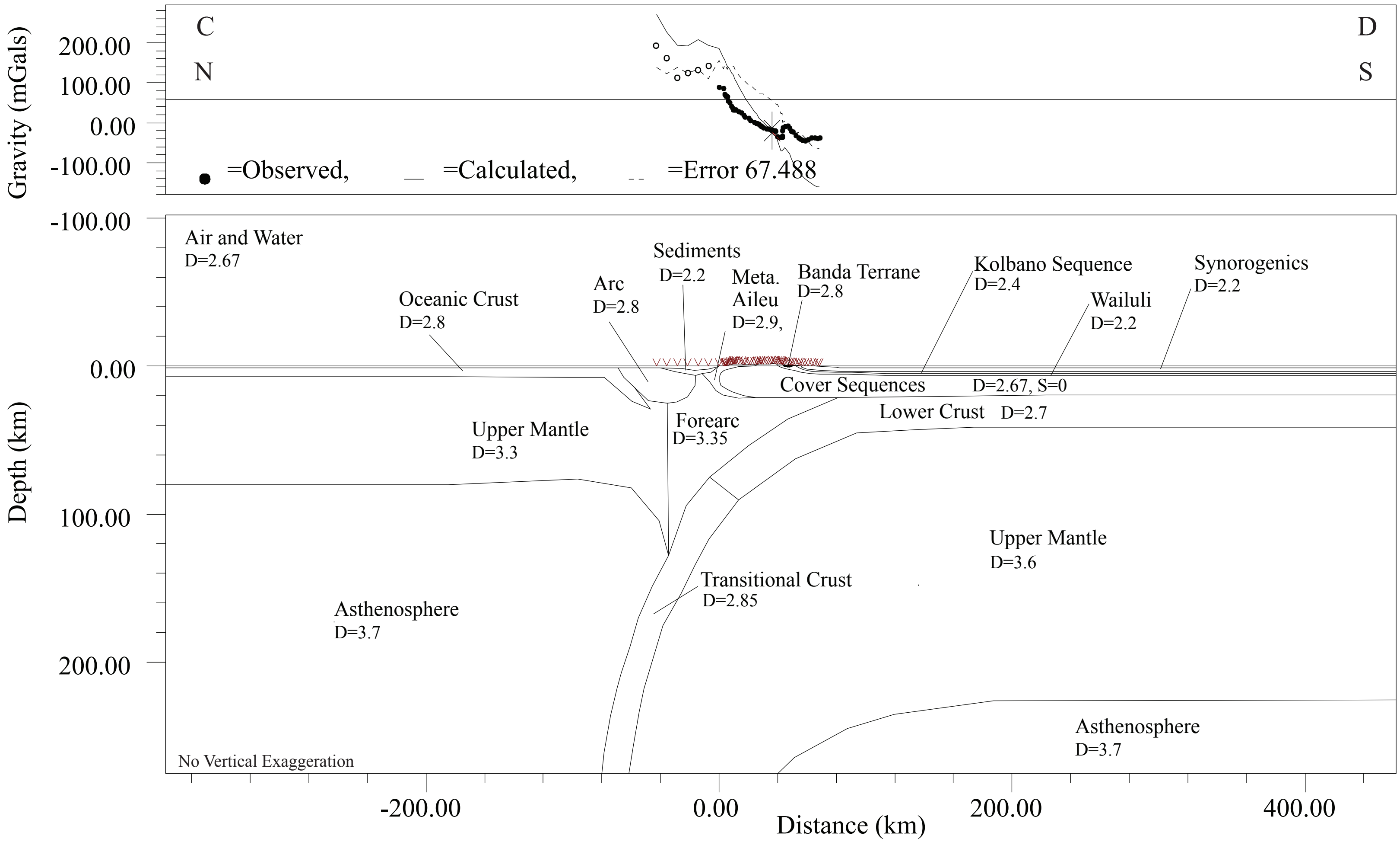

Figure 23: Gravity model of collisional geometry presented by Audley-Charles (2004) where forearc basement splits incoming cover sequences from underlying basement of Australian continental margin. Open circles represent offshore gravity data from Kaye and Milsom (1988). Filled circles from Chamalaun et al. (1975). The calculated gravity profile (this solid line) is the predicted gravity from this model and the residual (dashed) represents the difference between the calculated and observed gravity. Densities are in g/cm ^{3}. Line of section shown on figure 5.

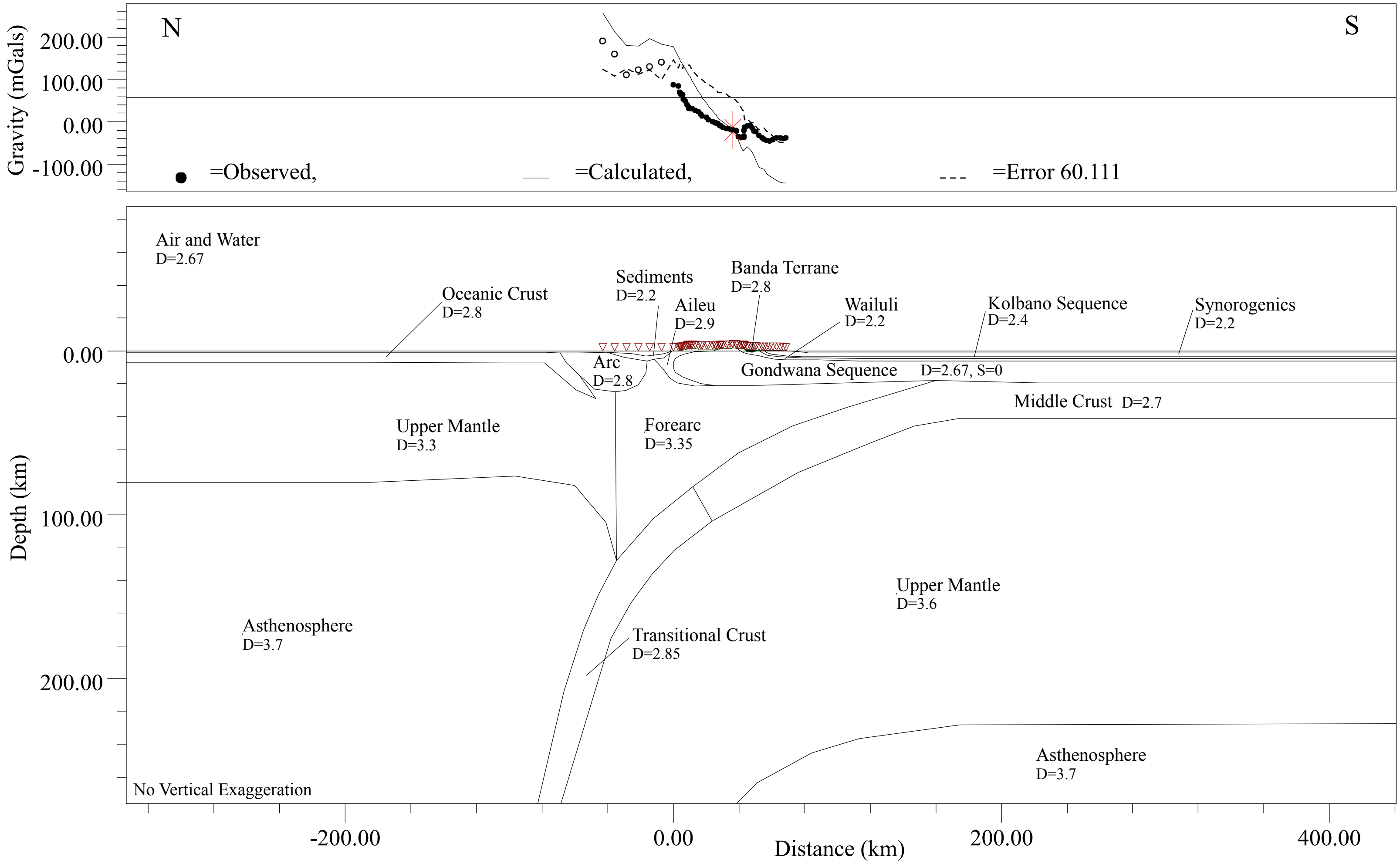

Figure 24: Modification of Audley-Charles (2004) in which the area of the forearc as calculated from Vorkink (2004) has been maintained. See figure 23 for other details.

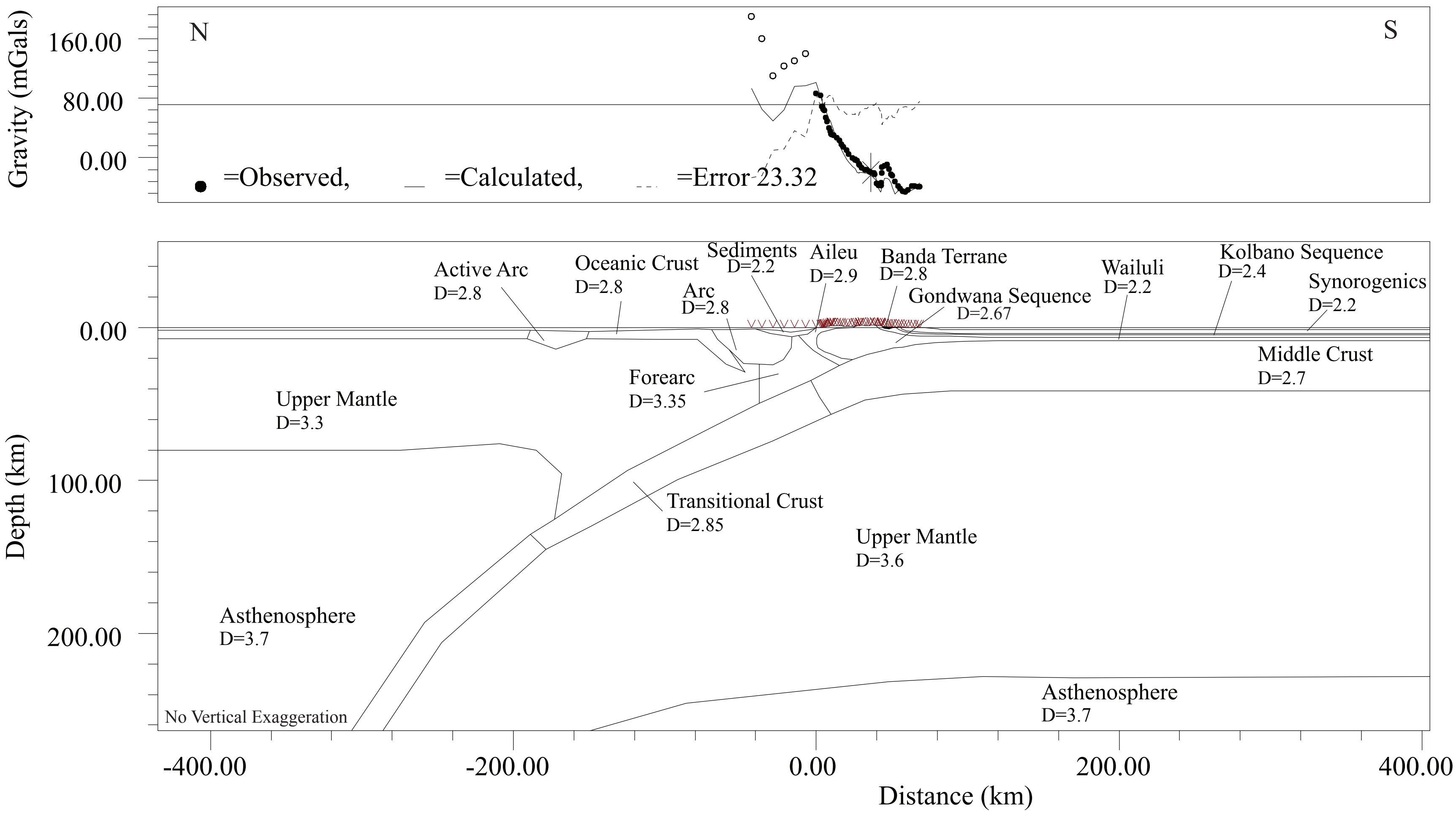

Figure 25: Displacement model of Harris (2003) in which the location of the active arc and forearc have been displace northward. This model and the lateral displacement model of Rutherford et al. (2001) also does not account for the steep gravity gradient north of Timor. See figure 23 for other details.

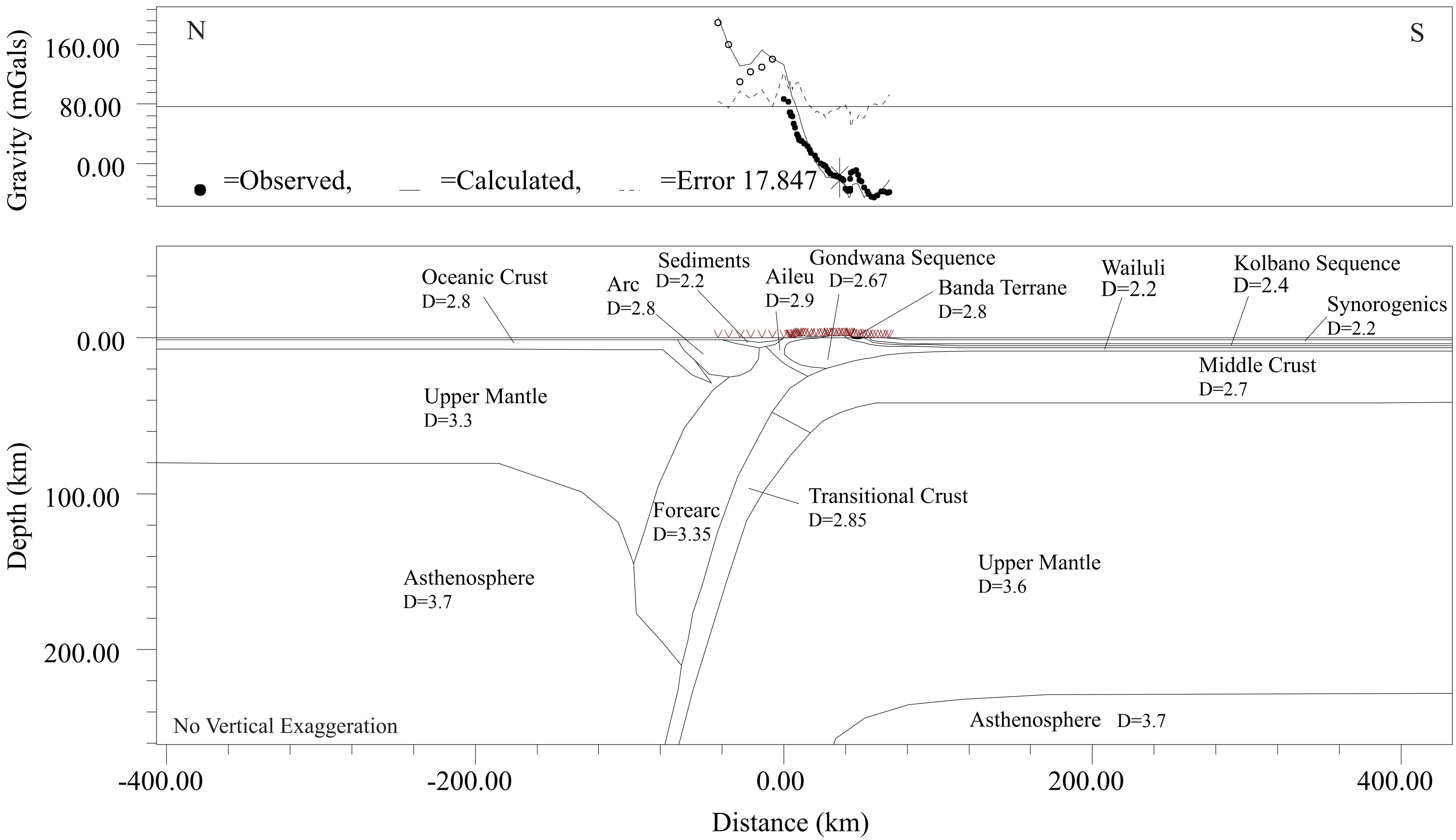

Figure 26: Area-balanced thickening model in which the forearc has been thickened in the initial stages of subduction erosion. See figure 23 for other details.

Arc magmatism north of Timor ended at 1-3 Ma (Abbott and Chamalaun, 1981; Silver et al., 1983). The best-fit model accounts for this by the insertion of cold forearc lithosphere into the asthenospheric wedge. We have extended the forearc along the subducting slab, which would cool the region formerly partial melting to produce arc magmatism. We hypothesize that this model is in the initial stages of subduction erosion, which eventually causes destruction of the forearc region.

The steep gravity gradient north of Timor is one of the steepest gradients documented on earth (McBride and Karig, 1987). It has been modeled as a local dense body of mantle by Milsom and Audley-Charles (1986). However, this model does not account for the location of the massive forearc slab. We prefer to use an internally thickened forearc beneath northern Timor and the arc to explain this anomaly because it is more consistent with other tectonic features. One of these features is high, but locally variable uplift rates of the south coast of the inactive volcanic arc, which should be subsiding due to thermal contraction, and coral terraces along the north coast of East Timor (Cox et al., 2006). From our modeling we conclude that the steep increase in gravity toward the back arc is a result of increasing thickness of the shortened forearc beneath the Banda Arc.

CONCLUSIONS

- The Gondwana Sequence was deposited by a proximal source to the northeast based on fresh mica, twinned feldspar, abundant lithic fragments, textural immaturity, and paleocurrent data.

- Detrital zircon ages for the Gondwana Sequence range from 254 – 385 and 1788 – 1874. Age similarities of detrital zircon and model ages of apatite grains of the Permian and Triassic Gondwana Sequence from East Timor to Savu indicate the same source for all Gondwana Sequence sandstones. The ages correspond closely with those from Northern Queensland and New Guinea, but these regions are too distant to account for its proximal facies indicators. We propose an Argoland source that would be an extension of the Northern Queensland granite belt that was rifted from the northwest margin of the Australia in the Jurassic.
- Differences in U/Pb detrital zircon ages between the Gondwana Sequence and the Banda Terrane provides a new application for distinguishing which units are of Australian affinity or Asian affinity.
- Structural measurements from the Gondwana Sequence in central East Timor indicate a maximum stress direction of northwest-southeast and fold axes oriented northeast-southwest, which is the same direction as rift structures of the northwest Australian margin. The maximum stress direction is a result of the upper plate accretionary backstop orientation (northeast-southwest). Most structures on Timor are sub-parallel to the Australian Continental margin indicating the influence of structural inheritance.
- Fault propagation folding is the dominate method of shortening for the Gondwana Sequence. Meso-scale folds have an average shortening of 35%. Total shortening for the Gondwana Sequence is approximately 50%, based on local line length and regional area balancing methods.

- The most likely method of forearc shortening north of East Timor is under stacking beneath the volcanic arc and north coast of Timor, which continues into the Holocene as indicated by uplifted coral terraces.

REFERENCES

Abbott, M.J. and Chamalaun, F.H., 1981. Geochronology of some Banda Arc volcanics. The Geology and Tectonics of Eastern Indonesia, Geological Research and Development Centre, Spec. Publ. No. 2, p. 253-268.

Audley-Charles, M.G., 2004, Ocean trench blocked and obliterated by Banda forearc collision with Australian proximal continental slope. Tectonophysics, 389, 65-79.

Audley-Charles, M.G., and Harris, R.A., 1990, Allochthonous terranes of the southwest Pacific and Indonesia. Philosophical Transactions of the Royal Society A31, 571-587.

Audley-Charles, M.G., 1968, The geology of Portuguese Timor: Geological Society of London Memoir 4, 76 pp.

Barber, A.J., Audley Charles, M.G., Carter, D.J., 1977, Thrust tectonics in Timor. Journal of the Geological Society of Australia, 24, 51-62.

Berry, R.F. and McDougall, I, 1986, Interpretations of 40Ar/39Ar dating evidence from the Aileu Formation, East Timor, Indonesia, Chem. Geol., 59, 43-58.

Berry, R.F., and Jenner, G.A., 1982, Basalt geochemistry as a test of tectonic models of Timor. Journal of the Geological Society of London, 139, 593-604.

Bird, P.R., and Cook, S.E., 1991, Permo-Triassic successions of the Kekneno area, West Timor: Implications for palaeogeography and basin evolution. Journal of Southeast Asian Earth Sciences, 6, 359-371.

Bird, P.R. (1987), The geology of the Permo-Triassic Rocks of the Kekneno, West Timor. Unpublished PhD Thesis, University of London.

Blake, D.H., and Stewart, A.J., 1992, Stratigraphic and tectonic framework, Mount Isa Inlier. In: Stewart, A.J., (eds) Detailed Studies of the Mount Isa Inlier, Australian Geological Survey Organisation Bulletin, 243, 1-11.

Blewett, R.S., and Black, L.P., 1998, Structural and temporal framework of the Coen Region, north Queensland: implications for major tectonothermal events in east and north Australia. Australian Journal of Earth Sciences, 45, 597-609.

Bodorkos, S., Cawood, P. A., and Oliver, N.H.S., 2000, Timing and duration of syn-magmatic deformation in the Mabel Downs Tonalite, northern Australia. Journal of Structural Geology, 22, 1181-2000.

Bowman, J.R., and Kennett, B.L.N., 1990, An investigation of the upper mantle beneath NW Australia using a hybrid seismograph array. Geophysical Journal International, 101, 411-424.

Bowin, C., Purdy, G.M., Johnston, C., Shor, G., Lawver, L., Hartono, M.S., and Jezek, P., 1980, Arc-continent collision in Banda Sea Region. The American Association of Petroleum Geologist Bulletin, 64, 868-915.

Breen, N., Silver, E.A., Hussong, D.M., 1986, Structural styles of an accretionary wedge south of the island of Sumba, Indonesia, revealed by Sea Marc II side scan sonar. Geological Society of America Bulletin, 97, 1250-1261.

Brouwer, H.A., 1942. Summary of the results of the expedition. Geological Expedition to the Lesser Sunda Islands under the leadership of H.A. Brouwer, 4, 345-402.

Burrett, C., and Stait, B., 1986, Southeast Asia as a part of an early Palaeozoic Australian Gondwanaland. Geol. Soc. Malaysia, 19, 103-107.

Caldwell, J.G., and Turcotte, D.L., 1979, Dependence of the thickness of the elastic oceanic lithosphere on age. Journal of Geophysical Research, 84, 7572-7576.

Carter, D.J., Audley-Charles, M.G., and Barber, A.J., 1976, Stratigraphic analysis of island arc-continental margin collision in eastern Indonesia. Journal of the Geological Society of London, 132, 197-198.

Chamalaun, F.H. and Grady, A.E., 1978, The tectonic evolution of Timor: A new model and its implications for petroleum exploration: Journal of the Australian Petroleum Exploration Association, 18, 102-108.

Chamalaun, F.H., Lockwood, K., and White, A., 1975, The bouguer gravity field and crustal structure of eastern Timor. Tectonophysics, 30, 241-259.

Charlton, T. R., 2002, The structural setting and tectonic significance of the Lolotoi, Laclubar and Aileu metamorphic massifs, East Timor: Journal of Asian Earth Sciences, 20, 851-865.

Charlton, T.R., Barber, A.J., Harris, R.A., Barkham, S.T., Bird, P.R., Archbold, N.W., Morris, N.J., Nicoll, R.S., Owen, R.S., Owens, R.M., Sorauf, J.E., Taylor, P.D., Webster, G.D., Whittaker, J.E., 2002, The Permian of Timor: stratigraphy, palaeontology and palaeogeography. Journal of Southeast Asian Earth Sciences, 20, 719-774.

Charlton T.R., 2000, Permo-Mesozoic rifting in Gondwanan eastern Indonesia. AAPG Bulletin, 84, 1411.

Cobbing, E.J., Pitfield, P.E.J., Darbyshire, D.P.F., and Mallick, D.I.J., 1992, The granites of the South-East Asian Tin Belt. British Overseas Geological Survey Memoir, 10, 369 p.

Cook, S.E., 1986, Triassic Sediments from East Kekneno, West Timor. Unpublished PhD thesis, University of London.

Cox, N., Merritts, D., Harris, R., Chen, Y., 2006, Quaternary uplift of coral terraces from active folding and thrusting along the northern coast of Timor-Leste. GSA Abstracts with Programs, 38, 509.

de Roever, W.P., 1940, Geological investigations in the Southwest Moetis region (Northern Timor). Unpublished PhD thesis, Amsterdam.

Dickinson, W.R., Beard, L.S., Brakenridge, G.R., Erjavec, J.L., Ferguson, R.C., Inman, K.F., Knepp, R.A., Lindber, F.A., Ryberg, P.T., 1983, Provenance of North American Phanerozoic sandstones in relation to tectonic setting. Geological Society of America Bulletin, 94, 222-235.

Dunlap, W.J., 1996, Palaeozoic alpine tectonics in central Australia and southern New Guinea. BMR Journal. Australia Geol. Geophysics., 1, 131-140.

Finney, S.C., Grubb, B.J., Hatcher, R.D. Jr., Graphic correlation of Middle Ordovician graptolite shale, Southern Appalachians; an approach for examining the subsidence and migration of a Taconic foreland basin. Geological Society of America Bulletin, 108, 355-371.

Grady, A.E., and Berry, R.F., 1977, Some Palaeozoic-Mesozoic stratigraphic-structural relationships in East Timor and their significance to the tectonics of Timor. Journal of the Geological Society of Australia, 24, 203-214.

Grady, A. E., 1975, A reinvestigation of thrusting in Portuguese Timor: Journal of the Geological Society of Australia, 22, 223-227.

Gehrels, G.E., Valencia, V., Pullen, A., 2006, Detrital zircon geochronology by Laser-Ablation Multicollector ICPMS at the Arizona LaserChron Center, in Loszewski, T., and Huff, W., eds., Geochronology: Emerging Opportunities, Paleontology Society Short Course: Paleontology Society Papers, 11, 10 p.

Genrich, J. F., Y. Bock, R. McCaffrey, E. Calais, C. W. Stevens, and C. Subarya, 1996. Accretion of the southern Banda arc to the Australian plate margin determined by Global Positioning system measurements, Tectonics, 15, 288-295.

Gianni, L., 1971, The geology of the Belu district of Indonesian Timor. Unpublished MPhil. Thesis, University of London, 122 pp.

Hamilton, W., 1979, Tectonics of the Indonesian region. United States Geological Survey Professional Paper, 1078.

Harris, R., 2006, Rise and fall of the Eastern Great Indonesian arc recorded by the assembly dispersion and accretion of the Banda Terrance, Timor. Gondwana Research, 10, 207-231.

Harris, R.A., 2003, Geodynamic patterns of ophiolites and marginal basins of the Indonesian and New Guinea regions, *in* Dilek, Y. and Robinson, P.T., eds., “Ophiolite in Earth History”, *Geol. Soc. London, Spec. Pub.*, 218, p. 481-505.

Harris, R., Kaiser, J., Hurford, A., Carter, A., 2000, Thermal history of Australian passive margin cover sequences accreted to Timor during Late Neogene arc-continent collision Indonesia. Journal of Asian Earth Sciences, 18, 47-69.

Harris, R. A. , Sawyer, R. K. and Audley-Charles, M. G., 1998, Collisional melange development: geologic associations of active melange-forming processes with exhumed melange facies in the western Banda orogen, Indonesia. Tectonics, 17, 458-480.

Harris, R.A., 1991, Temporal distribution of strain in the active Banda orogen: a reconciliation of rival hypotheses. Journal of Southeast Asian Earth Sciences, 6, 373-386.

Hillis, R., 1991, Australia-Banda Arc collision and in situ stress in the Vulcan Sub-basin (Timor Sea) as revealed by borehole breakout data. Exploration Geophysics, 22, 189-194.

Huang, C.Y., Yuan, P.B., and Tsao, S.J., 2006, Temporal and spatial records of active arc-continent collision in Taiwan: A synthesis. Geological Society of America Bulletin, 118, 274-288.

Huang, C.Y., Yuan, P.B., Lin, C.W., Wang, T.K., and Change, C.P., 2000, Geodynamic processes of Taiwan arc-continent collision and comparison with analogs in Timor, Papau New Guinea, Urals and Corsica, Tectonophysics, 325, 1-21.

Hunter, D.C., 1993, A stratigraphic and structural study of the Maubisse area, East Timor. Unpublished Master Thesis, West Virginia University, 107p.

Johnston, C.R., and Bowin, C.O., 1981, Crustal reactions resulting from the mid-Pliocene to Recent continent-island collision in the Timor region. BMR Journal of Australian Geology and Geophysics, 6, 223-243.

Karig, D.E., Barber, A.J., Charlton, T.R., Klemperer S., and Hussong, D.M., 1987, Nature and distribution of deformation across the Banda Arc-Australian collision zone at Timor. Geological Society of America Bulletin, 98, 18-32.

Kaye, S.J., and Milsom, J.S., 1988, A new bouguer anomaly map of Timor eastern Indonesia. University College London Gravity Research Group, pp. 31.

Leech, M.L., Singh, S., Jain, A.K., Klemperer, S.L., Manickavasagam, R.M., 2005, The onset of India-Asia continental collision; eatly, steep subduction required by the timing of UHP metamorphism in the western Himalaya. Earth and Planetary Science Letters, 234, 83-97.

Lemoine, P.M., 1959, Un exemple de tectonique chaotique: Timor. Revue de Geographie Physique et de Geologie Dynamique, 2, 205-230.

Liew, T.C., and Page, R.W., 1985, U-Pb zircon dating of granitoic plutons from the West Coast Province of Peninsular Malaysia. Journal of the Geological society of London, 142, 515-526.

Ludwig, K.R., 2003, Isoplot 3.00. Berkeley Geochronology Center, Special Publication 4, 70 p.

McBride J.H., and Karig, D.E.,1987, Crustal structure of the outer Banda Arc: new free-air gravity evidence. Tectonophysics, 140, 265-273.

Metcalfe, I., 2000, The Benton-Ruab suture zone. Journal of Asian Earth Sciences, 18, 691-712.

Metcalfe, I., 1996, Pre-Cretaceous evolution of SE Asian terranes. In: Hall, R., Blundell, D.J., (Eds.). Tectonic Evolution of Southeast Asia. Geological Society of London Special Publication 106, 97-122.

Mikolas, M., and Harris, R.A., 1996, Variation of stress in time and space of an oblique arc-continent collision: analysis of fractures in synorogenic deposits of Timor. Geological Society of America Abstracts with Programs, 28, 91.

Milsom, J., and Audley-Charles, M.G., 1986, Post-collision isostatic readjustment in the southern Banda Arc. Collision Tectonics, Geological society Special Publication, 19, 353-364.

Nugroho, H., Harris, R.A., King, R.W., Vorkink, M.W., Lestatiya, A.W., Maruf, B., Martin, D., and Harris, N., 2004, Strain partitioning in the active Banda arc-continent collision determined with GPS measurements: Geological Society of America Abstracts with Programs, 36, 505.

Page, R.W., and Williams, I.S., 1988, Age of the Barramundi Orogeny in northern Australia by means of ion microprobe and conventional U-Pb zircon studies. Precambrian Research, 40, 21-36.

Prasetyadi, C. and Harris, R.A., 1996. Hinterland structure of the active Banda arc-continent collision, Indonesia: constraints from the Aileu Complex of East Timor. Proc. 25th Conv. Indonesian Assoc. Geol., 144-173.

Price, N.J., and Audley-Charles, M.G., 1983, Plate rupture by hydraulic fracture resulting in overthrusting. Nature (London) 306, 572-575.
Petkovic, P., Collins, C.D.N., and Finlayson, D.M., 2000, A crustal transect between Precambrian Australia and the Timor Trough across the Vulcan Sub-basin. Tectonophysics, 329, 23-38.

Reed, D.L., Silver, E,A., Prasetyo, H., and Meyer, A.W., 1986, Deformation and sedimentation along a developing terrain suture: eastern Sunda forearc, Indonesia. Geology, 14, 977-1092.

Reusch, D.N., van Staal, C., Hibbard, J., 2006, A central Maine perspective on the Cambro-Ordvician Gander Terrane. Abstracts with Programs – Geological Society of America, 38, 72.

Rutherford, E., Burke, K., Lytwyn, J., 2001 Tectonic history of Sumba Island, Indonesia, since the late Cretacous and its rapid escape into the forearc in the Miocene. Journal of Asian Earth Sciences, 19, 453-479.

Sani, K., Jacobsen, M.L., and Sigit, R., 1995, The thin-skinned thrust structures of Timor. paper presented at Indonesian Petroleum Association 24^{th} Annual Convention, Jakarta, 227-293.

Sawyer , R.K., Sani, K. and Brown, S., 1993. The stratigraphy and sedimentology of West Timor, Indonesia, Proc. 22nd Conv. Indon. Pet. Assoc., 1-20.

Silver, E. A., D. R. Reed, R. McCaffrey, and Y. Joyodiwiryo, 1983. Back arc thrusting in the eastern Sunda arc, Indonesia: A consequence of arc-continent collision, Journal of Geophysical. Research, 88, 7429-7448.

Snyder, D.B., Prasetyo, H., Blundell, D.J., Pigram, C.J., Barger, A.J., Richardson, A. and Tjokosaproetro, S., 1996. A dual doubly vergent orogen in the Banda Arc continent-arc collision zone as observed on deep seismic reflection profiles, Tectonics, V. 15, p. 34-53.

Spiking, R.A., Foster, A.D., and Kohn, B.P., 1997, Phanerozoic denudation history of the Mount Isa Inlier, Northern Australia: Response of Proterozoic mobile belt to intraplate tectonics. International Geology Review, 39, 107-124.

Stacey, J.S., and Kramers, J.D., 1975, Approximation of terrestrial lead isotope evolution by a two-stage model. Earth and Planetary Science Letters, 26, 207-221.

Stampfli, G.M., and Borel, G.D., 2002, A plate tectonic model for the Paleozoic and Mesozoic constrained by dynamic plate boundaries and restored synthetic oceanic isochrones. Earth and Planetary Science Letters, 196, 17-33.

Standley, C.E., and Harris, R.A., in press, Tectonic evolution of the Lolotoi Complex of East Timor: Active accretion of an Asian forearc terrane to the NW Australian continental margin. Gondwana Research.

Symonds, P.A., Planke, S., Frey, O., and Skogseid, J., 1998, Volcanic Evolution of the western Australian continental margin and its implications for basin development, In:

Sedimentary Basin of Western Australia, Proceedings of Petroleum Exploration Society of Australia Symposium, 2, 33-54.

van der Plas, L., and Tobi, A.C., 1965, A chart for judging the reliability of point counting results. American Journal of Science, 263, 87-90.

van Wyck, N., and Willians, I.S., 2002, Age and provenance of basement metasediments from the Kubor and Bena Bena Blocks, central Highlands, Papua New Guinea: constraints on the tectonic evolution of the northern Australian cratonic margin. Australian Journal of Earth Sciences, 49, 565-577.

Vorkink, M., 2004, Incipient arc-continent collision: structural analysis of Savu Island, Indonesia. Unpublished. Masters Thesis, Brigham Young University, 87 pp.

Wanner, J., 1913, Geologie von Westtimor. Geologische Rundschau, 4, 136-150.

Williams, H.F., Turner, F.J., Gilbert C.M., 1982, Petrography, an introduction to the study of rocks in thin section, 2nd ed., W.H. Freeman and Co., San Francisco.

Appendix 1: Petrographic descriptions

Sample	Location	Latitude (S)	Longitude (N)	Rounding	Sorting	Grain Size	Contacts	Cementing
EZ-151	East Timor	819321	9010976	SA	Moderatelly	UF to VF	Point	Matrix
EZ-70	East Timor	825611	9019284	SA	Well	VF	Point	Matrix
EZ-69	East Timor	825445	9019036	SA	Well	LF to VF	Point	Calcite
EZ-88	East Timor	825217	9022536	SA	Well	VF	Point	Matrix
89 HS-11A	West Timor	786237	9023313	SR	Moderatelly Well	LF to VF	Long	Calcite
89 HS 14	West Timor	753095	9023158	SR	Poorly	UM to VF	Long	Calcite
90 HS 45	West Timor	782366	9025809	SA	Poorly	UM to VF	Long	Matrix
89 HS-16A	West Timor	777191	9006934	SA-SR	Well	VF	Long	Calcite
90 HS-73C	West Timor	781958	9041454	SA	Moderatelly Well	LF to VF	Point	Calcite
RA-24A	West Timor	787491	9055701	SA	Well	VF	Long	Calcite
SV-9	Savu	362402	8829691	SA-SR	Poorly	LC to F/VF	Long and Point	Matrix
SV-159	Savu	375147	8832885	SA	Well	F to VF	Point	Matrix
SV-155A	Savu	375419	8826472	SA	Well	F to VF	Point	Calcite
SV-28C	Savu	376130	8827396	SR	Poorly	LC to VF	Point	Calcite
SV-Bab	Savu	South part	of island	SA	Well	F to VF	Point	Calcite
SV-164	Savu	371652	8826375	SR	Poorly Sorted	UC to F/VF	Long	Matrix

Latitude and Longitude measurements are in UTM (m). SA = Sub-Angular, SR = Sub-rounded, LC = Lower Coarse, UM = Upper Medium
UF = Upper Fine, LF = Lower Fine, VF = Very Fine. Calcite cement is from an altered matrix.

Appendix 2: U-Pb (Zircon) Geochronologic Analysis Multicollector Inductively Coupled Plasma Mass Spectrometry

U (ppm)	206Pb 204Pb	U/Th	207Pb* 235U	± (%)	206Pb* 238U	± (%)	error corr.	206Pb* 238U	± (Ma)	207Pb* 235U	± (Ma)	206Pb* 207Pb*	± (Ma)	Best age (Ma)	± (Ma)
SV-164															
478	5993	0.8	4.83611	10.5	0.29158	10.3	0.98	1649.4	149.8	1791.2	88.4	1960.5	34.5	1960.5	34.5
554	62951	1.8	3.78429	2.1	0.27692	1.3	0.62	1575.8	18.3	1589.4	17.1	1607.5	31.3	1607.5	31.3
821	15777	1.2	5.60178	4.7	0.34704	4.2	0.89	1920.4	69.6	1916.4	40.4	1912.0	37.5	1912.0	37.5
58	12782	0.5	4.66157	3.8	0.31333	3.3	0.86	1757.1	50.8	1760.4	32.0	1764.3	35.2	1764.3	35.2
191	32616	1.4	5.58408	2.2	0.34745	1.1	0.50	1922.4	18.4	1913.6	19.0	1904.1	34.3	1904.1	34.3
172	30416	0.4	3.97884	1.9	0.28909	1.0	0.53	1637.0	14.5	1629.9	15.5	1620.7	30.2	1620.7	30.2
187	5624	1.0	0.38458	6.2	0.04966	4.4	0.71	312.4	13.4	330.4	17.6	458.9	98.0	312.4	13.4
98	17777	0.6	3.85131	2.6	0.28429	1.6	0.60	1612.9	22.2	1603.5	21.1	1591.2	39.3	1591.2	39.3
321	58599	2.1	5.55345	2.4	0.34662	1.3	0.54	1918.5	21.7	1908.9	20.7	1898.5	36.3	1898.5	36.3
127	32367	0.6	2.14922	2.3	0.19809	1.5	0.64	1165.0	15.7	1164.8	15.9	1164.4	35.0	1164.4	35.0
184	45124	1.0	5.40695	2.7	0.34113	1.0	0.37	1892.1	16.4	1886.0	23.1	1879.2	45.1	1879.2	45.1
276	55570	0.8	5.53000	3.7	0.34602	2.8	0.76	1915.5	46.4	1905.3	31.7	1894.1	43.2	1894.1	43.2
113	21956	1.0	5.31996	4.1	0.33959	2.0	0.49	1884.7	32.8	1872.1	34.7	1858.1	63.8	1858.1	63.8
126	33332	1.1	5.80313	2.0	0.35109	1.0	0.49	1939.8	16.8	1946.9	17.7	1954.4	31.8	1954.4	31.8
534	32672	1.8	1.39164	2.4	0.14741	1.9	0.78	886.4	15.4	885.4	14.1	882.8	30.8	886.4	15.4
424	52384	3.0	5.61938	2.7	0.34528	2.2	0.83	1912.0	36.7	1919.1	23.0	1926.7	26.5	1926.7	26.5
80	9031	0.9	1.45838	4.9	0.15072	1.0	0.20	905.0	8.4	913.3	29.6	933.5	98.9	905.0	8.4
333	15751	1.3	0.41085	3.2	0.05331	1.1	0.36	334.8	3.7	349.5	9.4	448.0	66.0	334.8	3.7
76	8347	0.5	2.43725	6.3	0.20804	2.2	0.35	1218.3	24.5	1253.7	45.4	1314.8	114.6	1314.8	114.6
187	6625	1.2	1.00155	4.0	0.11296	2.7	0.68	689.9	17.7	704.6	20.1	751.6	60.9	689.9	17.7
449	54538	1.2	5.31824	5.3	0.33860	4.4	0.84	1879.9	72.4	1871.8	45.4	1862.8	52.7	1862.8	52.7
469	11656	1.9	5.87448	8.3	0.35789	6.0	0.72	1972.1	101.2	1957.5	72.0	1942.0	102.9	1942.0	102.9
544	8601	1.5	5.23791	7.3	0.32281	5.8	0.80	1803.5	91.6	1858.8	62.3	1921.3	78.9	1921.3	78.9
371	48453	3.6	4.85669	6.5	0.31196	4.2	0.65	1750.3	64.8	1794.8	54.9	1846.8	89.8	1846.8	89.8
333	77391	1.0	5.32634	2.0	0.33957	1.1	0.54	1884.6	17.3	1873.1	16.7	1860.4	29.6	1860.4	29.6
375	17417	1.4	5.17168	7.5	0.32841	6.5	0.87	1830.7	103.5	1848.0	63.6	1867.5	66.7	1867.5	66.7
75	9985	1.2	1.46576	2.2	0.14773	1.5	0.68	888.2	12.1	916.4	13.0	984.8	32.1	888.2	12.1

353	78832	2.3	3.58238	1.9	0.27324	1.0	0.52	1557.2	13.8	1545.6	15.3	1529.8	30.9	1529.8	30.9
290	70299	1.7	5.39449	3.2	0.33950	3.0	0.93	1884.3	49.0	1884.0	27.7	1883.6	21.4	1883.6	21.4
196	36976	1.2	3.93831	2.5	0.28300	1.4	0.57	1606.5	20.0	1621.6	20.0	1641.3	37.7	1641.3	37.7
202	57727	1.7	5.63966	2.1	0.34585	1.7	0.81	1914.7	27.9	1922.2	17.8	1930.2	21.5	1930.2	21.5
341	87344	0.9	5.22234	1.8	0.33305	1.0	0.56	1853.2	16.1	1856.3	15.3	1859.7	26.9	1859.7	26.9
72	14679	0.7	3.88770	2.0	0.28125	1.4	0.71	1597.6	20.0	1611.1	16.1	1628.8	26.0	1628.8	26.0
430	22285	2.4	3.76769	3.3	0.27867	2.6	0.80	1584.7	37.2	1585.9	26.4	1587.5	36.5	1587.5	36.5
337	15194	1.3	0.42899	2.9	0.05487	1.2	0.41	344.3	4.0	362.5	8.7	480.0	57.3	344.3	4.0
911	31540	1.6	0.40542	2.2	0.05363	1.0	0.45	336.8	3.3	345.6	6.5	405.2	44.4	336.8	3.3
312	50338	1.6	3.76705	2.4	0.27995	1.3	0.55	1591.1	18.5	1585.8	19.3	1578.6	37.6	1578.6	37.6
297	68580	1.2	5.19934	3.2	0.33416	2.4	0.77	1858.5	39.6	1852.5	27.2	1845.7	37.1	1845.7	37.1
832	198464	16.5	4.69085	1.7	0.31417	1.0	0.58	1761.2	15.4	1765.6	14.4	1770.8	25.6	1770.8	25.6
306	63135	1.0	4.97752	2.7	0.32689	1.1	0.40	1823.3	17.2	1815.5	23.0	1806.6	45.3	1806.6	45.3
190	44302	2.1	5.13868	3.3	0.32886	2.2	0.65	1832.9	34.5	1842.5	28.3	1853.4	45.7	1853.4	45.7
476	56331	2.7	5.22719	2.2	0.33448	1.2	0.54	1860.1	19.7	1857.1	19.1	1853.7	34.0	1853.7	34.0
444	74090	2.8	5.50274	2.1	0.34192	1.7	0.78	1895.9	27.4	1901.0	18.3	1906.6	23.7	1906.6	23.7
219	9858	1.4	0.45093	2.5	0.05867	1.7	0.70	367.5	6.2	377.9	7.8	442.1	39.5	367.5	6.2
SV-159															
140	24453	0.8	12.66061	3.1	0.48826	2.1	0.69	2563.2	45.4	2654.7	29.5	2725.3	37.6	2725.3	37.6
512	11152	0.5	0.28300	3.7	0.03879	2.0	0.55	245.4	4.9	253.0	8.3	324.9	70.4	245.4	4.9
252	11098	1.7	0.69739	3.5	0.07845	1.6	0.46	486.9	7.7	537.2	14.8	757.1	66.4	486.9	7.7
359	3636	1.3	0.85344	8.0	0.09038	3.1	0.39	557.8	16.5	626.5	37.2	883.2	151.9	557.8	16.5
133	21320	1.0	5.46726	4.0	0.34365	1.7	0.43	1904.2	28.0	1895.5	34.1	1885.9	64.7	1885.9	64.7
655	21246	0.6	6.18667	6.7	0.35166	4.0	0.60	1942.5	67.5	2002.6	58.8	2065.1	94.9	2065.1	94.9
SV-155A															
170	6008	0.6	0.38195	9.6	0.04686	3.0	0.31	295.2	8.6	328.5	26.8	571.2	197.9	295.2	8.6
183	7087	1.6	0.42541	5.0	0.05425	2.2	0.44	340.6	7.3	359.9	15.2	486.4	99.6	340.6	7.3
215	14361	1.3	0.61115	3.2	0.07591	2.0	0.62	471.7	9.0	484.3	12.4	544.4	55.1	471.7	9.0
938	14519	1.1	0.36559	3.3	0.04861	1.5	0.46	306.0	4.5	316.4	8.9	393.8	65.1	306.0	4.5
396	45268	1.0	2.18599	2.6	0.19990	1.6	0.61	1174.8	17.1	1176.6	18.1	1179.9	40.5	1179.9	40.5
903	10362	1.6	0.44291	3.6	0.05644	1.3	0.36	353.9	4.6	372.3	11.3	488.2	74.7	353.9	4.6
187	13542	1.4	0.42908	3.8	0.05403	2.7	0.71	339.2	8.8	362.5	11.5	514.4	58.1	339.2	8.8
441	19938	1.6	1.58823	4.3	0.15556	3.5	0.81	932.1	30.6	965.6	27.0	1042.7	50.9	932.1	30.6
172	75668	1.0	5.26013	3.0	0.33853	1.1	0.37	1879.6	18.0	1862.4	25.3	1843.3	49.8	1843.3	49.8

	63	2727	1.1	0.48137	5.6	0.05567	2.3	0.41	349.3	7.9	399.0	18.6	698.3	109.7	349.3	7.9
	103	4028	0.7	0.36888	7.0	0.04601	3.1	0.44	290.0	8.7	318.8	19.2	535.3	138.7	290.0	8.7
	194	5684	0.5	0.29254	7.8	0.03706	1.8	0.22	234.6	4.0	260.6	18.0	501.0	168.5	234.6	4.0
	232	10507	0.8	0.39040	5.7	0.05211	2.9	0.51	327.5	9.1	334.7	16.1	384.9	109.6	327.5	9.1
	197	10213	1.0	0.38333	5.2	0.04862	3.3	0.63	306.0	9.8	329.5	14.6	498.6	88.6	306.0	9.8
	260	10862	0.7	0.36867	2.9	0.04669	1.4	0.50	294.2	4.1	318.7	8.0	501.9	55.6	294.2	4.1
	403	9218	0.9	0.28945	5.0	0.03825	2.7	0.55	241.9	6.5	258.1	11.3	407.7	93.2	241.9	6.5
	445	17230	1.4	0.33254	3.6	0.04436	2.9	0.79	279.8	7.9	291.5	9.2	386.4	49.8	279.8	7.9
	287	14812	1.2	0.37343	5.3	0.05014	3.0	0.57	315.4	9.4	322.2	14.7	371.7	98.8	315.4	9.4
	146	24654	0.7	2.19252	3.5	0.19552	2.3	0.66	1151.2	24.0	1178.7	24.1	1229.4	51.1	1229.4	51.1
	57	2189	1.7	0.42356	9.2	0.04287	6.2	0.67	270.6	16.4	358.6	27.8	976.4	138.4	270.6	16.4
	867	2644	1.6	0.42228	6.9	0.04558	3.7	0.55	287.3	10.5	357.7	20.7	843.7	119.6	287.3	10.5
SV-9																
	201	8767	0.8	0.34483	3.7	0.04671	2.5	0.68	294.3	7.2	300.8	9.6	351.5	61.1	294.3	7.2
	416	60033	2.5	5.27542	5.5	0.33265	3.8	0.70	1851.2	61.9	1864.9	47.1	1880.2	71.0	1880.2	71.0
	260	29199	0.7	2.19378	3.6	0.20039	3.4	0.96	1177.4	37.1	1179.1	25.0	1182.1	19.8	1182.1	19.8
	375	33931	0.5	6.34726	6.9	0.36494	5.5	0.80	2005.5	94.6	2025.0	60.4	2044.9	73.4	2044.9	73.4
	103	2379	0.9	0.38182	5.8	0.04769	2.9	0.50	300.3	8.5	328.4	16.3	532.2	110.1	300.3	8.5
	219	54623	1.2	5.03100	2.1	0.32125	1.0	0.47	1795.8	15.7	1824.6	18.1	1857.5	34.2	1857.5	34.2
	519	22430	0.6	0.40562	2.2	0.05423	1.1	0.50	340.4	3.6	345.7	6.4	381.3	42.6	340.4	3.6
	63	2693	0.6	0.39603	12.1	0.05175	7.8	0.65	325.2	24.8	338.8	34.9	432.7	206.3	325.2	24.8
	121	16273	0.9	1.45418	3.2	0.14805	1.0	0.32	890.0	8.3	911.6	19.1	964.2	61.4	890.0	8.3
	177	8786	0.9	0.36896	3.7	0.04853	2.3	0.61	305.5	6.8	318.9	10.2	417.7	66.4	305.5	6.8
	96	26183	0.5	6.85153	4.2	0.38913	2.3	0.55	2118.8	42.1	2092.4	37.4	2066.5	61.9	2066.5	61.9
	106	30107	0.9	3.71175	5.3	0.27504	3.1	0.58	1566.3	42.5	1573.9	42.5	1584.1	81.2	1584.1	81.2
	357	37620	0.9	1.27519	2.8	0.13951	1.4	0.49	841.9	10.7	834.7	15.8	815.7	50.6	841.9	10.7
	273	11663	0.9	0.59346	3.1	0.07562	1.2	0.38	469.9	5.4	473.1	11.8	488.3	63.6	469.9	5.4
	464	30431	1.0	1.35961	5.7	0.14461	4.1	0.72	870.7	33.5	871.7	33.4	874.3	81.6	870.7	33.5
	211	51126	1.2	5.32301	1.8	0.33745	1.5	0.84	1874.4	25.0	1872.6	15.7	1870.5	18.0	1870.5	18.0
	55	8742	0.5	2.10737	3.2	0.19489	2.6	0.82	1147.8	27.7	1151.2	22.2	1157.6	37.0	1157.6	37.0
	426	61867	0.7	9.12578	6.5	0.41652	6.3	0.97	2244.7	118.7	2350.7	59.3	2444.0	27.8	2444.0	27.8
	732	26049	0.7	0.46197	1.8	0.06186	1.3	0.71	386.9	4.9	385.6	5.9	378.0	28.9	386.9	4.9
	144	20340	0.7	2.21922	2.3	0.20294	1.1	0.46	1191.1	11.7	1187.1	16.2	1179.9	40.6	1179.9	40.6
	253	7547	0.5	5.13581	3.6	0.32092	3.2	0.88	1794.2	50.0	1842.0	30.7	1896.5	30.2	1896.5	30.2

189	39200	0.8	5.07629	2.2	0.33132	1.0	0.46	1844.8	16.0	1832.2	18.5	1817.8	35.2	1817.8	35.2
116	14825	0.5	3.92394	2.8	0.28117	1.8	0.64	1597.2	24.9	1618.6	22.4	1646.5	39.7	1646.5	39.7
225	5664	0.6	0.33832	2.6	0.04647	1.8	0.70	292.8	5.2	295.9	6.7	320.5	42.2	292.8	5.2
242	15291	0.6	5.59275	3.1	0.34814	2.1	0.70	1925.7	35.8	1915.0	26.3	1903.4	39.0	1903.4	39.0
776	44413	1.4	2.13592	4.6	0.19803	3.7	0.80	1164.7	39.5	1160.5	32.1	1152.6	55.6	1152.6	55.6
136	32839	0.9	11.47303	1.8	0.48854	1.1	0.58	2564.3	22.5	2562.4	17.1	2560.8	24.9	2560.8	24.9
319	25905	0.8	5.28739	2.8	0.33092	1.6	0.58	1842.8	25.8	1866.8	23.8	1893.7	41.0	1893.7	41.0
388	53148	1.6	5.35362	2.4	0.34140	1.6	0.65	1893.4	26.1	1877.5	21.0	1859.8	33.6	1859.8	33.6
469	14346	1.1	0.37316	3.5	0.05035	2.3	0.66	316.6	7.1	322.0	9.7	360.8	59.6	316.6	7.1
546	57367	3.4	5.05996	3.3	0.33023	2.1	0.64	1839.5	34.4	1829.4	28.4	1817.9	46.7	1817.9	46.7
205	4626	0.5	0.38526	8.6	0.04863	2.7	0.31	306.1	8.0	330.9	24.2	508.9	179.2	306.1	8.0
214	1859	0.4	2.08145	27.2	0.15207	10.7	0.39	912.6	90.9	1142.7	188.9	1610.4	474.4	1610.4	474.4
13	2645	0.6	4.40891	6.2	0.28617	5.7	0.91	1622.4	81.2	1714.0	51.4	1827.9	46.2	1827.9	46.2
74	10540	0.8	1.94985	3.9	0.17479	3.6	0.92	1038.5	34.3	1098.4	26.0	1219.1	29.1	1219.1	29.1
375	82642	1.6	5.22860	1.8	0.33466	1.0	0.57	1860.9	16.2	1857.3	15.1	1853.2	26.4	1853.2	26.4
594	25099	3.6	0.54774	2.7	0.07109	2.4	0.90	442.7	10.4	443.5	9.7	447.5	26.6	442.7	10.4
808	10212	1.1	0.39698	2.7	0.05296	1.8	0.66	332.6	5.7	339.5	7.7	386.4	44.9	332.6	5.7
312	56116	1.4	5.19320	1.8	0.33413	1.4	0.80	1858.4	23.2	1851.5	15.2	1843.8	19.2	1843.8	19.2
159	6792	0.8	0.43254	3.0	0.05691	1.9	0.64	356.8	6.6	365.0	9.1	417.1	51.3	356.8	6.6
230	62591	0.7	5.47333	2.0	0.34128	1.0	0.51	1892.8	16.4	1896.4	16.9	1900.3	30.6	1900.3	30.6
381	16998	1.2	0.33825	2.5	0.04739	1.8	0.74	298.5	5.4	295.8	6.4	275.1	38.8	298.5	5.4
146	4777	0.6	0.34510	5.3	0.04780	4.6	0.87	301.0	13.6	301.0	13.8	301.2	59.4	301.0	13.6
632	56782	1.0	5.40326	3.1	0.31637	2.6	0.82	1772.0	39.9	1885.4	26.9	2012.7	31.8	2012.7	31.8
94	3721	0.8	0.34003	7.9	0.04031	4.4	0.56	254.7	10.9	297.2	20.3	645.8	140.7	254.7	10.9
205	3477	0.9	0.37409	4.6	0.04880	2.2	0.48	307.1	6.7	322.7	12.9	436.5	90.9	307.1	6.7
320	7497	0.7	0.76564	12.1	0.08496	10.1	0.83	525.7	51.1	577.3	53.5	786.0	140.4	525.7	51.1
211	12466	0.6	0.52545	3.1	0.06885	2.0	0.66	429.2	8.4	428.8	10.8	426.4	52.0	429.2	8.4
242	64665	1.2	5.20733	2.7	0.33604	1.8	0.68	1867.6	29.6	1853.8	23.0	1838.4	36.0	1838.4	36.0
423	19823	1.1	0.42660	2.9	0.05707	1.3	0.43	357.8	4.4	360.8	8.9	379.9	59.6	357.8	4.4
307	72749	4.2	4.96773	1.9	0.32218	1.2	0.67	1800.4	19.5	1813.8	15.7	1829.4	25.0	1829.4	25.0
122	20816	0.5	2.11917	1.9	0.19587	1.0	0.53	1153.1	10.6	1155.1	13.0	1158.8	31.8	1158.8	31.8
486	35546	1.1	3.05250	6.1	0.23389	5.0	0.82	1354.9	61.3	1420.9	46.9	1521.2	66.4	1521.2	66.4
749	98236	3.5	5.62797	3.7	0.32268	3.1	0.85	1802.8	49.1	1920.4	31.6	2049.9	33.7	2049.9	33.7
186	62839	1.2	6.03172	4.9	0.35576	3.6	0.73	1962.0	60.8	1980.4	43.1	1999.7	60.2	1999.7	60.2

65	27016	1.0	13.17353	2.5	0.51552	1.7	0.68	2680.1	36.8	2692.2	23.2	2701.2	29.6	2701.2	29.6
183	8153	1.1	0.36088	4.0	0.04877	2.0	0.49	306.9	5.9	312.9	10.7	357.2	78.3	306.9	5.9
362	46389	1.4	3.41557	5.9	0.25442	5.0	0.84	1461.2	64.9	1508.0	46.6	1574.3	60.7	1574.3	60.7
195	46929	1.3	4.51549	3.4	0.30930	2.3	0.68	1737.3	34.9	1733.8	28.0	1729.7	45.2	1729.7	45.2
203	57657	1.4	5.42983	1.9	0.34156	1.3	0.65	1894.2	20.8	1889.6	16.6	1884.5	26.5	1884.5	26.5
396	12142	0.7	0.32525	4.9	0.04491	2.4	0.49	283.2	6.6	285.9	12.3	308.3	98.3	283.2	6.6
129	4938	0.9	0.36802	3.6	0.04921	2.0	0.54	309.7	6.0	318.2	9.9	380.9	68.6	309.7	6.0
159	9748	0.8	0.56041	4.7	0.07132	3.5	0.73	444.1	14.8	451.8	17.2	491.2	70.5	444.1	14.8
159	6832	0.7	0.39628	5.7	0.05089	4.2	0.74	320.0	13.2	338.9	16.4	471.3	84.5	320.0	13.2
227	41780	1.0	2.19212	2.9	0.19995	2.1	0.72	1175.1	22.3	1178.5	20.2	1184.9	39.9	1184.9	39.9
414	17046	1.2	0.35087	3.4	0.04848	2.6	0.77	305.2	7.8	305.4	9.0	306.7	49.4	305.2	7.8
203	37873	0.8	2.50259	2.3	0.21787	2.0	0.83	1270.6	22.5	1272.8	17.0	1276.4	25.2	1276.4	25.2
164	5901	0.5	0.34083	2.6	0.04742	1.7	0.63	298.6	4.8	297.8	6.8	291.2	46.7	298.6	4.8
351	9281	0.6	0.34427	3.6	0.04689	3.2	0.90	295.4	9.3	300.4	9.4	339.6	36.1	295.4	9.3
272	58226	1.7	5.43323	2.5	0.34024	2.0	0.78	1887.8	32.4	1890.1	21.8	1892.6	28.8	1892.6	28.8
258	9232	0.7	0.35599	4.9	0.04923	3.4	0.71	309.8	10.4	309.2	13.0	305.0	78.6	309.8	10.4
323	9533	0.9	0.35504	5.0	0.04782	4.6	0.92	301.1	13.5	308.5	13.3	364.5	45.1	301.1	13.5
227	5729	0.5	0.35481	5.8	0.04969	3.5	0.61	312.6	10.8	308.3	15.5	275.9	106.0	312.6	10.8
257	11100	0.8	0.38472	2.9	0.05230	1.8	0.62	328.7	5.8	330.5	8.2	343.5	52.0	328.7	5.8
122	11145	0.4	2.11608	1.8	0.19331	1.5	0.84	1139.3	16.1	1154.1	12.7	1181.9	19.8	1181.9	19.8
SV-28C															
138	5064	1.0	0.34860	11.5	0.04576	7.8	0.68	288.4	22.0	303.7	30.2	422.4	188.9	288.4	22.0
634	5506	1.4	0.45342	6.6	0.05758	5.8	0.87	360.9	20.2	379.7	21.0	496.0	72.2	360.9	20.2
672	49871	3.2	3.91071	2.7	0.28490	2.2	0.81	1616.0	31.1	1615.9	21.7	1615.7	29.4	1615.7	29.4
459	103134	4.1	4.00842	3.3	0.29286	2.1	0.63	1655.8	30.4	1635.9	26.8	1610.4	47.7	1610.4	47.7
407	11912	0.6	0.38616	3.2	0.05259	2.4	0.74	330.4	7.7	331.6	9.2	339.5	49.3	330.4	7.7
423	21827	1.4	0.51338	2.5	0.06798	1.6	0.64	423.9	6.6	420.7	8.6	403.0	42.6	423.9	6.6
883	113233	39.7	3.73244	2.1	0.27734	1.5	0.71	1577.9	20.4	1578.4	16.4	1578.9	26.9	1578.9	26.9
76	18555	0.8	4.60153	4.9	0.31080	2.4	0.50	1744.6	37.4	1749.5	40.8	1755.4	77.4	1755.4	77.4
483	52098	2.1	1.92199	3.7	0.18580	2.3	0.63	1098.6	23.5	1088.8	24.6	1069.1	57.3	1069.1	57.3
306	13113	0.6	4.48016	4.3	0.30658	2.0	0.46	1723.9	29.8	1727.3	35.5	1731.5	69.7	1731.5	69.7
348	49933	0.8	5.26942	2.8	0.33812	1.8	0.65	1877.6	29.1	1863.9	23.5	1848.7	37.8	1848.7	37.8
460	85468	1.2	5.31414	3.1	0.33985	2.4	0.75	1886.0	38.4	1871.1	26.7	1854.7	37.2	1854.7	37.2
299	18694	1.5	0.64012	2.9	0.08166	1.4	0.49	506.1	7.0	502.4	11.5	485.7	55.9	506.1	7.0

1005	4945	0.7	1.50944	5.4	0.09431	3.3	0.61	580.9	18.3	934.2	32.8	1896.8	76.1	1896.8	76.1
292	75460	0.9	5.27671	3.0	0.33534	2.2	0.75	1864.2	36.2	1865.1	25.5	1866.1	35.7	1866.1	35.7
355	6208	0.5	0.36081	2.5	0.04843	1.8	0.73	304.9	5.5	312.8	6.8	372.3	38.6	304.9	5.5
296	8518	0.8	0.30516	5.0	0.04275	3.4	0.67	269.9	8.9	270.4	11.9	275.3	85.3	269.9	8.9
332	1931	0.3	0.41870	9.3	0.04939	8.8	0.95	310.8	26.8	355.1	28.0	656.1	65.2	310.8	26.8
547	5369	0.7	0.34306	5.1	0.04649	2.2	0.43	292.9	6.2	299.5	13.2	351.0	104.1	292.9	6.2
425	14449	0.8	0.36306	4.6	0.04964	3.6	0.78	312.3	11.0	314.5	12.6	330.8	66.0	312.3	11.0
552	6987	0.4	0.37953	3.0	0.05045	1.9	0.63	317.3	5.9	326.7	8.4	394.0	52.4	317.3	5.9
405	69560	0.8	5.01797	4.1	0.32916	3.0	0.72	1834.3	47.2	1822.4	34.9	1808.7	52.0	1808.7	52.0
651	24700	0.6	0.46745	2.1	0.06174	1.8	0.87	386.2	6.7	389.4	6.7	408.7	22.6	386.2	6.7
481	19869	1.2	0.40865	3.4	0.05517	1.3	0.39	346.2	4.4	347.9	10.0	359.5	70.8	346.2	4.4
232	17476	0.4	4.68314	4.9	0.29407	4.5	0.94	1661.8	66.6	1764.2	40.7	1887.7	31.0	1887.7	31.0
212	7565	0.4	0.41967	3.2	0.05416	1.9	0.60	340.0	6.3	355.8	9.6	460.3	56.5	340.0	6.3
116	4129	0.5	0.38172	4.8	0.05118	2.8	0.57	321.8	8.7	328.3	13.6	374.8	89.6	321.8	8.7
297	38232	0.5	2.14538	2.7	0.20014	1.6	0.59	1176.0	17.4	1163.6	18.9	1140.4	43.6	1140.4	43.6
442	70668	1.1	5.26731	4.2	0.33559	3.5	0.83	1865.4	56.9	1863.6	36.3	1861.5	43.2	1861.5	43.2
159	7947	1.0	0.53142	2.8	0.06788	2.0	0.73	423.3	8.4	432.8	9.9	483.1	42.6	423.3	8.4
253	3861	0.6	4.77488	8.2	0.28426	7.4	0.90	1612.8	105.4	1780.5	68.7	1983.1	62.0	1983.1	62.0
820	20837	1.1	0.35110	2.8	0.04857	1.8	0.64	305.8	5.3	305.6	7.3	304.0	48.6	305.8	5.3
393	94080	1.9	4.38890	2.1	0.30413	1.8	0.88	1711.8	27.2	1710.3	17.1	1708.4	18.4	1708.4	18.4
338	15561	0.6	0.38712	3.8	0.05228	2.4	0.65	328.5	7.8	332.3	10.6	358.8	64.3	328.5	7.8
149	27502	1.2	2.24357	2.4	0.19997	1.3	0.54	1175.2	14.1	1194.8	17.1	1230.4	40.3	1230.4	40.3
665	14391	0.9	0.42425	4.9	0.05403	3.1	0.63	339.2	10.2	359.1	14.8	489.4	83.8	339.2	10.2
220	22582	1.2	4.94865	5.0	0.31213	4.1	0.81	1751.2	62.3	1810.6	42.6	1879.7	53.9	1879.7	53.9
295	14001	0.8	0.36233	3.8	0.04817	1.7	0.44	303.3	5.0	313.9	10.3	393.9	76.7	303.3	5.0
112	3938	0.5	0.40065	6.6	0.05049	2.5	0.37	317.5	7.6	342.1	19.2	512.6	135.0	317.5	7.6
204	53329	1.1	5.69129	4.9	0.35124	4.2	0.86	1940.5	70.6	1930.0	42.3	1918.8	44.7	1918.8	44.7
440	10895	0.9	0.41826	2.7	0.05526	1.1	0.41	346.7	3.6	354.8	7.9	408.0	54.3	346.7	3.6
109	8840	0.7	3.93023	5.6	0.26736	5.2	0.94	1527.4	71.2	1619.9	45.0	1742.3	34.0	1742.3	34.0
285	65615	1.0	5.26025	3.4	0.33824	2.0	0.60	1878.2	32.5	1862.4	28.6	1844.9	48.7	1844.9	48.7
309	64100	1.5	5.22668	3.1	0.33577	1.4	0.45	1866.3	22.7	1857.0	26.4	1846.6	49.9	1846.6	49.9
232	55880	0.7	6.15154	6.4	0.37008	3.4	0.53	2029.8	59.6	1997.6	56.0	1964.5	96.8	1964.5	96.8
447	18747	1.0	0.37029	3.4	0.04847	1.3	0.37	305.1	3.8	319.9	9.5	428.5	71.3	305.1	3.8
217	31020	1.0	3.92271	2.8	0.28412	2.4	0.85	1612.1	33.7	1618.4	22.6	1626.6	27.7	1626.6	27.7

138	2725	0.3	0.44167	5.1	0.05327	3.8	0.74	334.6	12.4	371.4	16.0	608.4	74.4	334.6	12.4
646	43056	2.5	3.77650	1.9	0.27946	1.4	0.75	1588.6	20.1	1587.8	15.3	1586.6	23.6	1586.6	23.6
654	17262	1.7	4.37274	4.1	0.27742	2.5	0.61	1578.3	35.4	1707.2	34.0	1869.2	58.6	1869.2	58.6
245	10864	0.7	0.41265	3.0	0.05553	2.0	0.68	348.4	6.9	350.8	8.8	366.5	49.1	348.4	6.9
159	8783	0.6	0.60750	2.6	0.07605	1.7	0.67	472.5	7.9	482.0	9.8	527.2	41.5	472.5	7.9
351	63185	0.8	5.22263	2.4	0.33502	1.2	0.49	1862.6	19.1	1856.3	20.4	1849.2	37.6	1849.2	37.6
371	19376	0.8	5.01070	6.0	0.31380	5.2	0.87	1759.4	80.6	1821.1	51.2	1892.5	54.3	1892.5	54.3
321	49890	3.2	1.73304	4.1	0.16507	3.2	0.79	984.9	29.2	1020.9	26.2	1098.8	50.2	1098.8	50.2
132	1626	0.8	0.41813	8.8	0.04450	2.2	0.25	280.6	5.9	354.7	26.2	873.2	176.2	280.6	5.9
496	106601	1.2	4.55241	2.0	0.30925	1.0	0.51	1737.0	15.2	1740.6	16.4	1744.9	31.1	1744.9	31.1
126	5664	0.5	0.40401	3.6	0.05228	2.0	0.56	328.5	6.5	344.6	10.5	454.1	66.3	328.5	6.5
239	9087	0.9	4.89027	7.4	0.30505	7.2	0.97	1716.3	108.1	1800.6	62.5	1899.6	33.3	1899.6	33.3
221	1557	0.4	0.51815	4.2	0.05957	2.1	0.50	373.0	7.6	423.9	14.4	710.9	76.6	373.0	7.6
73	12686	0.4	4.45663	3.3	0.29510	2.0	0.58	1667.0	28.6	1722.9	27.8	1791.6	49.6	1791.6	49.6
117	21456	0.5	10.43200	4.3	0.45595	2.7	0.63	2421.7	55.1	2473.9	40.1	2517.1	56.3	2517.1	56.3
265	41279	0.5	3.84563	2.1	0.28319	1.6	0.76	1607.4	23.3	1602.4	17.3	1595.7	26.0	1595.7	26.0
142	945	0.6	0.92296	10.3	0.08909	3.4	0.33	550.2	17.9	663.9	50.5	1072.1	196.9	550.2	17.9
573	16814	0.8	0.36624	2.5	0.04684	1.4	0.56	295.1	4.0	316.9	6.7	480.2	45.2	295.1	4.0
94	14821	0.8	5.51528	2.8	0.34454	1.9	0.69	1908.5	31.8	1903.0	24.1	1897.0	36.5	1897.0	36.5
396	35130	0.8	5.06058	2.5	0.32355	1.8	0.73	1807.0	28.9	1829.5	21.3	1855.2	30.9	1855.2	30.9
628	7067	4.2	2.82017	7.6	0.20239	7.3	0.96	1188.2	79.1	1360.9	56.9	1643.7	39.1	1643.7	39.1
550	43306	1.0	5.22998	3.1	0.33304	2.3	0.76	1853.1	37.7	1857.5	26.2	1862.5	35.9	1862.5	35.9
224	33510	0.8	4.79566	3.6	0.32161	3.1	0.87	1797.6	48.7	1784.1	29.9	1768.4	31.6	1768.4	31.6
313	65333	1.3	4.62213	2.0	0.31100	1.0	0.51	1745.6	15.3	1753.3	16.4	1762.4	30.9	1762.4	30.9
544	58912	3.3	4.62786	3.6	0.29455	3.1	0.86	1664.2	44.9	1754.3	29.9	1863.4	33.2	1863.4	33.2
287	22858	0.7	2.32339	2.2	0.19551	1.0	0.46	1151.1	10.5	1219.5	15.4	1342.4	37.1	1342.4	37.1
266	65630	1.1	4.72739	2.1	0.31702	1.0	0.48	1775.2	15.5	1772.1	17.5	1768.5	33.4	1768.5	33.4
91	2359	0.7	0.33305	3.6	0.04233	1.7	0.48	267.2	4.6	291.9	9.2	494.2	70.5	267.2	4.6
559	64047	1.9	3.30442	3.5	0.25275	3.0	0.87	1452.7	39.0	1482.1	27.0	1524.5	32.6	1524.5	32.6
936	17038	3.3	0.30570	3.1	0.04271	2.6	0.81	269.6	6.7	270.8	7.5	281.3	41.7	269.6	6.7
733	16232	1.0	0.38993	1.7	0.05237	1.3	0.80	329.1	4.3	334.3	4.7	370.9	22.7	329.1	4.3
289	31629	0.8	5.03443	3.2	0.32271	1.0	0.31	1803.0	15.7	1825.1	27.3	1850.5	55.3	1850.5	55.3
116	26239	1.1	5.25527	4.4	0.33677	2.2	0.49	1871.1	35.1	1861.6	37.4	1851.0	68.9	1851.0	68.9
330	21188	0.5	9.78489	11.0	0.41750	10.6	0.96	2249.1	200.7	2414.7	102.1	2557.4	53.7	2557.4	53.7

279	11480	2.2	0.54069	3.6	0.06659	2.5	0.70	415.6	10.1	438.9	12.7	563.0	55.4	415.6	10.1
355	4986	3.5	0.48060	3.6	0.05718	2.6	0.73	358.4	9.1	398.5	11.8	637.8	52.9	358.4	9.1
240	42903	1.1	4.56017	2.2	0.30962	1.0	0.45	1738.8	15.2	1742.0	18.6	1745.9	36.5	1745.9	36.5
683	28874	8.4	3.64469	7.1	0.26472	6.0	0.86	1514.0	81.6	1559.3	56.3	1621.3	67.6	1621.3	67.6
289	70122	1.6	11.71954	3.0	0.49146	2.0	0.68	2577.0	42.8	2582.3	27.6	2586.4	36.1	2586.4	36.1
197	7995	0.7	0.49720	3.2	0.06414	2.8	0.88	400.8	11.0	409.8	10.9	461.0	33.5	400.8	11.0
217	9161	1.0	0.39771	5.6	0.05241	4.1	0.73	329.3	13.2	340.0	16.2	413.9	85.0	329.3	13.2
150	14330	1.2	1.83435	5.4	0.17612	3.4	0.64	1045.7	33.1	1057.8	35.3	1082.9	83.0	1082.9	83.0
525	20657	1.3	4.66189	6.2	0.28724	5.7	0.93	1627.7	82.7	1760.4	51.9	1921.7	41.6	1921.7	41.6
679	8006	1.0	0.37730	9.2	0.04909	8.8	0.95	309.0	26.5	325.1	25.7	441.9	64.1	309.0	26.5
469	12124	0.5	0.51571	3.7	0.06405	2.4	0.65	400.2	9.4	422.3	12.9	544.7	61.8	400.2	9.4
444	17245	1.9	0.47596	2.9	0.05891	1.4	0.48	369.0	5.0	395.3	9.5	552.3	55.3	369.0	5.0
151	31629	1.0	5.59315	3.3	0.34833	2.0	0.60	1926.6	32.9	1915.0	28.2	1902.5	46.9	1902.5	46.9
1253	5640	1.9	2.84695	4.4	0.20214	4.1	0.94	1186.8	44.4	1368.0	32.7	1663.4	27.3	1663.4	27.3
74	1571	0.8	0.40165	11.3	0.04870	7.2	0.64	306.6	21.5	342.8	32.9	596.8	189.3	306.6	21.5
175	10883	1.0	4.87414	3.4	0.32123	2.4	0.71	1795.7	38.1	1797.8	29.0	1800.2	44.4	1800.2	44.4
EZ-151															
645	10477	0.7	0.30103	4.0	0.04191	3.1	0.76	264.6	7.9	267.2	9.4	289.6	59.0	264.6	7.9
848	2351	0.9	1.13830	8.6	0.10779	8.2	0.95	659.9	51.3	771.7	46.6	1110.5	54.6	659.9	51.3
407	87412	1.0	5.57755	2.2	0.34725	1.3	0.60	1921.5	21.5	1912.6	18.5	1903.1	30.9	1903.1	30.9
263	20671	0.7	4.54705	3.2	0.30688	2.9	0.92	1725.3	43.8	1739.6	26.3	1756.8	22.9	1756.8	22.9
627	39884	1.4	3.57424	2.1	0.26981	1.5	0.73	1539.9	20.8	1543.8	16.6	1549.3	27.1	1549.3	27.1
232	12040	0.7	0.61583	2.5	0.07919	2.2	0.88	491.3	10.4	487.2	9.7	468.3	26.9	491.3	10.4
199	5754	0.6	0.42110	7.7	0.05300	4.9	0.64	332.9	16.0	356.8	23.3	515.4	131.2	332.9	16.0
164	6045	0.4	0.39512	3.3	0.05306	2.5	0.75	333.3	8.0	338.1	9.4	371.5	48.4	333.3	8.0
318	13118	0.7	0.37616	3.6	0.05058	3.1	0.86	318.1	9.7	324.2	10.1	368.6	42.4	318.1	9.7
644	2346	1.0	0.53927	5.3	0.06435	3.1	0.58	402.0	11.9	437.9	18.9	631.4	93.2	402.0	11.9
385	14151	0.9	0.36059	4.4	0.04911	2.3	0.52	309.0	6.9	312.7	11.9	339.6	85.8	309.0	6.9
234	26697	0.4	4.72428	3.3	0.31558	2.6	0.80	1768.1	40.7	1771.6	27.7	1775.6	36.3	1775.6	36.3
578	15181	0.7	0.35519	4.5	0.04548	2.8	0.62	286.7	7.9	308.6	12.1	477.5	78.5	286.7	7.9
243	10776	0.5	0.45186	2.3	0.05598	1.7	0.75	351.1	5.9	378.6	7.3	550.0	33.7	351.1	5.9
571	101800	1.2	3.64760	2.3	0.27452	1.8	0.78	1563.7	24.7	1560.0	18.1	1555.0	26.7	1555.0	26.7
321	38427	1.1	5.36384	4.6	0.33908	1.5	0.33	1882.2	24.6	1879.1	39.7	1875.6	79.0	1875.6	79.0
477	44860	2.3	4.31446	4.8	0.30333	3.7	0.77	1707.8	55.6	1696.1	39.6	1681.7	56.5	1681.7	56.5

230	2658	0.7	0.34030	5.1	0.04290	4.3	0.85	270.8	11.4	297.4	13.0	512.1	58.6	270.8	11.4
576	15946	0.7	0.28881	4.1	0.04026	2.5	0.62	254.5	6.3	257.6	9.2	286.5	72.7	254.5	6.3
182	18228	1.1	1.63661	6.8	0.12482	5.8	0.86	758.2	41.7	984.4	42.7	1530.0	64.7	1530.0	64.7
375	59142	0.8	4.48337	3.3	0.30376	2.3	0.69	1709.9	33.9	1727.9	27.2	1749.7	43.4	1749.7	43.4
58	1521	0.5	0.34905	8.5	0.04019	7.2	0.84	254.0	17.8	304.0	22.3	707.8	97.5	254.0	17.8
191	14923	0.8	5.81995	3.6	0.33920	2.0	0.55	1882.8	32.4	1949.4	31.2	2020.8	53.2	2020.8	53.2
396	67920	2.2	3.62296	4.6	0.23925	4.1	0.89	1382.8	51.1	1554.6	36.7	1796.5	38.0	1796.5	38.0
209	71519	1.1	5.74473	3.7	0.35400	2.7	0.73	1953.7	45.0	1938.1	31.8	1921.5	45.4	1921.5	45.4
108	14277	0.4	2.25404	3.0	0.20386	2.6	0.85	1196.0	27.9	1198.0	21.1	1201.7	30.9	1201.7	30.9
401	3304	0.6	4.77563	5.2	0.30166	3.5	0.67	1699.6	52.3	1780.6	43.7	1877.0	69.4	1877.0	69.4
284	6334	0.8	0.34778	3.8	0.04707	1.5	0.40	296.5	4.4	303.0	10.0	353.9	79.6	296.5	4.4
267	10163	0.5	0.42277	4.6	0.05534	3.6	0.78	347.2	12.1	358.0	13.8	428.5	63.4	347.2	12.1
227	37568	1.4	3.56540	3.5	0.24747	2.6	0.74	1425.4	32.8	1541.9	27.5	1705.4	43.1	1705.4	43.1
583	14698	0.8	0.41619	2.6	0.05512	2.0	0.78	345.9	6.9	353.3	7.8	402.7	37.0	345.9	6.9
637	22506	0.8	0.43536	2.5	0.05795	1.8	0.74	363.1	6.5	367.0	7.7	391.4	37.4	363.1	6.5
758	9066	0.8	0.39494	4.3	0.04908	3.1	0.73	308.9	9.5	338.0	12.5	543.2	65.3	308.9	9.5
156	4860	0.7	0.33500	4.8	0.04099	4.6	0.95	258.9	11.7	293.4	12.3	577.4	32.0	258.9	11.7
316	7787	0.5	0.60251	2.8	0.07386	2.3	0.82	459.4	10.1	478.8	10.6	573.0	34.8	459.4	10.1
296	5030	0.7	0.39157	3.3	0.05059	2.4	0.74	318.2	7.6	335.5	9.4	457.6	49.4	318.2	7.6
480	1798	0.8	0.25329	7.0	0.03819	2.5	0.36	241.6	5.9	229.2	14.3	104.4	154.2	241.6	5.9
159	3746	0.4	0.30480	4.5	0.04061	3.6	0.79	256.6	8.9	270.1	10.7	389.1	61.7	256.6	8.9
188	7345	0.3	0.76233	2.9	0.08983	2.0	0.68	554.5	10.4	575.4	12.7	658.5	45.7	554.5	10.4
350	7168	0.5	0.36880	4.8	0.04953	2.8	0.58	311.7	8.5	318.8	13.2	371.0	88.4	311.7	8.5
362	9905	0.7	0.40436	2.9	0.05473	2.3	0.80	343.5	7.6	344.8	8.4	353.6	39.1	343.5	7.6
303	8537	0.6	0.29693	3.6	0.04140	3.3	0.89	261.5	8.4	264.0	8.5	286.2	37.3	261.5	8.4
712	14474	0.9	3.85711	5.2	0.25611	4.9	0.93	1469.9	64.2	1604.8	42.2	1786.5	33.9	1786.5	33.9
182	4359	0.8	0.29768	5.4	0.03895	3.0	0.57	246.3	7.3	264.6	12.5	429.6	98.4	246.3	7.3
638	12029	0.8	0.29518	2.5	0.04080	1.2	0.51	257.8	3.1	262.6	5.7	305.8	48.4	257.8	3.1
346	7433	0.9	0.38216	4.3	0.04973	2.8	0.65	312.9	8.4	328.6	11.9	441.9	72.2	312.9	8.4
188	7872	1.2	0.38016	3.7	0.05043	2.5	0.66	317.1	7.6	327.2	10.4	399.0	62.6	317.1	7.6
452	16096	1.0	0.47201	3.2	0.06092	1.2	0.36	381.2	4.4	392.6	10.6	459.9	67.1	381.2	4.4
479	32830	0.9	4.74357	1.4	0.31434	1.0	0.70	1762.0	15.4	1775.0	12.0	1790.2	18.6	1790.2	18.6
504	51391	1.1	3.67192	7.0	0.27177	1.2	0.17	1549.8	16.2	1565.3	55.7	1586.3	128.6	1586.3	128.6
393	14274	0.8	4.94223	5.6	0.30985	5.1	0.92	1739.9	78.5	1809.5	47.5	1890.6	40.5	1890.6	40.5

507	9619	0.6	0.42384	20.5	0.05006	5.0	0.24	314.9	15.4	358.8	61.9	653.5	429.5	314.9	15.4
232	8705	0.7	0.37743	3.6	0.05028	2.9	0.82	316.2	9.1	325.1	10.0	389.4	46.9	316.2	9.1
533	24239	0.6	0.28177	3.5	0.03949	3.1	0.87	249.7	7.5	252.1	7.9	274.3	39.2	249.7	7.5
123	3703	0.8	0.29375	4.4	0.03937	2.9	0.65	248.9	7.0	261.5	10.1	376.0	74.7	248.9	7.0
222	6811	0.5	0.30240	3.1	0.04072	2.7	0.88	257.3	6.9	268.3	7.3	365.3	32.8	257.3	6.9
424	19939	2.6	0.72771	2.4	0.08906	1.9	0.78	550.0	10.1	555.2	10.4	576.6	33.1	550.0	10.1
237	4243	0.6	0.29472	8.6	0.03882	2.4	0.28	245.5	5.9	262.3	19.9	414.5	184.5	245.5	5.9
106	3157	0.6	0.31299	6.6	0.04101	4.4	0.66	259.1	11.1	276.5	16.0	426.4	110.4	259.1	11.1
69	16674	0.2	4.14970	4.1	0.28691	3.0	0.73	1626.0	43.0	1664.1	33.8	1712.5	52.3	1712.5	52.3
326	9787	0.7	0.30179	4.8	0.04038	3.1	0.63	255.2	7.7	267.8	11.4	379.5	84.5	255.2	7.7
538	4074	1.0	0.42345	11.2	0.05127	3.1	0.28	322.3	9.9	358.5	34.0	600.0	234.4	322.3	9.9

All uncertainties are reported at the 1-sigma level, and include only measurement errors.
Systematic errors would increase age uncertainties by 1-2%
U concentration and U/Th are calibrated relative to NIST SRM 610 and are accurate to ~20%.
Common Pb correction is from 204Pb, with composition interpreted from Stacey and Kramers (1975) and uncertainties of 1.0 for 206Pb/ 204Pb, 0.3 for 207Pb/ 204Pb, and 2.0 for 208Pb/ 204Pb.
U/Pb and 206Pb/ 207Pb fractionation is calibrated relative to fragments of a large Sri Lanka zircon of 564 ± 4 Ma (2-sigma).
U decay constants and composition as follows: 238U = 9.8485 x 10 -10, 235U = 1.55125 x 10 -10, 238U/ 235U = 137.88

Appendix 3: Timor structural measurements (using right hand rule) (Lat. And Long. In UTM)

Turquetti Measurements

Bedding		Bedding		Axial Surfaces		Mode 1 Fractures		Faults		
Strike	Dip	Stike	Dip	Strike	Dip	Strike	Dip	Strike	Dip	Type
0174261 S		354	28	20	62	15	90	278	50	
9037884 E		320	24	240	25	205	84	266	60	
243	46	278	20	280	14	241	40	120	30	
260	30	280	32	31	5	250	60	260	48	
220	38	310	30	278	26	284	70	110	60	
240	26	320	22	270	8	314	82	80	33	
266	25	245	47	140	48	340	88	328	38	
246	58	331	35	172	40	270	62	130	86	Normal
196	60	311	43			86	90	326	66	
222	32	280	48			124	22	57	31	Thrust
180	18	290	45					354	35	Thrust
0174364 S		289	40					200	20	
9037612 E		282	50					351	26	
49	28	300	40					211	38	
40	31	310	50					83	45	
94	25	0175706 S						206	20	Thrust
61	25	9040016 E						272	20	
43	20	300	41					270	46	
40	8	267	20							
68	8	276	16							
270	10	252	22							
82	12	290	20							
134	19	273	24							
90	24	103	30							
183	12	250	12							
100	9	90	30							
94	31	241	21							
58	28	280	26							
43	26	272	18							
350	41	318	12							
7	50	336	15							
49	40	276	26							
52	40	280	43							
103	10	20	28							
46	38	320	25							
79	31	256	24							
59	25	211	42							
57	10	186	30							
42	12	230	40							
38	30	0176741 S								
10	28	9043062 E								
352	22	50	80							
13	20	48	82							
0174748 S		236	48							
9039090 E		320	58							
368	10									

Cribas Measurements										
Bedding		Bedding		Axial Surfaces		Mode 1 Fractures		Faults		
Strike	Dip	Stike	Dip	Strike	Dip	Strike	Dip	Strike	Dip	Type
0828541 S		251	40	180	12	0	89	17	69	Normal
9038156 E		231	52	159	18	81	82	125	32	Thrust
163	26	179	23	200	18	310	84	120	42	Normal
224	25	190	13	220	20	302	84	51	12	Thrust
107	20	0823477 S		189	15	90	84	126	62	Normal
69	8	9031932 E		176	28	356	60	341	61	Normal
100	12	108	29	225	24	260	84	194	24	Normal
136	9	145	46	260	43	348	60	142	70	Normal
320	78	240	20	298	35	288	81	164	66	Thrust
196	40	22	10	124	32	268	75	149	67	
224	44	130	20	0827602 S		225	88	256	19	
277	26	160	34	9033982 E		306	70	213	38	Thrust
181	30	50	25			90	86	138	76	
191	35	330	15	0827081 S		253	80	236	40	
169	41	25	38	9034940 E				100	45	
167	39	290	40	209	27			204	8	Thrust
186	22	220	22	201	30			350	42	
229	59	264	34	169	27			150	30	Roof
200	59	248	52	154	40			162	35	Floor
193	57	252	5	224	68	Axial Planes		97	46	Normal?
197	52	241	30	139	80	Strike	Dip	116	62	
200	22	10	76	90	23	16	22	179	52	Normal
197	29	255	46	306	26	51	23			
326	44	48	83	272	22	40	0			
304	49	240	42	280	26	306	7			
180	23	246	48	155	24	296	66			
123	11	174	42	248	40					
226	16	188	35	0825430 S						
228	43	199	54	9033452 E						
238	42	164	67							
185	41	149	70							
185	32	220	40							
104	44	220	83							
200	22	185	50							
106	84	190	32							
174	45	154	26							
107	54	134	28							
262	21	180	60							
230	22	172	32							
193	22	44	20							
185	66	110	20							
230	27	224	40							
0826713 S		140	42							
9037205 E		170	26							

Soibada Measurements

Bedding		Bedding		Bedding		Bedding	
Strike	Dip	Stike	Dip	Strike	Dip	Stike	Dip
0824111 S		40	88	0822916 S		238	24
9025132 E		148	18	9011594 E		180	30
239	89	40	90	69	20	146	32
143	43	167	63	50	41	197	48
125	25	197	78	338	67	194	18
141	71	6	86	206	44	208	29
123	28	28	30	187	44	90	27
171	72	0825452 S		330	33	180	26
161	64	9021942 E		7	63	0823661 S	
163	31	201	12	17	50	9010724 E	
24	21	217	25	15	42	59	10
29	10	31	82	30	54	334	14
17	30	220	20	46	44	339	26
297	30	220	66	50	64	180	11
256	20	243	50	90	80	180	23
332	36	218	34	359	66	83	10
177	42	231	13	42	42	171	40
262	71	58	44	20	57	161	36
357	14	90	55	41	24	132	22
331	31	239	76	0823181 S		165	78
4	82	238	43	9010452 E		17	61
54	25	262	87	200	32	153	67
0824773 S		230	40	38	88	266	48
9023294 E		260	32	18	74	276	18
206	76	206	56	70	13	319	26
170	30	346	22	192	46	0828089 S	
211	34	216	22	10	74	9004094 E	
228	26	283	40	20	40		
224	42	297	22	201	18	0823893 S	
159	36	284	63	31	63	9011134 E	
211	52	227	38	273	2	264	9
149	59	217	38	45	18	289	40
182	44	185	47	218	78	216	26
158	30	209	50	212	82	287	9
232	46	151	25	26	24	162	38
218	34	237	46	271	30	5	42
210	72	230	70	29	48	11	34
0825288 S		230	40	93	15	21	48
9021988 E		182	60	36	48	169	27
78	64	217	25	236	28	41	85
40	70	213	28	232	22	0824205 S	
80	40	195	11	216	24	9011622 E	
210	80	262	40	53	23		
30	70	248	48	59	13		
136	28	222	28	223	32		
46	62	237	22	250	32		
153	30	0822495 S		270	16		
		9011885 E		192	40		

Soibada Measurements

Axial Surfaces		Mode 1 Fractures		Faults		
Strike	Dip	Strike	Dip	Strike	Dip	Type
135	34	97	84	330	56	
135	48	256	60	223	66	
135	49	138	26	232	64	
68	57	224	50	143	60	Normal
194	52	107	89	223	68	Normal
30	85	117	54	153	18	
187	65	50	69	1	71	
198	67	188	97	290	78	Normal
200	71	313	78	261	64	Normal
199	57	31	85	0	22	Thrust
205	52	151	79	148	73	
205	50	211	83	114	50	Normal
195	75	278	84	283	58	Normal
183	70	199	70	132	53	
191	86	296	66	257	62	
13	58	297	68	264	64	
212	61	254	58	260	46	
220	43	216	79			
236	75	29	42			
249	63	158	79			
192	42	186	18			
350	84	224	82			
317	80	112	74			
24	71	206	29			
191	76	130	90			
200	79	297	90			
208	68	117	80			
213	59	166	90			
229	82	3	76			
39	60	257	82			
215	80	131	78			
30	61	332	80			
		42	60			
		270	62			
		344	14			
		4	84			
		120	78			
		120	74			
		130	67			
		112	90			
		218	60			
		229	76			
		232	42			
		40	70			
		125	82			
		324	62			

Fatu Berliu Measurements

Bedding		Bedding		Axial Surfaces		Mode 1 Fractures	
Strike	Dip	Stike	Dip	Strike	Dip	Strike	Dip
0821209 S		231	46	359	86	214	83
9004290 E		236	38	359	86	98	80
252	42	229	40	270	74	286	80
250	21	224	31	243	70	97	76
183	33	283	78	203	82	328	28
354	25	204	40	223	56	224	76
334	20	222	48	216	67	223	78
190	49	0819675 S		200	63	158	69
202	34	9009574 E		204	60	332	80
187	31	178	32			113	84
158	15	205	76			70	62
201	50	334	49			296	24
96	30	243	48			41	76
201	81	197	76			66	65
240	32	352	83			340	68
7	38	253	46			105	63
87	22	238	66			90	41
13	18	203	63			147	88
337	22	198	66				
38	21	8	56				
6	44	27	42				
227	38	195	44				
336	84	335	65				
248	45	228	52				
139	32	195	44				
0819926 S		177	37				
9007872 E		211	42				
323	30	0819321 S					
357	54	9010976 E					
29	72						
47	18						